To the Graduate Council:

I am submitting herewith a thesis written by Alok Maheshbhai Patel entitled "Two-Phase Hydraulics State Identification using linear and non-linear time series analysis: Distillation Column Flooding Sensor". I have examined the final electronic copy of this thesis for form and content and recommend that it be accepted in partial fulfillment of the requirements for the degree of Masters of Science, with a major in Chemical Engineering.

Duane Bruns

Major Professor

We have read this thesis
and recommend its acceptance.

David Keffer

Charles Moore

Accepted for the Council:

Carolyn R. Hodges
Vice Provost and
Dean of Graduate Studies

(Original signatures are on file with official student records)

TWO-PHASE HYDRAULICS STATE IDENTIFICATION USING LINEAR AND NON-LINEAR TIME SERIES ANALYSIS: DISTILLATION COLUMN FLOODING SENSOR

A Thesis Presented for the
Master of Science Degree

The University of Tennessee, Knoxville

Alok Maheshbhai Patel
December 2007

Copyright © 2007 by Alok Patel
All rights reserved.

DEDICATION

I would like to dedicate this thesis to my parents Mahesh and Chhaya, Meena, and to my brother Priyank. This thesis is also dedicated to my aunt and uncle - Trupti and Dinesh, my grandparents and all my friends and family who gave me their unconditional support during the course of my education and life.

ACKNOWLEDGEMENT

First of all I would like to thank all the organizations, all my professors, and the Chemical Engineering Dept. for their never ending support. I would like to give special thanks Dr. Duane Bruns for all the help, trust and motivation to complete this project. I would also like to thank Team Chaos: Jason Walker, Scott Owens, Clinton Sattler, and all other undergraduate students who helped me directly or indirectly in running the experiments on the distillation column. I am also very thankful for the advice and guidance from Dr. Charles Finney and Dr. Stuart Daw. I would like to thank Dr. David Kefer and Dr. Charles Moore for serving on my committee. Dr. Rob Whitely (Oklahoma State University, Sweet Water), Anand, CP, and Dr. Chen (Fractional Research Institute) provided data and insight for this project. I am very thankful to Dr. Frymier and Dr. Weber for recommending me to join the GTA program which helped me in improving my teaching skills and paid most of my student fees. Last but not least, I want to thank Doug Feilden and his crew in the machine shop for all the help and support toward this project and the distillation column.

ABSTRACT

A novel sensor to detect and predict hydraulic flooding in the distillation column was developed in this research. High speed (1000 Hz) differential pressure data sets were collected across distillation trays. The distillation column at University of Tennessee, Knoxville (UTK) was the main research and demonstration site. The UTK column is 9 inches inside diameter, has 4 trays each of a different type not counting the reboiler. Many data sets were collected synchronously across the top tray (sieve tray) and across the next tray (bubble cap) from the top. Flooding always occurred on the sieve tray. To prove the application of this 'flooding sensor' in the field, data available from a pilot plant distillation column (low pressure, 4 foot diameter) located at Fractionation Research Inc. (FRI), Stillwater, OK was also analyzed. These time series were analyzed using linear and nonlinear methods such as autocorrelation, frequency analysis, mutual information and residual Shannon entropy. There was no separation of material carried out in the distillation column at UTK as it ran with water at total reflux. For the sieve tray, the magnitude of the first maxima peak in the autocorrelation, frequency analysis, mutual information and residual Shannon entropy plots increases, as the column moves towards the flooding. The behavior of the plots for the bubble cap tray also showed clear trends with increasing column throughput. Online monitoring of the chosen peak or peaks allows tracking of the hydraulic state and to predicting flooding.

TABLE OF CONTENTS

CHAPTER 1 INTRODUCTION 1

CHAPTER 2 THEORY 6

2.1 LINEAR METHODS 7

2.2 NON-LINEAR METHODS 8

2.3 SYMBOLIZATION 10

2.4 CHOICE OF SYMBOLIZATION PARAMETERS 14

CHAPTER 3 EXPERIMENTAL SETUP 23

3.1 UNIVERSITY OF TENNESSE, KNOXVILLE DISTILLATION COLUMN SETUP 23
3.11 Distillation column, University of Tennessee, Knoxville (UTK) 23
3.12 Instrumentation and Human Machine Interface 26
3.13 Differential pressure sensor hardware and interface 32
3.14 Signal Conditioning 37
3.15 Experimental campaigns 39

3.2 FRACTIONAL RESEARCH, INC. (FRI), FACILITY STILLWATER, OKLAHOMA 45

CHAPTER 4 DATA ANALYSIS 49

4.1 CHOICE OF TIME SERIES SEGMENTS 49

4.2 ANALYSIS OF TIME SERIES DATA 55
4.2.1 UTK distillation column data 55
4.2.1.1 Mean and standard deviation 55
4.2.1.2 FFT analysis - UTK data 59
4.2.1.3 A candidate Flooding Sensor: Autocorrelation function (ACF) analysis – UTK data 71
4.2.1.4 A candidate Flooding Sensor: Mutual Information (MI) analysis – UTK data 78
4.2.1.5 Residual Shannon Entropy (RSE) – UTK data 85
4.2.2 FRI DISTILLATION COLUMN DATA 89
4.2.2.1 Mean and Standard deviation 89
4.2.2.2 FFT analysis – FRI data 92
4.2.2.3 Autocorrelation function (ACF) analysis – FRI data 95

4.2.2.4 Mutual Information (MI) analysis – FRI data 98
4.2.2.5 Residual Shannon Entropy (RSE) – FRI data 98

CHAPTER 5 CONCLUSIONS AND FUTURE WORK 102

5.1 CONCLUSIONS 102

5.2 FUTURE WORK 106

BIBLIOGRAPGY 108

APPENDICES 112

APPENDIX A: LINEAR ANALYSIS FOR DIFFERENT RUNS 113

APPENDIX B: NON-LINEAR ANALYSIS FOR DIFFERENT RUNS 126

APPENDIX C: RUNNING MEAN AND VARIANCE FOR UTK DATA 135

VITA 159

LIST OF FIGURES

Figure 2.1 Typical behavior of random, chaotic and periodic data for (a) autocorrelation and (b) mutual information function (symbolic analysis of experimental data) [1] 11

Figure 2.2 Symbolization of a time series. 13

The time series is partitioned with Symbol-set size n=2. Three symbols are used to create the code, therefore the symbol sequence length L=3. The interval is 1 for this time series. If every other data point is used to create the code, then the interval will be equal to 2. 13

Figure 2.3 Residual Shannon entropy plot for different set sizes varying from 2 to 5, with constant sequence length of n=3 and symbolization interval τ =1 and sample = 0.001 second. 16

Figure 2.4 Residual Shannon entropy plot for different sequence lengths varying from 2 to 5, with constant set size of n=4 and symbolization interval τ =1 and sample = 0.001 second. 17

Figure 2.5 Symbol sequence histogram with symbol set size n= 4, sequence length L=2, symbolization interval τ =1 and sample = 0.001 sec..... 18

Figure 2.6 Symbol sequence histogram with symbol set size n= 2, sequence length L=3, symbolization interval τ =1 and sample = 0.001 sec..... 19

Figure 2.7 Symbol sequence histogram with symbol set size n= 3, sequence length L=3, symbolization interval τ =1 and sample = 0.001 sec..... 20

Figure 2.8 Symbol sequence histogram with symbol set size n= 4, sequence length L=3, symbolization interval τ =1 and sample = 0.001 sec..... 21

Figure 3.1 Distillation column located on first floor of unit operations lab. 24

Figure 3.2 Picture of the thermosiphon reboiler connected with steam on the shell side and column fluid on the tube side. 25

Figure 3.3 Shell and tube condenser located on the second floor of the unit operations lab..... 27

Figure 3.4 The feed tank (left) used to feed the liquid to the reboiler and the storage tank (right) to hold the final product. 28

Figure 3.5 The accumulator holds the liquid which is condensed in the condenser before feeding it back in the column. The liquid can be also diverted to the storage tank or the feed tank. 29

Figure 3.6 P&ID of the distillation column at University of Tennessee, Knoxville prepared by the class of ChE 447 (Applied Process Automation Laboratories) Fall 2005. 30

Figure 3.7 Portion of the HMI front panel from LabVIEW code that is used for controlling the instruments and collecting data on the workstation. 31

Figure 3.8 A pressure tap above tray 2 collection of pressure data in the vapor space above that particular tray. 33

Figure 3.9 Differential pressure sensor - MKS Baratron Type 223 34

Figure 3.10 Differential pressure sensor - Validyne P55D 35

Figure 3.11 Picture of the FRI distillation column building 47

Figure 4.1 Three different segments extracted from a continuous time series raw signal and bandpass filtered. 51

Figure 4.2 Mutual information plots for the time series segments from figure 4.1. 52

Figure 4.3 Running mean for non-overlapping segments of 2.048 sec (2048 points) for time series segments 1 and 2 from figure 4.1 54

Figure 4.4 Mean and standard deviation vs. reboiler steam pressure plot for tray 3 differential pressure data. 56

Figure 4.5 Mean and standard deviation vs. reboiler steam pressure plot for tray 4 differential pressure data. 58

Figure 4.6 FFT plot of differential pressure data collected across tray 3 for reboiler pressure range of 0 to 27.96 psig. 60

Figure 4.7 FFT plot (frequency 0 to 100 Hz) of differential pressure data collected across tray 3 for reboiler pressure range of 29.59 to 31.02 psig (flooded) and15.02 psig (post flooding). 61

Figure 4.8 FFT plot (frequency 0 to 25 Hz) of differential pressure data collected across tray 3 for reboiler pressure range of 0 to 27.96 psig. ... 63

Figure 4.9 FFT plot (frequency 0 to 25 Hz) of differential pressure data collected across tray 3 for reboiler pressure range of 29.59 to 31.02 psig (flooded) and15.02 psig (recovered post flooding). 64

Figure 4.10 FFT plot (frequency 0 to 2.5 Hz) of differential pressure data collected across tray 3 for reboiler pressure range of 0 to 27.96 psig 65

Figure 4.11 FFT plot (frequency 0 to 2.5 Hz) of differential pressure data collected across tray 3 for reboiler pressure range of 29.59 to 31.02 psig (flooded) and15.02 psig (post flooding). 66

Figure 4.12 FFT plot of differential pressure data collected across tray 4 for reboiler pressure range of 0 to 27.96 psig. 67

Figure 4.13 FFT plot (frequency 0 to 100 Hz) of differential pressure data collected across tray 4 for reboiler pressure range of 29.59 to 31.02 psig (flooded) and15.02 psig (post flooding). 68

Figure 4.14 FFT plot (frequency 0 to 25 Hz) of differential pressure data collected across tray 4 for reboiler pressure range of 0 to 27.96 psig. ... 69

Figure 4.15 FFT plot (frequency 0 to 25 Hz) of differential pressure data collected across tray 4 for reboiler pressure range of 29.59 to 31.02 psig (flooded) and15.02 psig (post flooding). 70

Figure 4.17 Autocorrelation plot for tray 3 data for reboiler pressure range of 9.97 to 27.96 psig..... 73

Figure 4.18 Autocorrelation plot for tray 3 differential pressure data for reboiler pressure range of 29.59 to 31.02 psig and15.02 psig (post flooding) 74

Figure 4.19a Autocorrelation plot for tray 4 differential pressure data. 76

Figure 4.19b Autocorrelation plot for tray 4 differential pressure data without 0, 31.02 (flooding) and 15.02 (post flooding) psig curves..... 77

Figure 4.20 Mutual Information plot for tray 3 data..... 79

Figure 4.21 Mutual Information plot for tray 3 data for reboiler pressure range of 9.97 to 27.96 psig..... 80

Figure 4.22 Mutual Information plot for tray 3 data for reboiler pressure range of 29.59 to 31.08 psig without 0, 31.02 (flooding) and 15.02 (post flooding) psig curves. 81

Figure 4.23a Mutual Information plot for tray 4 data..... 83

Figure 4.23b Mutual Information plot for tray 4 differential pressure data without 0, 31.02 (flooding) and 15.02 (post flooding) psig curves. 84

Figure 4.24 Residual Shannon Entropy plot for tray 3 data for reboiler pressure range of 9.97 to 27.96 psig..... 86

Figure 4.25 Residual Shannon entropy plot for tray 3 data for reboiler pressure range of 29.59 to 31.02 psig and 15.02 psig (post flooding).... 87

Figure 4.26 Residual Shannon entropy plot for tray 4 data for all reboiler pressures. 88

Figure 4.27 Mean and standard deviation vs. time graphs for FRI data. 90

Figure 4.28 FFT plot (frequency 0 to 100 Hz) for FRI differential pressure data. 93

Figure 4.29 FFT plot (frequency 0 to 25 Hz) for FRI differential pressure data. 94

Figure 4.30 Autocorrelation plot for FRI differential pressure data (Lag 0-500). 96

Figure 4.31 Autocorrelation plot for FRI differential pressure data (Lag 0-150). 97

Figure 4.32 Mutual information plot for FRI differential pressure data (Lag 0 to 1000)..... 99

Figure 4.34 Shannon Entropy plot for FRI differential pressure data (Lag 0 to 100). 101

Figure A.1 Mean and standard deviation vs. reboiler steam pressure plot for tray 4 differential pressure data (UTK column, tray 4 data, November 16, 2006). Figure 4.5 repeated from section 4. 114

Figure A.2 Mean and standard deviation vs. reboiler steam pressure plot (UTK column, tray 4 data, September 18, 2006)..... 115

Figure A.3 Mean and standard deviation vs. reboiler steam pressure plot (UTK column, tray 4 data, October 2, 2006) 116

Figure A.4 Mean and standard deviation vs. reboiler steam pressure plot (UTK column, tray 4 data, October 3, 2006) 117

Figure A.5 FFT plot of differential pressure data collected across tray 4 for reboiler pressure range of 0 to 27.96 psig. (UTK column, tray 4 data, November 16, 2006). Figure 4.12 repeated from section 4. 118

Figure A.6 FFT plot (UTK column, tray 4 data, September 18, 2006) 119

Figure A.7 FFT plot (UTK column, tray 4 data, October 2, 2006) 120

Figure A.8 FFT plot (UTK column, tray 4 data, October 3, 2006) 121

Figure A.9 Autocorrelation plot for tray 4 differential pressure data. (UTK column, tray 4 data, November 16, 2006). Figure 4.19 repeated from section 4. 122

Figure A.10 Autocorrelation plot (UTK column, tray 4 data, September 18, 2006) 123

Figure A.11 Autocorrelation plot (UTK column, tray 4 data, October 2, 2006) 124

Figure A.12 Autocorrelation plot (UTK column, tray 4 data, October 3, 2006) 125

Figure B.1 Mutual Information plot for tray 4 with all differential pressure data. (UTK column, tray 4 data, November 16, 2006). Figure 4.23 repeated from section 4 127

Figure B.2 Mutual information plot (UTK column, tray 4 data, September 18, 2006) 128

Figure B.3 Mutual information plot (UTK column, tray 4 data, October 2, 2006) 129

Figure B.4 Mutual information plot (UTK column, tray 4 data, October 3, 2006) 130

Figure B.5 Residual Shannon entropy plot for tray 4 data for all reboiler pressures. (UTK column, tray 4 data, November 16, 2006). Figure 4.26 repeated from section 4. 131

Figure B.6 Residual Shannon entropy plot (UTK column, tray 4 data, September 18, 2006) 132

Figure B.7 Residual Shannon entropy plot (UTK column, tray 4 data, October 2, 2006) 133

Figure B.8 Residual Shannon entropy plot (UTK column, tray 4 data, October 3, 2006) 134

Figure C.1 Running mean and variance for tray 3 time series at reboiler pressure = 0 psig 135

Figure C.2 Running mean and variance for tray 3 time series at reboiler pressure = 9.97 psig 136

Figure C.3 Running mean and variance for tray 3 time series at reboiler pressure = 15.04 psig 137

Figure C.4 Running mean and variance for tray 3 time series at reboiler pressure = 20.08 psig 138

Figure C.5 Running mean and variance for tray 3 time series at reboiler pressure = 24.98 psig 139

Figure C.6 Running mean and variance for tray 3 time series at reboiler pressure = 27.96 psig 140

Figure C.7 Running mean and variance for tray 3 time series at reboiler pressure = 29.59 psig 141

Figure C.8 Running mean and variance for tray 3 time series at reboiler pressure = 29.94 psig 142

Figure C.9 Running mean and variance for tray 3 time series at reboiler pressure = 30.02 psig 143

Figure C.10 Running mean and variance for tray 3 time series at reboiler pressure = 31.08 psig 144

Figure C.11 Running mean and variance for tray 3 time series at reboiler pressure = 31.02 psig 145

Figure C.12 Running mean and variance for tray 3 time series at reboiler pressure = 15.02 psig 146

Figure C.13 Running mean and variance for tray 4 time series at reboiler pressure = 0 psig 147

Figure C.14 Running mean and variance for tray 4 time series at reboiler pressure = 9.97 psig 148

Figure C.15 Running mean and variance for tray 4 time series at reboiler pressure = 15.04 psig 149

Figure C.16 Running mean and variance for tray 4 time series at reboiler pressure = 20.08 psig 150

Figure C.17 Running mean and variance for tray 4 time series at reboiler pressure = 24.98 psig 151

Figure C.18 Running mean and variance for tray 4 time series at reboiler pressure = 27.96 psig 152

Figure C.19 Running mean and variance for tray 4 time series at reboiler pressure = 29.59 psig 153

Figure C.20 Running mean and variance for tray 4 time series at reboiler pressure = 29.94 psig 154

Figure C.21 Running mean and variance for tray 4 time series at reboiler pressure = 30.02 psig 155

Figure C.22 Running mean and variance for tray 4 time series at reboiler pressure = 31.08 psig 156

Figure C.23 Running mean and variance for tray 4 time series at reboiler pressure = 31.02 psig 157

Figure C.24 Running mean and variance for tray 4 time series at reboiler pressure = 15.02 psig 158

Nomenclature

τ	delay or lag; symbolization interval
c_τ	correlation coefficient
x(t)	time domain representation of the time signal
X(f)	frequency domain representation
p_i	probability that a measurement will fall in the i^{th} bin
Z	total number of non-empty bins
H_s	Shannon Entropy
H_{SM}	modified Shannon entropy
H'_{SM}	residual Shannon entropy
I	Mutual information
n	Symbol-set size
L	symbol sequence length
W_n	natural frequency (radians/sec)
F_n	natural frequency (Hz)
C	velocity of sound in media (ft/sec)
a	cross sectional area of tubing (cu ft)
L	length of tubing (ft)
Q	transducer cavity volume (cu ft)

Acronyms

DOE	United States Department of Energy
UTK	University of Tennessee, Knoxville
FRI	Fractionation Research, Inc.
NTSAS	Nonlinear Time Series Analysis Software©
MCEC	Measurement and Control Engineering Center
ORNL	Oak Ridge National Laboratory
FFT	fast Fourier transform
P&ID	Piping and Instrumentation diagram
PT	Pressure transmitter
FCV	Flow control valve
ΔP	Differential pressure
HMI	Human-Machine-Interface
NI	National Instruments
SCB	Signal Connector Block
DAQ	Data Acquisition
PI	Proportional Integral

CHAPTER 1 INTRODUCTION

Distillation is the most common process used for separation of chemicals in the chemical industry. Distillation is a process that separates two or more miscible liquids based on the differences of their respective boiling points. In today's modern world of transportation, gasoline is an important commodity. The United States Department of Energy (DOE) has previously estimated that operation of distillation columns at capacity (very close to flooding) could save 2.4 trillion Btu of feedstock energy, 7 trillion Btu of heat/steam energy, and 0.11 MMTCE/year in carbon emissions by 2020 (DOE, 2003a). The petrochemical industry is the largest consumer of energy in the chemical industry because distillation is the most energy consuming process in the chemical plants. Approximately 35 – 40% of the total energy in refining crude oil is used in distillation process. Approximately 8% of the total energy used in the US industrial sector is used in running distillation columns [1]. To increase the efficiency of the distillation column, one has to increase the throughput of the column.

In most petrochemical plants, one of the most effective ways to increase the plant efficiency is to increase the throughput per distillation column. There are two aspects where increased column throughput provides economic rewards. One is that large savings are made if one column out of a set of columns can be shut down. This is highlighted in a 2004 Office of Information Technology Solicitation for Distillation [21]. Another is increased production in

those situations where flooding in a distillation column represents the bottleneck in a manufacturing unit (a common occurrence). The distillation expert for a major U.S. petrochemical company estimates that capacity gains of up to 5% to 15% may be achievable [22, 30]. For commodity processes, the economic impact of increasing capacity with essentially no capital investment is tremendous.

When the distillation columns are pushed towards the operating limits, the operators are faced with an unwanted problem of flooding. Flooding occurs when excess liquid accumulates within the column resulting in loss of mass transfer capabilities [8]. Nearly 10% of the columns in the US experience flooding. There are different mechanisms through which flooding occurs:

1. Spray entrainment flooding – occurs when the vapor velocity increases to a point where the liquid drops get entrained in the vapor and are transported to the tray above. The separation achieved by the tray is partly negated.
2. Froth entrainment flooding – occurs due to the froth height increasing as the vapor rate increases, when the tray spacing is insufficient, the froth gets entrained to the tray above resulting in liquid accumulation on that tray.
3. Downcomer backup flooding – occurs when the aerated liquid in the downcomer exceeds the tray spacing causing liquid to accumulate in the tray above. This is due to differential pressure through tray being too large.

4. Downcomer choke flooding – occurs when the liquid flow rate increases above the hydraulic capacity of the downcomer causing the tray liquid level to increase.

This results in large changes in tops and bottoms flow rate, loss of mass transfer capability and off-spec product which leads to column shut down. The end result is loss of energy consumed in production of off-spec product. Loss of mass transfer efficiency results in off specification product and shut down of the distillation column. The final result of all this is capital loss to the chemical industry.

The phenomenon of flooding is very complex and there are many definitions of flooding, in part, due to various flooding mechanisms. In general, there is no specific operating point which can be defined as a flooding point. This makes the prediction of flooding more difficult. To prevent the occurrence of flooding, distillation columns are typically operated at 80-85% of flood [8, 22, 30]. Flooding is also a problem in packed columns and predicting the onset of flooding is considered much harder than in tray columns. Therefore the packed towers are operated at 70-80% of flooding.

Flooding can be detected in columns when one or more of the following observations are made [8]

1. Excessive column average differential pressure
2. Sharp rise in column average differential pressure
3. Loss of bottoms
4. Rapid rise of entrainment from column tray

5. Loss of separation (generally detected by lab analysis or temperature profile)

Most of the distillation columns are operated by measuring the average differential pressure across different sections of the distillation column to detect excessive column differential pressure, which indicates flooding. These indications generally occur after the column has already flooded or the differential pressure representing the flooding constraint changes with the operating conditions; therefore there is a well established need for a method or sensor to more accurately detect the onset of flooding. Much research has been done in the field of distillation but there has been little success in detection of incipient flooding.

This thesis documents the research in developing the detection of incipient flooding in distillation columns. The experiments are carried out on the distillation column located in the Unit Operations Lab at University of Tennessee, Knoxville (UTK). Data from Fractionation Research, Inc. (FRI) will also be analyzed and presented in the results section. FRI is a non-profit organization which performs only commercial size distillation research for member companies from all over the world.

The author will analyze appropriately collected high speed differential pressure data sampled at the rate of 1000 Hz using Nonlinear Time Series Analysis Software© (NTSAS) Matlab toolkit developed by collaboration of Measurement and Control Engineering Center (MCEC), UTK and Oak Ridge National Laboratory (ORNL). The time series will be symbolized to enhance

the detection of chaotic patterns. Nonlinear analysis techniques such as mutual information and the Residual Shannon entropy will be utilized to analyze the symbolized data. Linear parameters such as mean, standard deviation and autocorrelation will be calculated. This approach has had success as indicated by patents and patent applications for other chaotic processes as large fluidized bed polyethylene reactors [31], flames in coal combustors [27] and spark ignition engines [32]. The bubbling phenomenon studies at UTK from a single orifice and fluidized bed using non-linear techniques have showed similar results.

The layout of the thesis is as follows. This chapter provides a review of the concept of flooding and motivation for developing an online sensor to quantify the percent of flooding. Chapter 2 discusses the theoretical concepts applied on the experimental data. Chapter 3 describes the experiments carried out to collect the data used for this thesis and the equipment set up. Chapter 4 discusses the results obtained from the linear and nonlinear analysis of the high speed differential pressure time series data and the implementation of the ‘flooding sensor’. Chapter 5 outlines the conclusion and recommended future work for additional development, testing and utilization of the new hydraulics (flooding) sensor.

CHAPTER 2 THEORY

A novel sensor is developed to detect and predict hydraulic flooding in the distillation columns. The most common way of detecting flooding in the field is measuring the differential pressure across the whole column, a certain section of the column or a tray. In this research the method used for detection of incipient flooding is through measuring high speed (1000 Hz) differential pressure data across a tray. There have been very few research projects targeted at detecting incipient flooding in columns in the recent years. One such work that has presented some promising results is by Dzyacky [5, 28]. The Dzyacky method implements software that measures several time averaged output variables. These variables are differential pressure, temperature, flow rates, etc. These variables are measured on macro time scales of seconds and minutes. The software is based on recognizing patterns in different variables measured during the column run and detecting instability in the column. It requires calculating derivatives of several of the measured variables. The software is based on recognizing patterns in different variables measured during the column run and detecting instability in the column. The Dzyacky prediction algorithm does not incorporate nonlinear time series concepts and is not a sensor but a complex software program. The system has not been widely implemented by industry.

This research involves detecting incipient flooding by collecting high frequency differential pressure time series, symbolizing the data and

calculating non-linear parameters for the symbolized data. The nonlinear concepts employed are Mutual information and Shannon entropy. Quantitative linear techniques such as calculating autocorrelation function and fast Fourier transform (FFT) to generate Power Spectral Density plots are also utilized.

2.1 LINEAR METHODS

The autocorrelation function calculates the correlation between observations separated by a certain lag in samples. The correlation coefficient for observations separated by lag τ is given by

$$c_\tau = \frac{E(x_i \bullet x_{i+\tau})}{E(x_i{}^2)} \qquad (2.1)$$

where E is the expected value. The value of the correlation coefficient c_τ varies from 0 to 1 [3]. If the process is non-linear, autocorrelation does not provide confident results because it assumes linear relationship between data points [9].

The function of the FFT is to transform a signal from the time domain to the frequency domain. The FFT is commonly used in analysis of time-invariant systems and spectral analysis [10]. Equation 2.2 defines the two sided Fourier transform

$$X(f) = F\{x(t)\} = \int_{-\infty}^{\infty} x(t) e^{-j2\pi ft} dt \qquad (2.2)$$

where x(t) the time domain representation of the time signal and X(f) is the frequency domain representation [10].

2.2 NON-LINEAR METHODS

Bubble formation on column trays is a complex process. Yang and Glasgow have proven that bubbling is a low dimensional deterministic process and have considered it as a non-linear process [11]. They analyzed the bubbling on the sieve tray using a photomultiplier and measuring light scattering caused by bubbles passing through focused white light and proved that low dimensional deterministic chaos by calculating the correlation dimension and largest Lyapunov exponent. The phenomenon of bubble formation and the impact of electrostatic fields on the dynamics of bubble formation is also studied using non-linear techniques such as delay embedding and time return maps [26].

Entropy is the measure of amount of disorder in a signal or alternatively, the amount of information in a signal. Entropy was first introduced to the area of data communication by Shannon and Weaver [12]. Common Entropy definition used with engineering data is the Shannon entropy. Shannon Entropy (H_s) is the "degree of randomness or lack of predictability of the signal". It is defined as

$$H(X) = -\sum_i p_i \ln p_i \qquad (2.3)$$

where p_i is the probability that a measurement will fall in the i^{th} bin. The modified Shannon Entropy (H_{SM}) is defined as

$$H_{SM} = -\frac{1}{\ln Z}\sum_i p_i \log p_i \qquad (2.4)$$

where Z is the total number of non-empty bins[4]. The modified version of Shannon entropy by Daw et al [4] prevents bias in entropy calculations and therefore is used in analysis of the distillation column data. The entropy is 0 when one is absolute certain about the outcome of an event and 1 when one is only making a random guess. Shannon entropy has been used in many experimental analyses such as investigating dynamic behavior in bubbling fluidized beds [14]. It is the basis for calculating Mutual information.

Consider a time series $X(t)= x(t_1), x(t_2), x(t_3), \ldots, x(t_n)$ and the τ delayed version of the time series be $X(t+\tau)= x(t_1+ \tau), x(t_2+\tau), x(t_3+\tau), \ldots, x(t_m+\tau)$. The joint average entropy for these two time series is defined as

$$H(X, X+\tau) = -\sum_i^N \sum_j^M p(x_i, x_j) \ln p(x_i, x_j) \qquad (2.5)$$

where $p(x_i, x_j)$ represents the probability of x(t) falling in i^{th} bin and the delay version $x(t+ \tau)$ falling in j^{th} bin [9].

Mutual information and Shannon entropy were developed as concepts mainly used in the theories of communication. Today both concepts are widely used in experimental data analysis. Mutual information was first introduced by Fraser and Swinney to analyze chaotic data from an experiment on the Belousov-Zhabotinskii reaction [7]. Mutual information (I) is

the amount of information one variable (X) provides about another variable (Y) knowing one of the variables (X or Y). In the following example the second variable is represented as the delayed version (X+ τ) of the first variable X. It is defined as

$$I(X, X+\tau) = 2H(X) - H(X, X+\tau) \qquad (2.6)$$

The first minimum of the Mutual information plot is often used to determine the time delay for plotting the phase portrait plots [7, 9]. Karamavruc et. al [9] used mutual information to analyze the temperature and differential pressure data from a fluidized bed. Figure 2.1 shows Autocorrelation and the Mutual Information plots for periodic, chaotic and random time series. The probabilities for calculating Shannon entropy and Mutual Information are calculated using symbolization of the differential pressure time series data.

2.3 SYMBOLIZATION

In recent years data analysis techniques such as symbolization has been very fruitful in analysis of chaotic and non-linear systems. Early use of symbolization can be referred to Crutchfield [16] and Tang [15]. Symbolization was used to find correlation time scales at high noise levels [15]. Daw et al (1997) used the symbolization technique to quantitatively define “temporal irreversibility” in time series. Symbolization was also used by Daw et al [4] for modeling nonlinear dynamics in internal combustion engine.

Symbolization is a technique involving coarse graining where the original time series is partitioned into a finite number of regions. Each region is specified

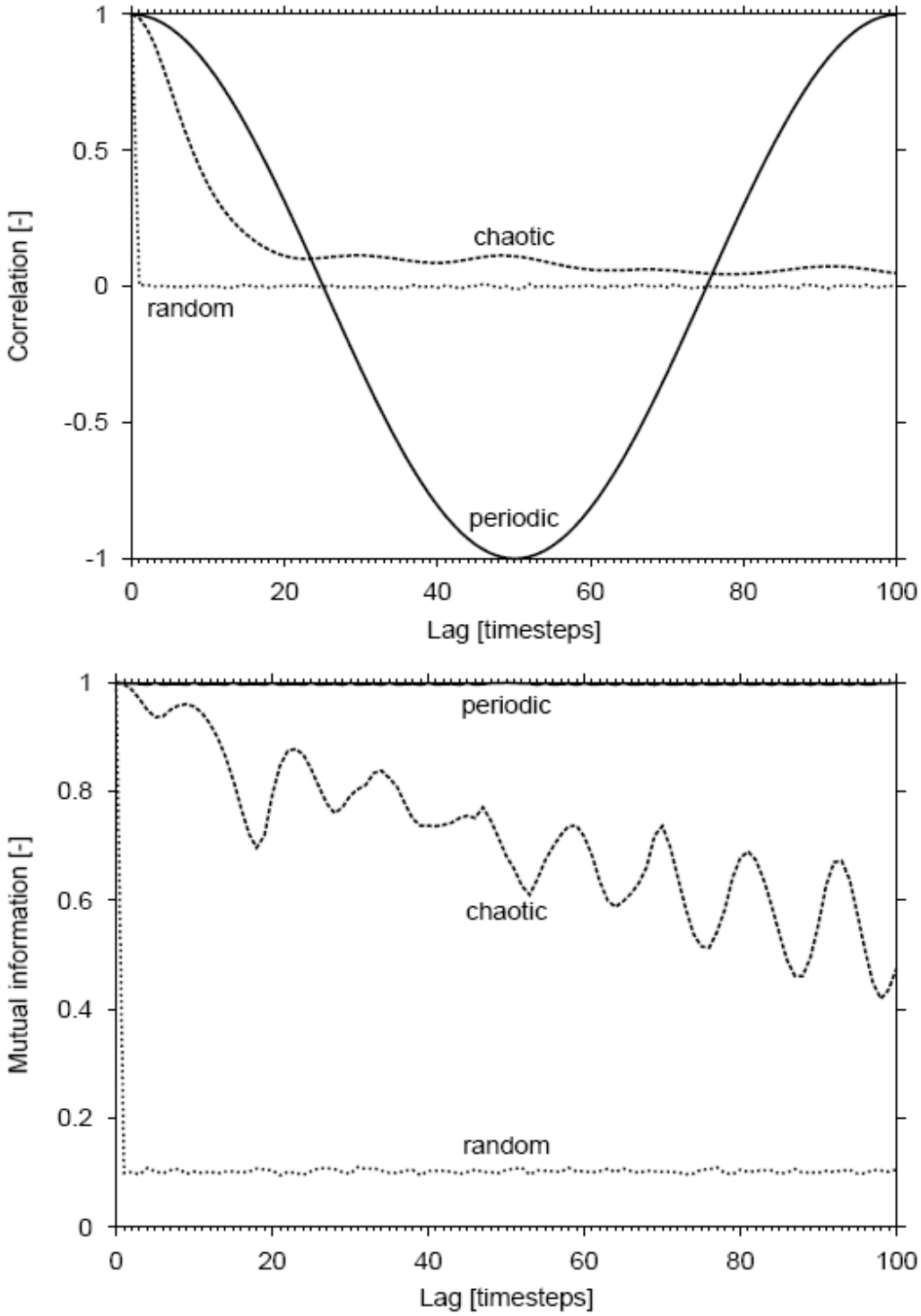


Figure 2.1 Typical behavior of random, chaotic and periodic data for (a) autocorrelation and (b) mutual information function (symbolic analysis of experimental data) [1]

as a certain number called the symbol (n=0, 1, 2…). As shown in figure 2.2, the original data points in the time series *x (t)* are assigned specific symbols (0, 1, 2…) according to the region it falls into. The total number of possible symbols is called the Symbol-set size or the Alphabet size [1]. The next step after obtaining the symbol series is to formulate the *symbol sequences*. Symbol sequences (words) depends on the number of symbols used, which is also referred as "*symbol sequence length (L)*". The total number of possible symbol sequence is equal to n^L. For example, if the time series is divided into two partitions with symbols 0 and 1 with the sequence length equal to three, then the total number of possible symbol sequences is equal to $2^3 = 8$. To facilitate the calculation of the frequency of each symbol sequence, the symbol sequence is assigned "a unique number by evaluating the equivalent base-10 value of each base-n sequence" [2].

The unique number series formed from the symbol sequence is called the *code series*. The base-10 values for a *symbol-set size* of n and a symbol *sequence length* of L are 0, 1, 3…. n^L. For the example if the key is *symbol-set size*, n, of 2 and *sequence length*, L, of 3, the *code series* can take on values of 0, 1, 2, 3, 4, 5, 6, 7 and 8. The probability distribution of the code series, also called the *symbol sequence histogram* gives an idea about different patterns of symbol sequences occurring in the time series. Partitioning of the time series can be done in different manners such as mean partitioning or equiprobable partitioning (relative frequency of each possible

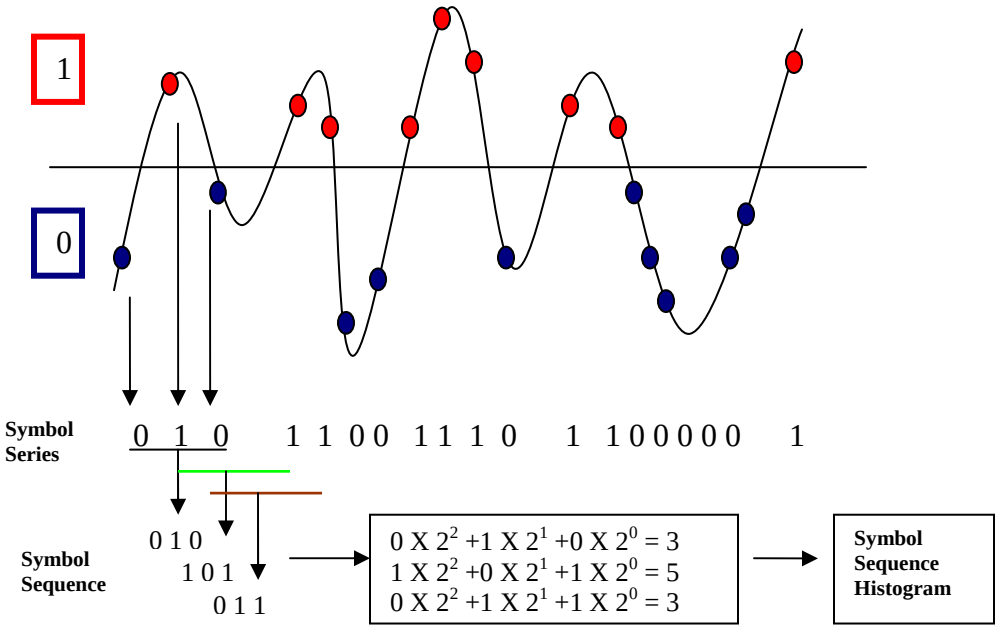


Figure 2.2 Symbolization of a time series.

The time series is partitioned with Symbol-set size n=2. Three symbols are used to create the code, therefore the symbol sequence length L=3. The interval is 1 for this time series. If every other data point is used to create the code, then the interval will be equal to 2.

sequence for truly random data will be equal). For this project the time series is partitioned in equiprobable bins.

2.4 CHOICE OF SYMBOLIZATION PARAMETERS

The symbolization parameters are the set size (n), sequence length (L) and the interval (τ). This set of parameters is called the key for the symbolization. The choice of the parameters in the key highly depends on the dynamics of the process. There is no one particular theory that can be applied to all experiments for choosing symbolization parameters [1]. The sequence length and the interval should be chosen according to the dynamics of the process [13]. If the time series is complex, it should have finer partitions therefore higher set size value. Otherwise for a simple time series, one might just choose a smaller set size. A lot of times scientist and engineers have to choose the symbolization parameters based on trial and error methods.

In this application we will study the residual Shannon entropy plots for different symbolization parameters. The residual Shannon entropy is defined as $H'_{SM} = 1 - H_{SM}$. Peaks in Shannon entropy plot indicate high unpredictability, whereas a peak in residual Shannon entropy indicates high predictability in the time series at that particular interval.

Let $H'_{SM}(n, L, \tau)$ be the residual Shannon entropy of a time series at set size n, sequence length L and symbolization interval τ. Many values of the symbolization key (n, L, τ) were evaluated to determine a best key. The results of the key selection are illustrated in figures 2.3 and 2.4. The time

series used in figure 2.3 and 2.4 is collected across tray 3 (reboiler pressure = 20.08 psig) on November 16, 2006. Figure 2.3 shows the residual Shannon entropy plots for various set sizes. The value for the set size is varied from 2 to 5, with sequence length equal to 3 and interval equal to 1. By visually inspecting figure 2.3, set size of 2, 3 and 4 can be used for further analysis. As set size increases the tail, lag of 80 and higher, rises with lag. For n = 1, 2 and 3 the tail stays around zero. Increasing the set size increases the peaks in residual entropy plot and the value of entropy for higher lags increases. In figure 2.4, the set size and symbolization interval are constant (n=4 and τ=1). The sequence length is increased from 2 to 5. Increasing the sequence length while holding the set size and interval constant, the residual entropy curve becomes flat and the peaks at lag of 25 and 45 diminish. There is no peak at lag of 25 for sequence length of 2. Thus a key with set size equal to 4, sequence length equal to 3 and interval equal to 1 is selected as the best choice of symbolization parameters based on figure 2.3 and 2.4.

To support the above choice of symbolization keys, figure 2.5 through 2.8 shows symbol sequence histogram using different keys for the same data set used in figure 2.3 and 2.4 (key 1 where n=4 and L=2, key 2 where n=2 and L=3, key3 where n=4 and L=3, key 4 where n=3 and L=3). Figure 2.5 shows that there is maximum probability of symbol sequences with values of [0 0], [1 1], [2 2] and [3 3] (sequence codes with 0, 5, 10 and 15). Similarly in figure 2.6 there is maximum probability for symbol sequences with value of [0 0 0] and [1 1 1]. In general the symbol sequence histogram should have

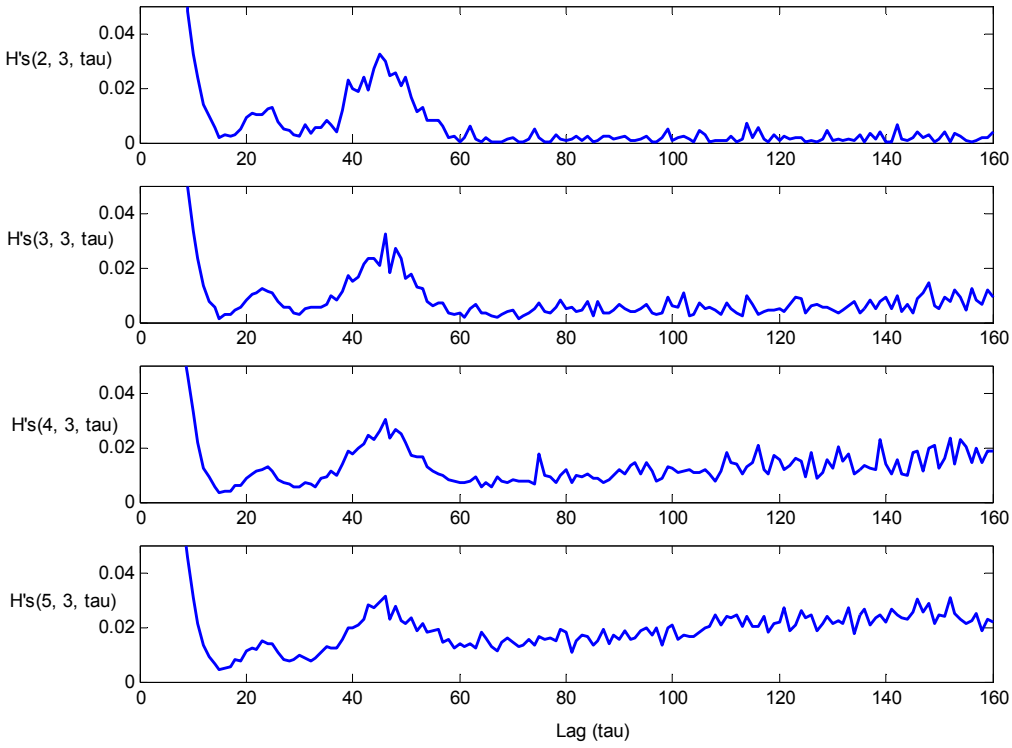


Figure 2.3 Residual Shannon entropy plot for different set sizes varying from 2 to 5, with constant sequence length of n=3 and symbolization interval τ =1 and sample = 0.001 second.

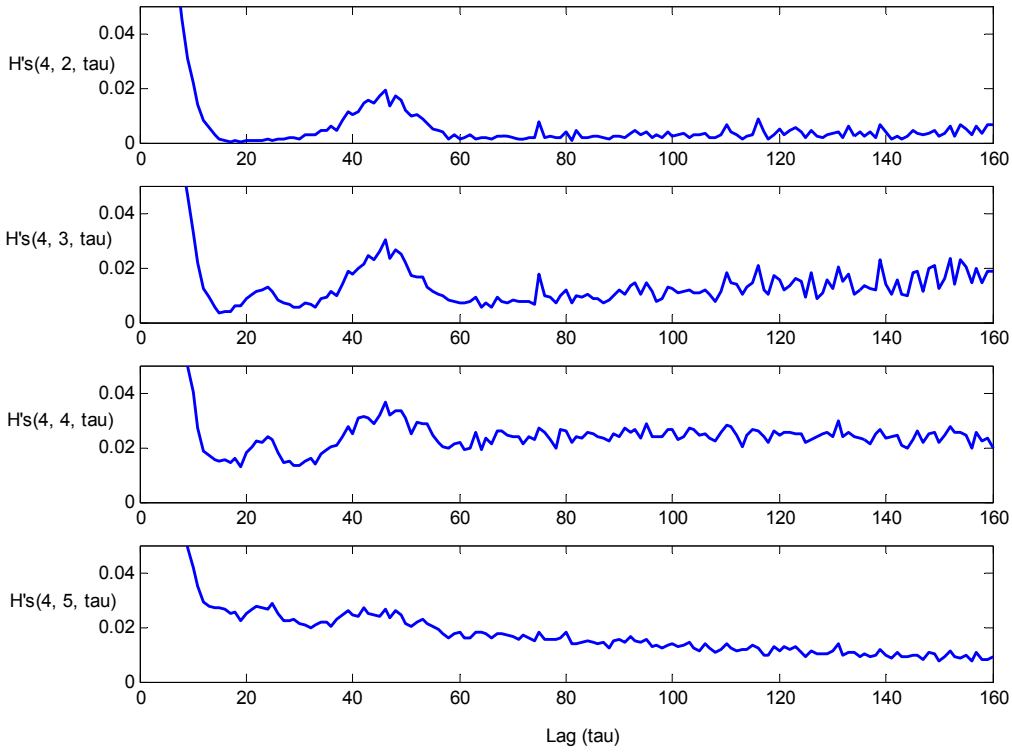


Figure 2.4 Residual Shannon entropy plot for different sequence lengths varying from 2 to 5, with constant set size of n=4 and symbolization interval τ =1 and sample = 0.001 second.

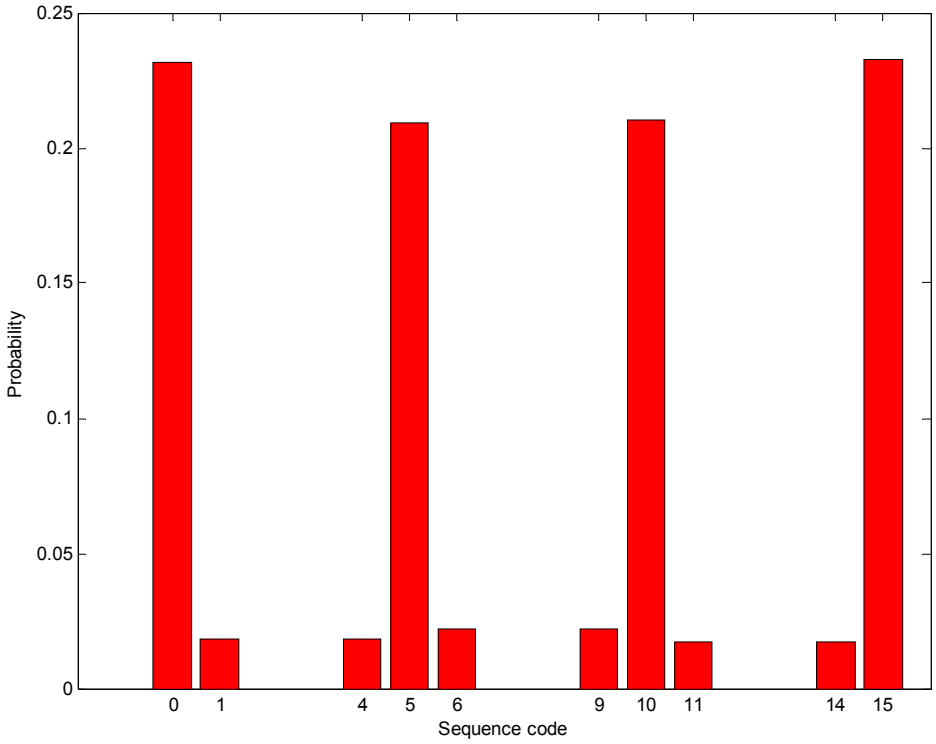


Figure 2.5 Symbol sequence histogram with symbol set size n= 4, sequence length L=2, symbolization interval τ =1 and sample = 0.001 sec.

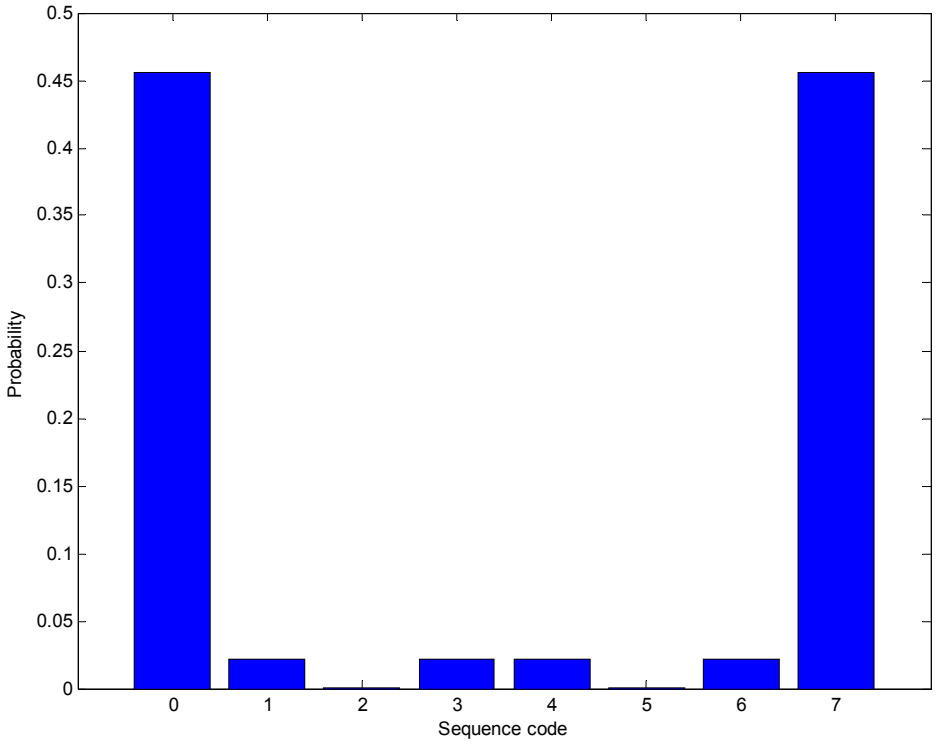


Figure 2.6 Symbol sequence histogram with symbol set size n= 2, sequence length L=3, symbolization interval τ =1 and sample = 0.001 sec.

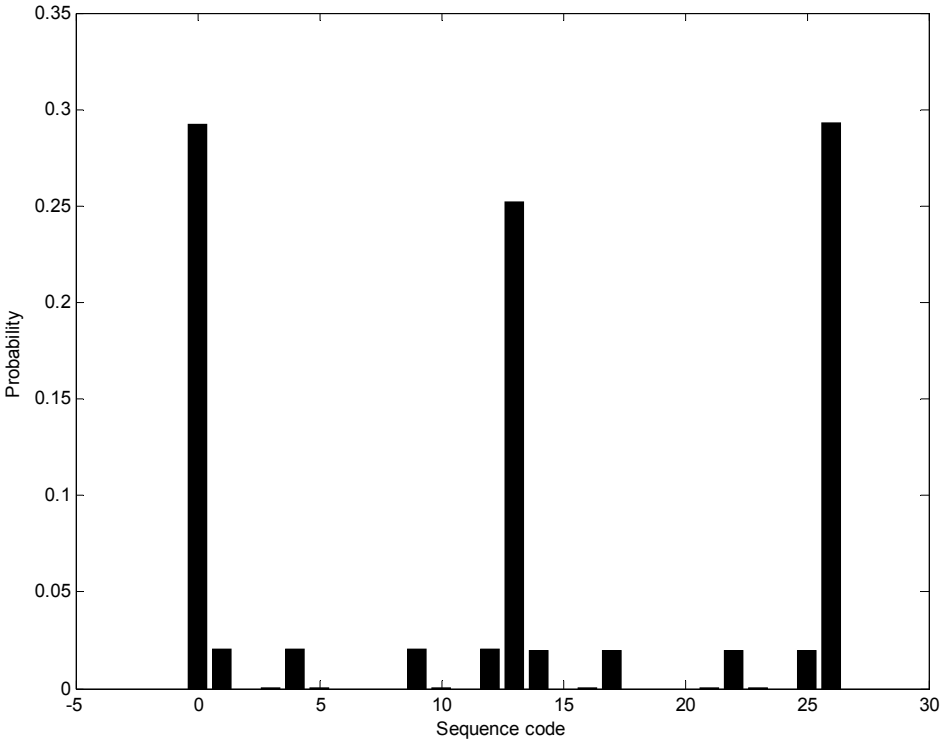


Figure 2.7 Symbol sequence histogram with symbol set size n= 3, sequence length L=3, symbolization interval τ =1 and sample = 0.001 sec.

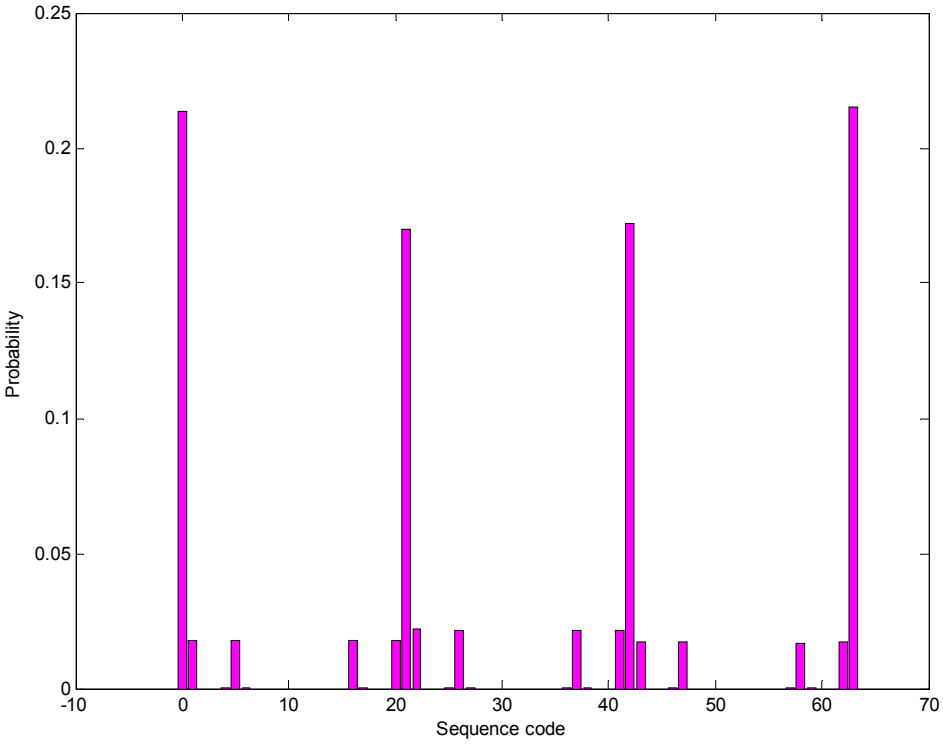


Figure 2.8 Symbol sequence histogram with symbol set size n= 4, sequence length L=3, symbolization interval τ =1 and sample = 0.001 sec.

variety of possible symbol sequence codes not just [0 0 0] or [1 1 1]. Figure 2.7 is the symbol sequence histogram for set size of 3 and sequence length of 3. There are more sequence codes in figure 2.7 and 2.8 in comparison with figure 2.5 and 2.6. Charles E. A. Finney (Nonlinear analysis expert) recommends that the number of symbol sequences be around 64 for low dimensional time series [private communication]. Figure 2.8 which has 64 symbol sequences shows several peaks indicating a variety of symbol sequence code possible with a symbolization key of set size = 4 and sequence length =3.

CHAPTER 3 EXPERIMENTAL SETUP

3.1 UNIVERSITY OF TENNESSE, KNOXVILLE DISTILLATION COLUMN SETUP

3.11 Distillation column, University of Tennessee, Knoxville (UTK)

The distillation column at the University of Tennessee, Knoxville is located in the Unit Operations Laboratory for the purpose of experimental use for the students. It consist of four trays (bottom to top) – Glitsch V-1 ballast tray (bottom), Glitsch A-1 ballast tray, bubble cap tray and a sieve tray (top). All the trays in this column are different because the column is primarily used for instructional purposes. The tray blueprints show that the sieve tray has the smallest open cross section for liquid and gas passage. Therefore it is anticipated that the sieve tray is the one that will flood as the throughput is increased in the column (private communication as per Dr. Rob Whiteley, Oklahoma State University).

Figure 3.1 shows the distillation column set up at the university's unit operations lab. It utilizes a vertical thermosiphon type reboiler with one gallon liquid capacity and can be supplied with 120 psig high pressure steam. The reboiler is a shell and tube heat exchanger with the heating material (steam) in the shell and the product to be separated (water) on the tube, see Figure 3.2. The condenser is a shell and tube heat exchanger with 15

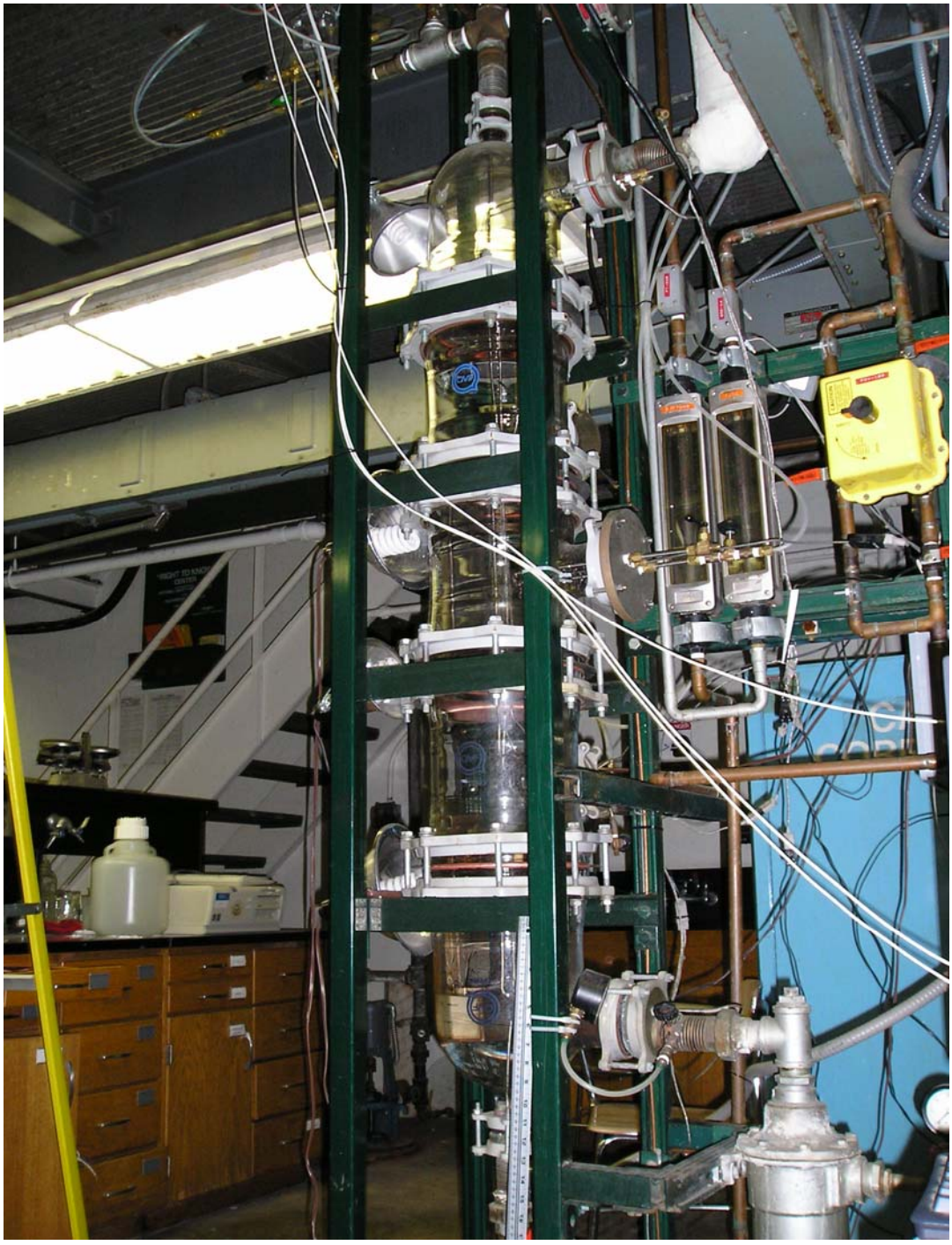


Figure 3.1 Distillation column located on first floor of unit operations lab.



Figure 3.2 Picture of the thermosiphon reboiler connected with steam on the shell side and column fluid on the tube side.

stainless steel tubes cooled by utility water, see Figure 3.3. The distillation column and the reboiler are situated on the lower floor while the condenser, product feed tanks (Figure 3.4), product storage tanks (Figure 3.4), accumulator (Figure 3.5) and the pressure sensors are on the second floor with metal grates.

3.12 Instrumentation and Human Machine Interface

The distillation column is fully instrumented and automated. Figure 3.6 shows the P&ID of the instrumentation mounted on the distillation column. The main instruments utilized while running experiments on the distillation column were the pressure sensors on the steam pressure line (PT-001 and PT-002), the steam flow control valve (FCV-301), the accumulator level indicator (ΔP-003) and the reflux control valve (FCV-109). All the final control elements (control valves, motor speed controllers, on/off valves, start/stop motors) and sensor transmitters on the distillation column are interfaced to the control and data acquisition system. The values of all IO (Inputs and Outputs) can be archived. National Instrument's LabVIEW software provides the control and data acquisition system and Human-Machine-Interface (HMI). Figure 3.7 shows a portion of the front panel of LabVIEW which was used to control and monitor the column. The steam supply pressure and the accumulator level were maintained at the set point values using the in-built PI controller function. The PI controller would send an output to the valve to



Figure 3.3 Shell and tube condenser located on the second floor of the unit operations lab.



Figure 3.4 The feed tank (left) used to feed the liquid to the reboiler and the storage tank (right) to hold the final product.

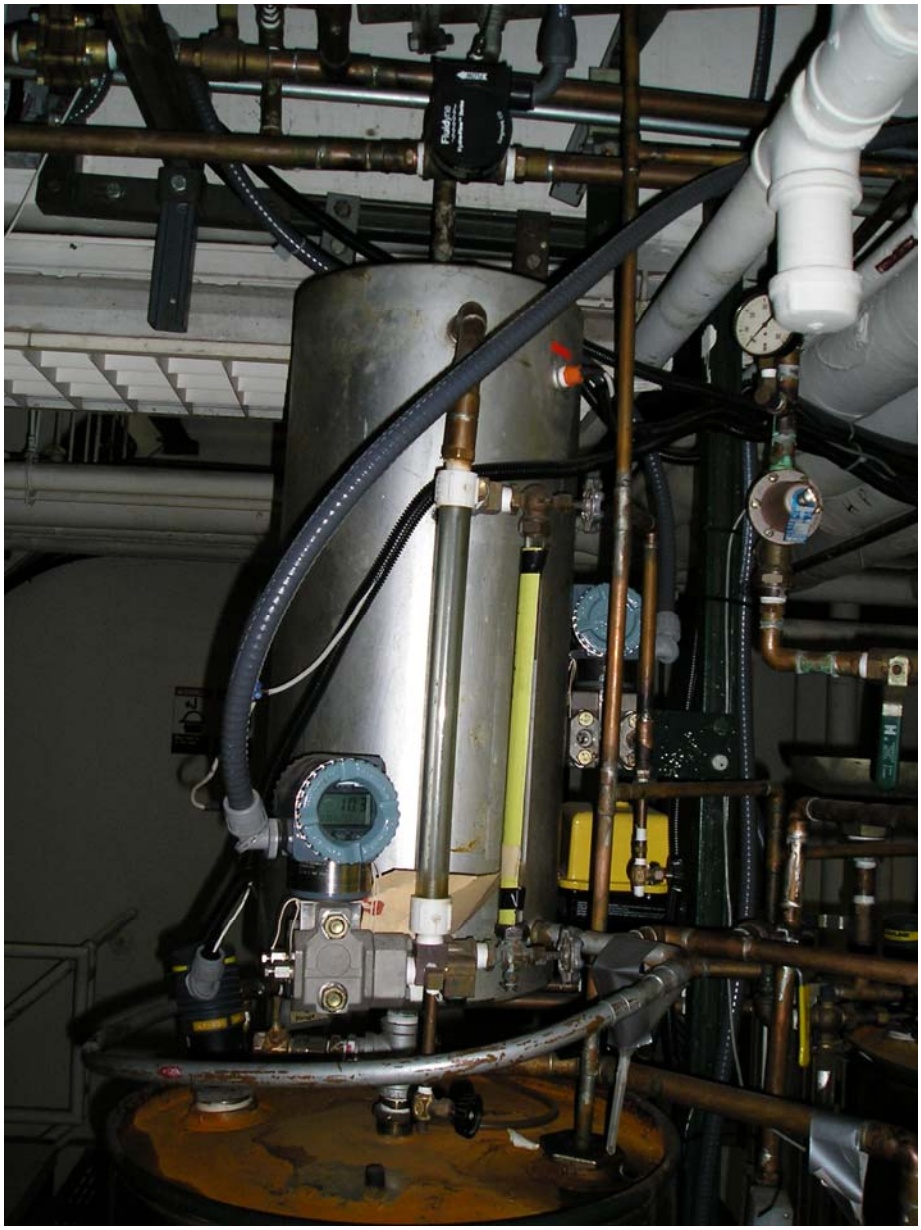


Figure 3.5 The accumulator holds the liquid which is condensed in the condenser before feeding it back in the column. The liquid can be also diverted to the storage tank or the feed tank.

PROCESS and INSTRUMENTATION DIAGRAM

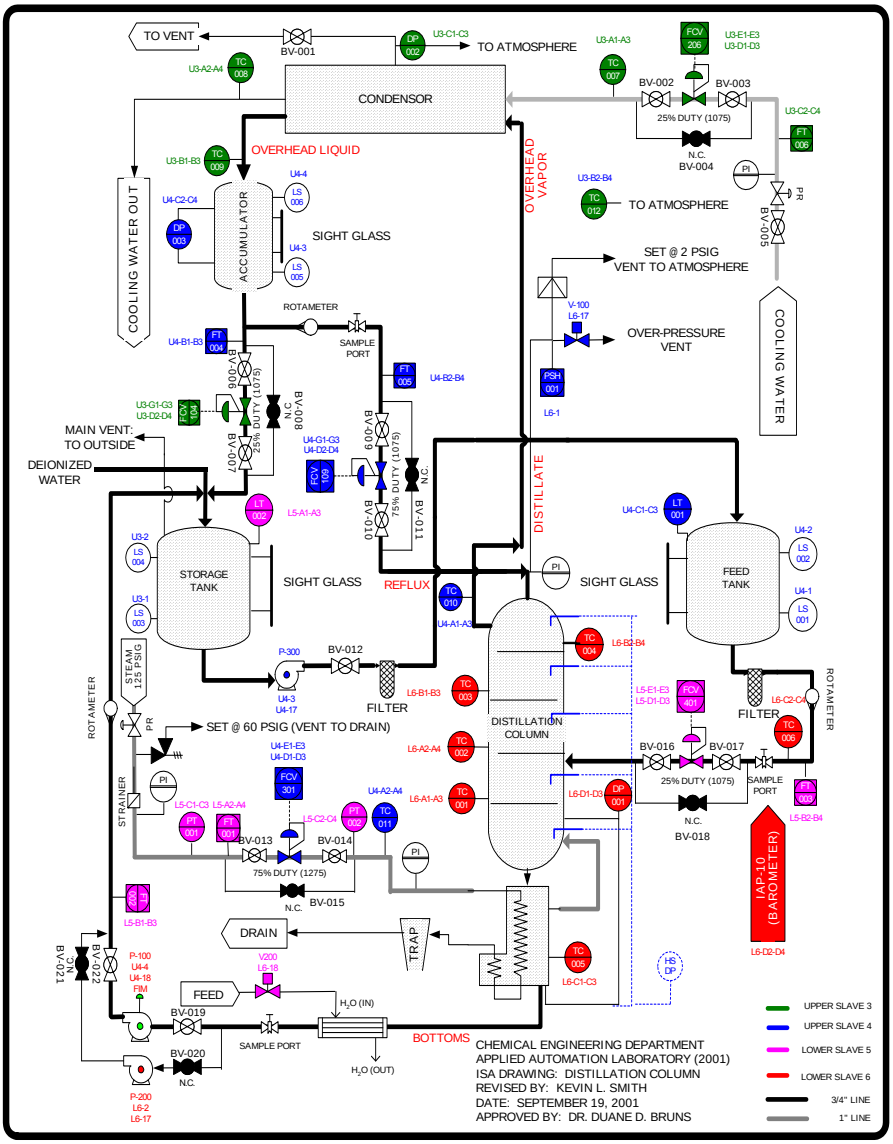


Figure 3.6 P&ID of the distillation column at University of Tennessee, Knoxville prepared by the class of ChE 447 (Applied Process Automation Laboratories) Fall 2005.

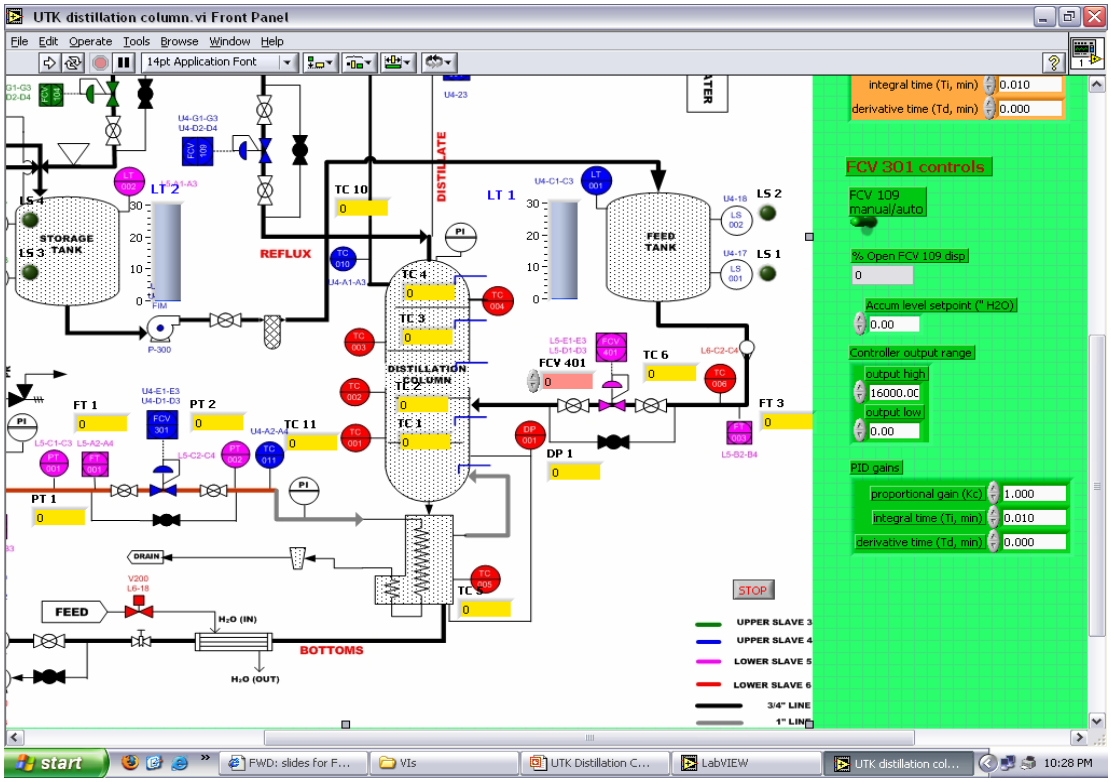


Figure 3.7 Portion of the HMI front panel from LabVIEW code that is used for controlling the instruments and collecting data on the workstation.

open or close depending on the downstream steam pressure (or the accumulator level).

3.13 Differential pressure sensor hardware and interface

The differential pressure across the selected trays is measured in the vapor space through the pressure taps located above and below each tray (see figure 3.8). A constant purge of air (approximately 15 cc/sec) using sonic flow was blown through the 1/4” plastic tubing lines to prevent vapor condensation that could cause accumulation of water in the pressure tap line or in the sensor cavity. Water in the pressure taps would cause errors in the differential pressure measurements while the sensors were rated for vapor only. The purge air was introduced in sonic flow through orifices to keep the purge air flow rate constant even though the pressure in the column and thus the pressure tap lines varies with time. This eliminated concerns that purge system dynamics would interact with the pressure dynamics being measured and analyzed. Two pressure sensors were used to measure the differential pressure – MKS Baratron Type 223 (serial # 55572 – 1A) shown in figure 3.9 and Validyne P55D (serial # 116046) shown in figure 3.10. The MKS differential pressure (ΔP) sensor requires gas contact. It has a range of 0 – 50 inches of H_2O with an output of 0 – 5 Volts DC. It claims a resolution of 1 in 10,000. Variable capacitance is used for the pressure sensing technique. A metal diaphragm defects with pressure and modulates an oscillator signal that



Figure 3.8 A pressure tap above tray 2 collection of pressure data in the vapor space above that particular tray.

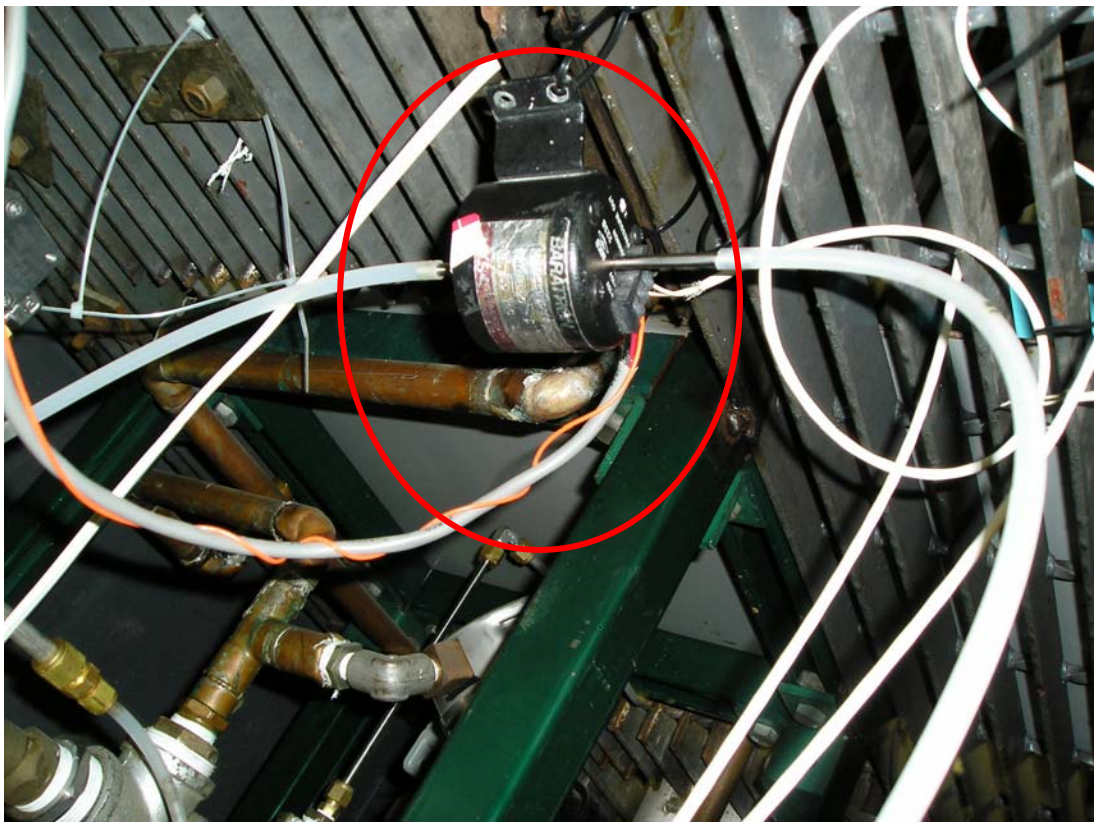


Figure 3.9 Differential pressure sensor - MKS Baratron Type 223

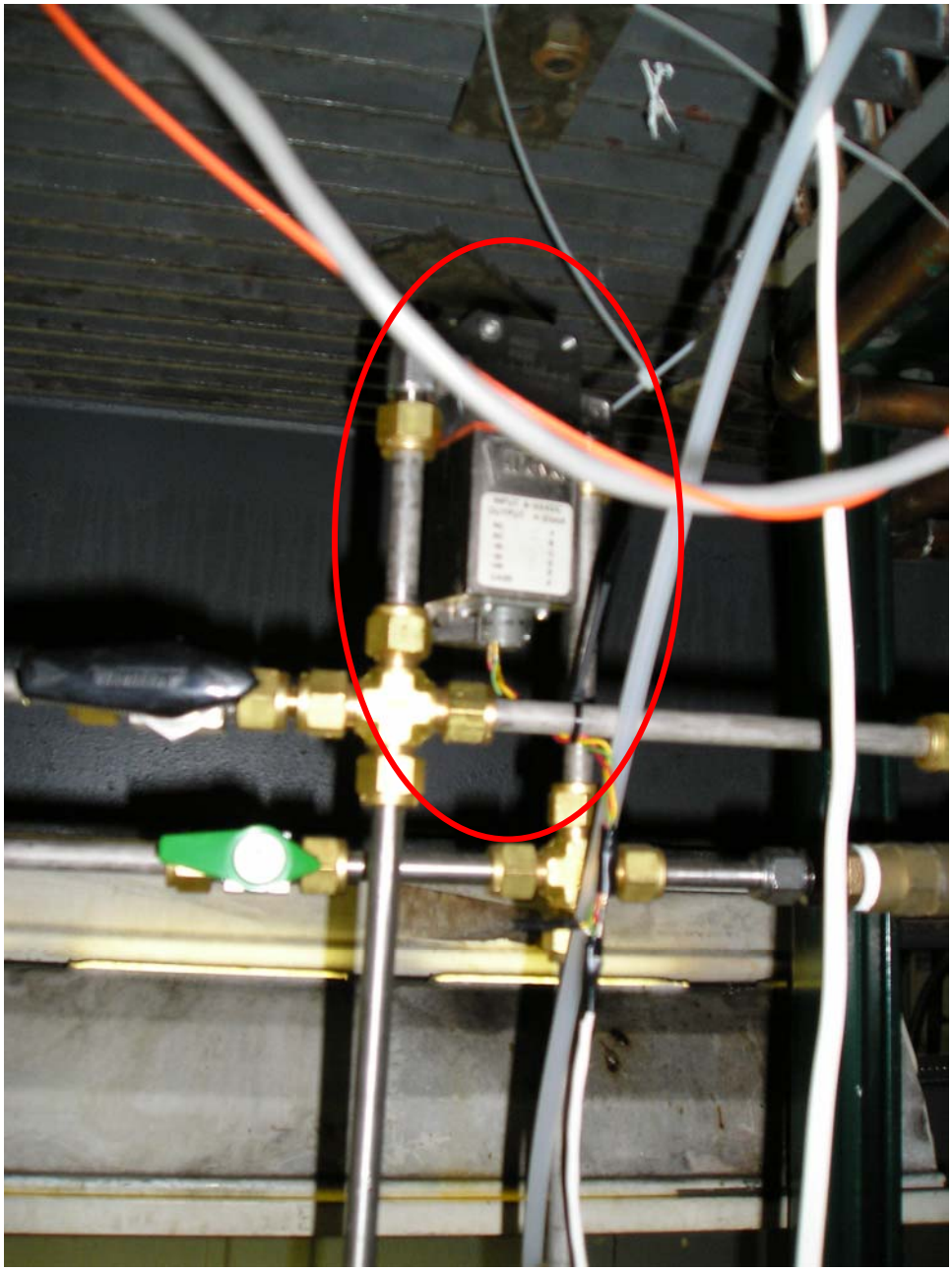


Figure 3.10 Differential pressure sensor - Validyne P55D

has a frequency of around 12,000 Hz the modulated signal is then converted into a high level (0-5 VDC) that is linear with pressure. It is considered to be capable of tracking pressure at 100 Hz.

The Validyne sensor has a range of 0 – 30 inches of H_2O with an output of 4 – 20 milliamps, which is converted to a voltage range of 1 – 5 Volts DC using a 250 Ω resistor. The Validyne sensor uses variable reluctance technology that measures the resistance to flow of magnetic flow. It is capable of tracking pressure at 100 Hz with lines filled with gas and 200 Hz when filled with liquid. The frequency observed in the time series data also depends on the plumbing response. Equation 2.7 calculates the natural frequency of plumbing as a function of sensor cavity volume and tubing dimension [33].

$$W_n = \frac{C}{L\sqrt{\frac{1}{2} + \frac{Q}{aL}}} \qquad (2.7)$$

where W_n (radians/sec) is the natural frequency, F_n (Hz)= $W_n/2\pi$ is the natural frequency, C (ft/sec) is the velocity of sound in media, a (cu ft) is the cross sectional area of tubing, Q (cu ft) is the transducer cavity volume and L (ft) is the length of tubing. The piping at UTK was ¼" plastic piping (most of the length) and stainless steel piping (at the column joints) with maximum length of 20. The FRI column set up has approximately 120 ft of copper piping. The natural frequency calculated using equation 2.7 for UTK piping is around 167 Hz which was filtered out using analog filters. The natural frequency for FRI

piping is around 14 Hz which was not filtered out from the signal. The piping at FRI was not straight and had many elbows in piping run.

The voltage output signal from the ΔP sensors was split with one branch of the signal analog band-pass filtered (0.1 Hz high pass and 100 Hz low pass) using Rockland analog filters (model #852). The filtered and the unfiltered signals are then sent to the National Instruments (NI) SCB-68 (Signal Connector Block) box where all the IO (input-output) wires carrying the pressure signals are connected. The SCB-68 is connected to the NI DAQ (Data Acquisition) card which is mounted inside the workstation. National Instruments LabVIEW software was used for the collection of data from the sensors. There were two different workstations used. The instrumentation on the distillation column communicates over Siemens Profibus. Profibus has a limited sampling rate that would not support the 1000 Hz differential pressure measurements used for hydraulic state identification. Thus one workstation was used for operating the distillation column and collecting data over the Profibus intranet. The second workstation was used for collecting the high-speed differential pressure data from the pressure sensors.

3.14 Signal Conditioning

In the analysis of time series data taken from process sensors it is important to minimize the signal to noise ratio or keep this ratio below some

acceptable value. This was done following standard wiring procedures. Our grounding procedure is to ground all instruments and wire shields at a common ground near the IO interface to the data acquisition system to avoid ground loops. Changes to the data acquisition were made until the noise level was acceptable. The data collection protocol is to always collect a set of data before the column was operating and another set taken after the column was shutdown to validate the operation of the data collection system.

Another essential requirement for collecting good time series data, especially high speed data, is to avoid aliasing in the digitized data. This requires knowledge of the sensors response capabilities, measurement techniques and natural frequencies. Our anti-aliasing procedure is to require the sensors response frequency or natural frequency to be more than twice the highest frequency of interest, the signal must be sampled more than twice the frequency of interest and the analog signal be low pass analog filtered at or below the Nyquist frequency of the sensor. When the data analysis is based only on variations with time in the data and not on the magnitude, the data was also analog high pass filtered. When an electrical signal is analog high pass filtered the DC bias (signal average) is removed.

3.15 Experimental campaigns

The purpose of these experiments was to collect high speed differential pressure data to identify hydraulic characteristics that could be used to quantify the percent flooding on a tray and to predict hydraulic flooding. This would provide the underling fundamentals for the 'hydraulic flooding sensor'. Thus the consideration of separation criteria during the experimental run was not needed and only water was used during the experimental runs.

The column was also run at total reflux. This simplified operating the column at stationary conditions. At this stage of sensor development, it is desired to the column as stationary as possible. Typically tray efficiency and pressure drop curves are evaluated in columns with standard hydrocarbon mixtures at total reflux. Once the appropriate time scales are identified and analysis procedures developed for hydraulic state identification needed for the flooding sensor, future work should involve sensor evaluation under more transient conditions.

There were many runs made before the final data was collected. Some of the significant events along the way were learning about thermosiphon surge and correcting the design of a down comer. Initially the inlet valve to the thermosiphon was set fully open. This caused the thermosiphon to surge

during operation. The tubes in the thermosiphon contained too much water and as steam was formed it blew out slugs of water. This slugging or ‘surge’ occurred at a nearly constant rate of about 1 Hz that was a weak function of steam pressure. The surge caused the pressure in the column to vary by approximately 5 inches of water, and dominated the time series. This is probably a chaotic process. The thermosiphon was then operated by setting the thermosiphon valve so that a fine spray entered the column and caused no or very little pressure variations. It was then important to adjust this valve as the reboiler steam pressure was increased and guard against the heat exchanger going dry.

Bubbles from the bubble cap next to the down comer from the sieve tray went directly into the down comer. This provided a mechanism for flooding that should never occur in a correctly designed column. Downcomer flooding occurs when the pressure drop provided by the liquid in the downcomer is less than the differential across the tray so the vapor flow switches to going up through the downcomer instead of through the tray. During a visit to the project by Dr. Whiteley, it was decided to correct this problem by putting a vertical shield next to the bubble cap to block the bubbles that were going directly into the down comer.

High speed pressure data was only collected across the sieve tray (tray # 4) and the bubble cap tray (tray # 3) for the final experimental campaigns where good quality data was collected. The last campaign carried out on November 16, 2006 was conducted with the Validyne sensor

measuring ΔP across tray 4 and MKS sensor measuring ΔP across tray 3 with taps of minimum length to avoid resonance. The taps were around 2 feet with stainless steel tubing of inside diameter of ¼". The taps on MKS sensor were of polyethylene plastic tubing with ¼" inside diameter with approximately the same length of taps as of Validyne sensor.

For the experimental campaigns on September 18, October 02 and October 03, 2006, pressure data was only collected across tray 4. During these runs, the length of the polyethylene taps on the MKS sensor were around 20 ft. Tray 4 is the tray that floods during an experimental run as it has the smallest cross section for liquid and gas flow; therefore the data collected across tray 4 is the most important.

Before starting the column the water level in the reboiler is set between 5 and 8 inches and the accumulator water level is checked to see how it compares to the typical set point of 10 inches. The nitrogen purge is turned on and flowing through the pressure taps to the differential pressure sensors. A set of 'base or reference' data is collected from the sensor(s). This data provides partial validation of the data collection system. The differential pressure signals should read close to zero and contain little noise especially 60 Hz from the 120 or 240 VAC at 60 Hz in the lab. All the connections on the pipes are checked for leaks and tightened if needed. After finishing the initial leak test and the collection of base data, the column startup procedure is followed

Column startup procedure

1. The product flow control valve (FCV-104) is closed from the HMI so the column will operate in total reflux.
2. Air purge established through the pressure taps by setting the nitrogen regulator at 45 psig.
3. Base differential pressure data is collected.
4. If the water level in the accumulator is high, the reflux flow control valve (FCV-109) is opened in manual mode from the HMI until the level (ΔP-003) is about 1 inch above the desired set point (typically 10 inches) and then the reflux valve is closed. If the water level in the accumulator is low, it is known that some column inventory will be needed to fill the accumulator during column startup.
5. Water level in reboiler is maintained by visual inspection of the water level. If additional water is needed quickly, it is added through the feed line entering on tray 2. If the accumulator height is above the desired height, water can be added from the accumulator.
6. Water flow to condenser is started with a constant flow rate. The flow rate of the water flowing through the condenser is not controlled during the experiment. The flow rate is set manually so that the temperature difference across the condenser is about15 °F.
7. The main supply ball valve on the steam line is manually opened.
8. The steam regulator is manually set at 60 psig.
9. The reboiler PI (proportional integral) controller is put into automatic and 10 psig entered as the set-point. The measured or controlled variable for

this loop is the steam pressure in the reboiler (PT-102). The controller manipulates the steam flow control valve (FCV-301) on the steam line to maintain the reboiler pressure.

10. After the column has run with the steam pressure at 10 psig for roughly 10 minutes, the reboiler steam pressure is slowly ramped over approximately 4 minutes to the steam pressure where the first set of differential pressure data is to be collected.
11. Once there is some overhead condensate the accumulator level is watched by the operator. When the accumulator level (ΔP-003) rises about 2 inches above the desired set-point, the accumulator PI controller is set to auto mode to control the level in the accumulator and the set point to 10 inches.
12. The reboiler level is adjusted as needed as some of the column inventory is now on the trays and some of the inventory may have been used to get the accumulator level to set-point. Liquid is added slowly through the feed valve which is otherwise off.
13. The column is allowed to reach stationarity. When the reboiler level and the accumulator level variations are minimum but not constant, the column is considered to be at stationary state.

The HMI allows most of the startup to be completed through the automation system. The steam pressure in the reboiler and the accumulator level are controlled using built-in PI controllers in LabVIEW software. Two people are required to be in the lab when any equipment is operated for

safety. The column can now be operated by one person leaving the second person free to observe the behavior on the trays, monitor the time series displayed on the second workstation and collect video of the column.

Once stationarity is established a set of data is collected across the selected tray(s). The reboiler pressure is increased in increments of 0.5-5 psig depending on whether the column is close to the flooding state. After each reboiler pressure increase the reboiler level is adjusted if needed and the column is allowed to reach a stationary state (when the level in the reboiler and the accumulator approximately remain constant) and a set of data is collected.

The data set consist of a time series collected at a frequency of 1000 Hz for duration of 60 seconds. The date set was collected at frequency of 1000 Hz to capture all the frequencies that might be occurring due to the bubbling phenomenon and also prevent anti-aliasing using a low pass analog filter with the low pass frequency one half or less than sampling frequency. A typical data set would consist of 60 seconds of differential pressure data and not show any trend in the average of the data. The length of the data set might vary according to the necessity of the experiment. As the column gets close to the flooding state, the program is set to collect continuous data from the pressure sensor(s). As the column approaches flooding, tray 4 gets loaded with liquid.

A point is reached when the liquid seal in the downcomer from tray 4 to tray 3 that prevents the vapors from flowing up through the downcomer

breaks. Then the high gas flow through downcomer acts like a vacuum cleaner and all the liquid from tray 3 gets sucked up onto tray 4. Once gas break through occurs all of the liquid on tray 3 is remove in roughly a second. At this point the column is considered 100% flooded and the efficiency of the column has decreased drastically. After approximately 30 seconds of flooding data is collected, then column reboiler steam pressure is decreased to 15 psig. Excess liquid drops from tray 4 onto tray 3 and lower trays and the column recovers. A set of post flooding data set is collected roughly after 2 minutes after recovery with the reboiler pressure at 15 psig.

3.2 FRACTIONAL RESEARCH, INC. (FRI), FACILITY STILLWATER, OKLAHOMA

A joint project with Professor James “Rob” Whitely in the Chemical Engineering Department at Oklahoma State University (OSU), Fractionation Research, Incorporated, (FRI) and this research work allowed a limited amount of data to be acquired from an industrial scale tray distillation column with 4 and 8 foot diameters. Funding was provided by FRI as a Measurement and Control Engineering Center project. FRI also provided significant in-kind support by purchasing all equipment, instrumentation, and wiring runs of 1200 feet needed at their field site to collect the high speed differential pressure data. FRI also provided personnel to install and assist in the data collection.

Fractionation Research, Inc. (www.fri.org) is a non-profit facility located in Stillwater, Oklahoma on the edge of OSU campus. The facility is supported by petroleum and chemical member companies from all over the world. The facility strictly runs commercial scale experiments with hydrocarbons systems with pressure ranging from deep vacuum to 400psia. The FRI experimental facility has two commercial size distillation columns with their supporting equipment (see figure 3.11). Each column can run independently or as a two-column system. Both the columns are closed-system design used for studying the efficiency and capacity of a given tray or packing.

The high pressure column measures 48 inches in diameter and has a height of 31 feet. The high pressure column can withstand 525 psig to full vacuum at 400 deg F. The low pressure column consists of two independent constructed sections joined together. The lower section is 48” in diameter and has a height of 27’-6”. The upper section is 22’ in height with a 12’ middle section and 96” diameter tapering to 48” at the end. The design pressure for low pressure column is 175 psig to full vacuum at 350 deg F. The columns will accommodate up to ten trays at 24” spacing or 18’ of packing [18].

The FRI data that is presented in this thesis is from an experiment carried out on the low pressure column. The data was collected on December 15, 2005. The low pressure column was installed with proprietary trays which were to be analyzed by the FRI engineers for efficiency curves, capacity to flooding and differential pressure



Figure 3.11 Picture of the FRI distillation column building

drop. The column operating pressure was 150 psig. The distance between the pressure drop taps was 112” which contained 4 trays. The differential pressure was measured using the Validyne P55D (serial # 116046, 0 to 30 inches of water) sensor. The data acquisition system for collection of 1000 Hz pressure data was similar to the one at UTK (refer section 3.13). A major difference was the differential pressure was measured across 4 trays.

The experiments are carried out according to the requirements of the company which is testing their trays. This information is confidential; therefore most details are not available to the public. The differential pressure time series data with some notations on operation state (startup, increasing reboiler pressure, etc.) are basically the all of the information available from the experimental run.

CHAPTER 4 DATA ANALYSIS

The objective of this research was to develop novel sensor technique to detect and predict hydraulic flooding in distillation columns. The first step was collecting high frequency (1000 Hz) differential pressure data across a selected tray or trays in the distillation columns at UTK and FRI. Predicting the flooding state in the distillation column at UTK was achieved by analyzing the time series of differential pressure using linear and non-linear techniques. Mean, standard deviation, power spectral density and autocorrelation of the time series were calculated for linear analysis. Shannon entropy and mutual information plots using symbolized time series data were calculated for non-linear analysis. Autocorrelation, Shannon entropy and mutual information are calculated using Non-Linear Time Series Analysis Software® developed by collaboration of UTK, MCEC and ORNL. The result section discusses data collected from one of the experimental runs at FRI and UTK.

4.1 CHOICE OF TIME SERIES SEGMENTS

The differential pressure time series data was usually collected when the distillation column was at a stationary state. This was determined by carefully observing the level in the reboiler and the accumulator as detailed in section 3.15. In this analysis the main emphasis is on the trend of the autocorrelation, mutual information and residual Shannon entropy plots at stationary states as a function of reboiler steam pressure. After the time

series data were collected on the workstation, the time series for each reboiler steam pressure was visually inspected stationarity. A necessary condition for stationarity is that the time series mean and standard deviation are nearly constant with time. The time series also were inspected by calculating the mean and standard deviation with a moving window. Any signals not meeting the mean and standard deviation condition are flagged.

Figure 4.1 shows time series segments of 19 seconds extracted from a continuous time series of differential pressure measured across the trays in the distillation column at FRI. Segments 1, 2 and 3 are low-pass filtered at 100 Hz. These data are used to calculate the average pressure to give an indication of column throughput. An increase in average pressure drop across the trays indicates an increased throughput. Segment 1 in figure 4.1 does not posses any trend in the data. Segment 2 has an increasing trend whereas segment 3 has a decreasing trend. The time series below the segments are band-pass filtered versions with 0.1 Hz high pass and 100 Hz low pass. The high pass filter removes the local signal average (DC bias) and thus helps in removing the trend from the data.

Figure 4.2 shows the effect of a trend in the time series on the mutual information plot. The time series segments 2 and 3 with trend in the data have higher mutual information values than segment 1. The mutual information plots for both the unfiltered and filtered time series segment 1 with no trend (time series appears stationary) are similar. The mutual information curve for the band-pass filtered time series with a trend (segments 2 and 3) are lower

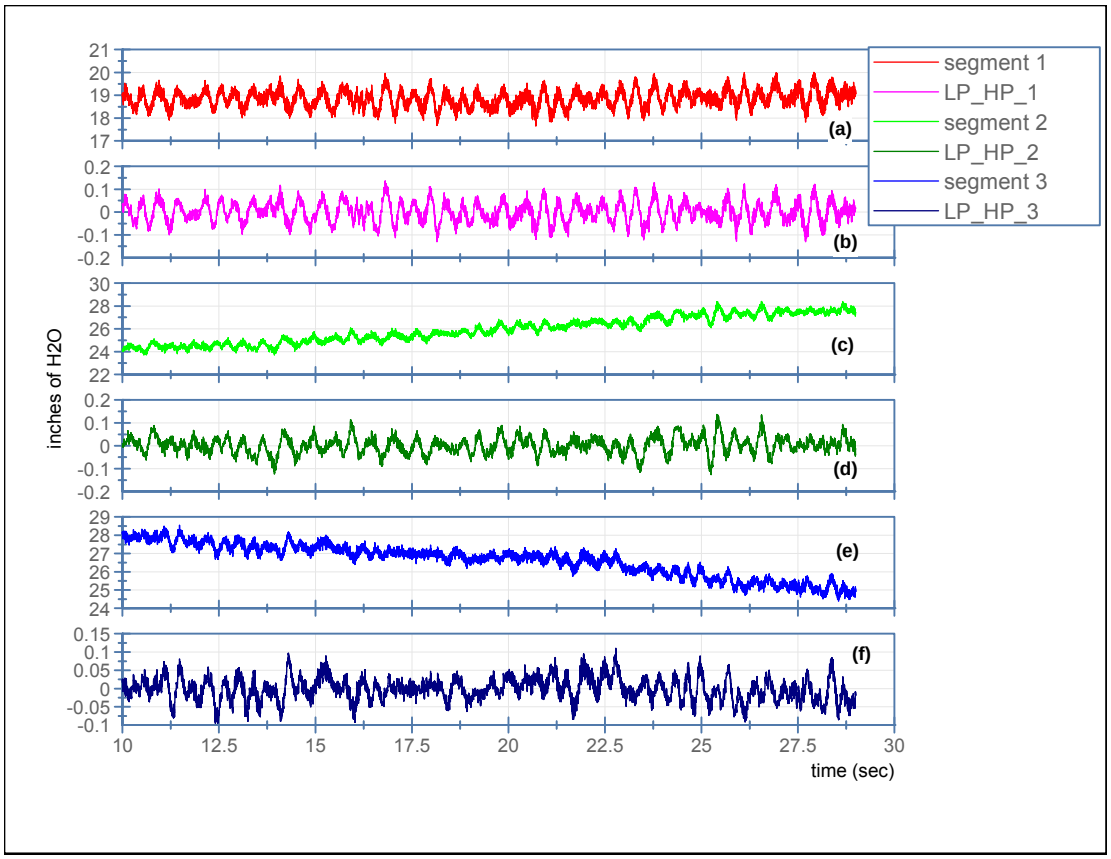


Figure 4.1 Three different segments extracted from a continuous time series raw signal and bandpass filtered.

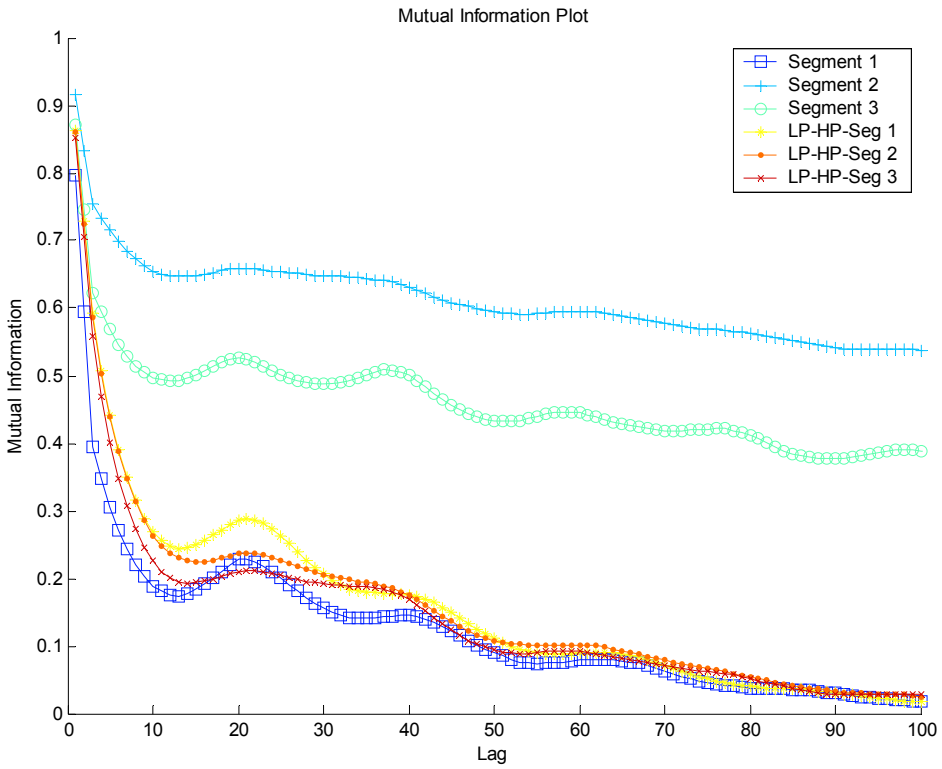


Figure 4.2 Mutual information plots for the time series segments from figure 4.1.

than the non-filtered segments and closer to the filtered segment 1. This indicates that band-pass filtering helps in removing trends and preventing one from incorrect conclusions due to the presence of trend. This is an important issue in application of the new sensor in an industrial environment and is presented as a topic for future research.

There are several tests for quantifying the stationarity of a time series. Stationarity of time series is a research area within itself. For present purposes we tested the time series for stationarity with a necessary but not sufficient requirement that a time series is considered stationary if the mean and the variance remain constant for an appropriate window length throughout the time series. Figure 4.3 shows the running mean of time series segments 1 and 2. The mean and the error bars (standard deviation) are calculated from non-overlapping segments of 2048 points in the time series. There is not much variation in the mean for segment 1 and it remains within all the standard errors bars, but the mean for segment 2 increases as the time series progresses and does not stay within all the standard error bars. This test confirms our visual feeling for the stationarity of a time series and provides a simple quantitative procedure for flagging non-stationary time series.

In chaotic systems, it is possible for a parameter to drift without noticeable change in mean and the standard deviation. Checking mean and standard deviation is a test for weak stationarity. Refer to Kantz and Schreiber [19] suggestions for more in depth stationarity analysis on chaotic and nonlinear

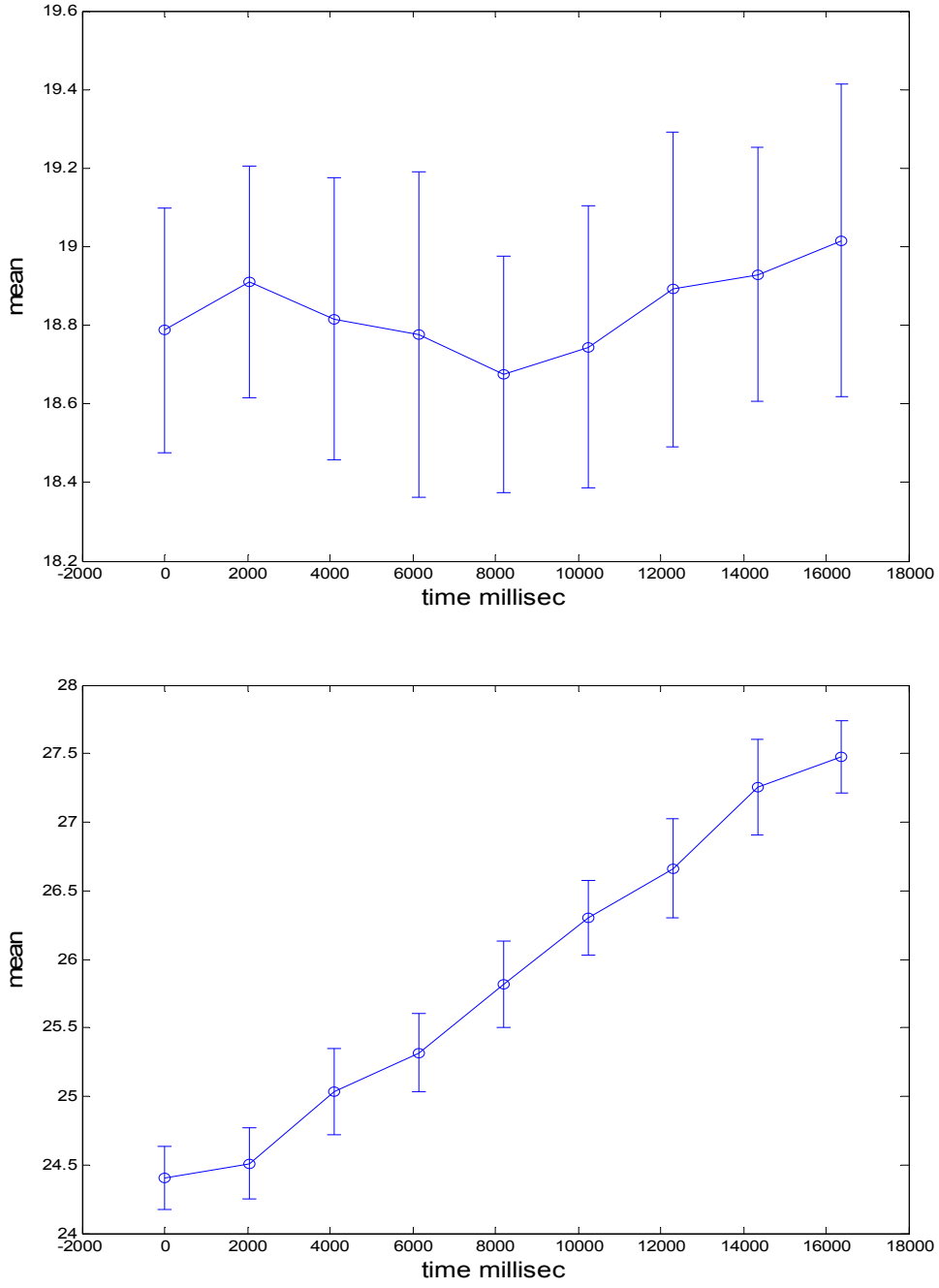


Figure 4.3 Running mean for non-overlapping segments of 2.048 sec (2048 points) for time series segments 1 and 2 from figure 4.1

time series. Running mean and variance plots for the UTK data are included in the appendices.

4.2 ANALYSIS OF TIME SERIES DATA

4.2.1 UTK distillation column data

The results that are presented and discussed in this section are for the experimental run conducted at UTK on November 16, 2006. There was no separation done in the column as it was run with water at total reflux. Water was the only liquid used for these experiments. Two differential pressure (ΔP) time series were measured one across tray 3, the bubble cap, with MKS sensor; and another across tray 4, the sieve tray, with the Validyne sensor during this run. The length of the time series was generally 60 seconds, except when the column was close to flooding and there was no way of predicting when the column would flood then data was collected continuously until the column flooded.

4.2.1.1 Mean and standard deviation

Figure 4.4 shows the mean and standard deviation for the differential pressure time series measured across tray 3, the bubble cap tray with increasing throughput caused by increasing reboiler pressure. The mean ΔP across tray 3 increases from 1.1 to over 1.6 inches of water as the reboiler steam pressure is increased from 10 to near 30 psig. The mean suddenly drops to 0.64 inches of H_2O at 31.02 psig steam pressure. This is

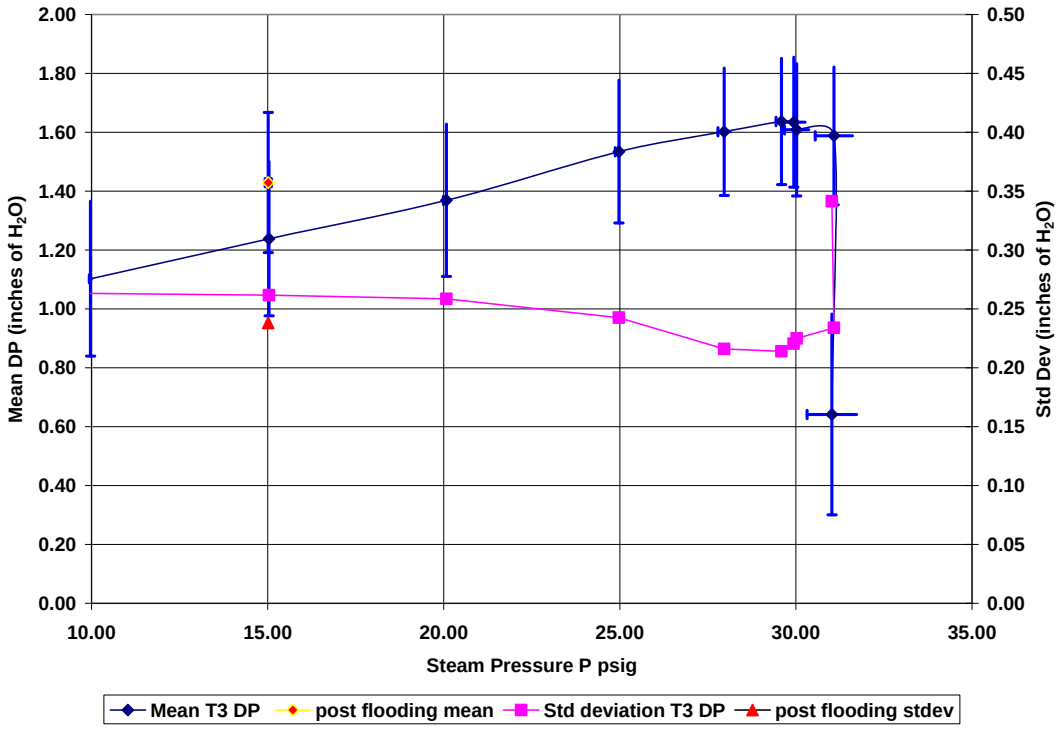


Figure 4.4 Mean and standard deviation vs. reboiler steam pressure plot for tray 3 differential pressure data.

due to flooding in the column. The liquid on tray 3 gets evacuated up through the downcomer to tray 4 when the liquid seal is broken between tray 3 and tray 4. The standard deviation of the time series decreases from 0.27 to 0.22 as the reboiler steam pressure is increased until the column approaches flooding near 29 psig reboiler pressure, then the standard deviation increases slightly to 0.24. After the column is flooded the standard deviation jumps to 0.34. The mean for post-flooding data is higher than the pre-flooding data at the same reboiler pressure. Standard deviation for post-flooding data is lower than pre-flooding data at the same steam pressure. This is maybe due to the column not being stationary as the post-flooding data was taken as soon as liquid was recovered on both tray 3 and 4. The mean bar test for all time series segments is presented in Appendix D. Both of these time series at 15 psig appear very stationary according to this test. This indicates that extra liquid was built up in the top of the tower while it was in a flooded state. When the pressure was drastically reduced from about 30 to 15 psig to drop liquid from the flooded tray 4 to the dry tray 3 and trays below, and the column operation was recovered, there still was an excess inventory in the upper part of the column.

Figure 4.5 shows the mean and standard deviation data for the time series data measured across tray 4 (sieve tray). The mean ΔP across tray 4 has similar characteristics as those across tray3. It increases from 2.8 to 11 inches of water as reboiler steam pressure is increased from 10 to 30 psig. The mean ΔP suddenly drops to 4.08 inches of H_2O at 31.02 psig (flooding).

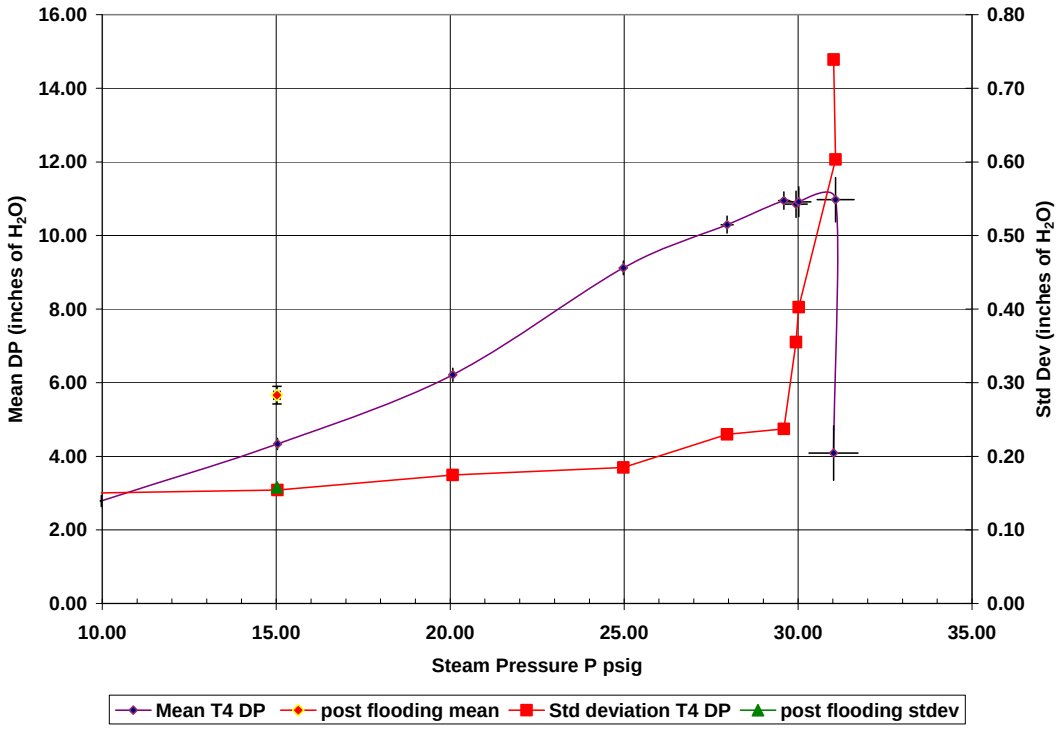


Figure 4.5 Mean and standard deviation vs. reboiler steam pressure plot for tray 4 differential pressure data.

However, the standard deviation of the ΔP across tray 3 and across tray 4 exhibit different trends. The time series standard deviation across tray 4 increases as the reboiler steam pressure is increased. As the reboiler pressure is increased above 29.5 psig, standard deviation increases more rapidly. The post-flooding mean ΔP is higher than pre flooding but standard deviation of the post and pre-flooding data is nearly the same.

The mean ΔP behavior exhibited by these 2 trays illustrates the often noted operation procedure used in industry of constraining the ΔP across the whole column or sections of the column. Often industrial columns are pushed to flooding during tests to “finger print” a column. Part of the finger print would be ΔP measurements [23]. The finger print is then used to constrain the column throughput.

4.2.1.2 FFT analysis - UTK data

Bubble cap, Tray 3

The FFT plots are calculated and created using National Instruments (NI) DIADEM software (version 9). FFT plots are calculated using an interval length of 2048 points with 25% overlap. Figure 4.6 and 4.7 are FFT plots for tray 3 (bubble cap) for reboiler steam pressure range of 0 to 31.02 psig. The column flooded at 31.02 psig. Frequency peaks or bands of peaks are observed around 0.5 Hz, 5-15 Hz and 32 Hz for tray 3 data in figures 4.6 and 4.7 as the reboiler pressure is increased from 0 to 30 psig. Flooding data has the maximum magnitude for the frequency peaks observed at 0.5 Hz, 5-15 Hz

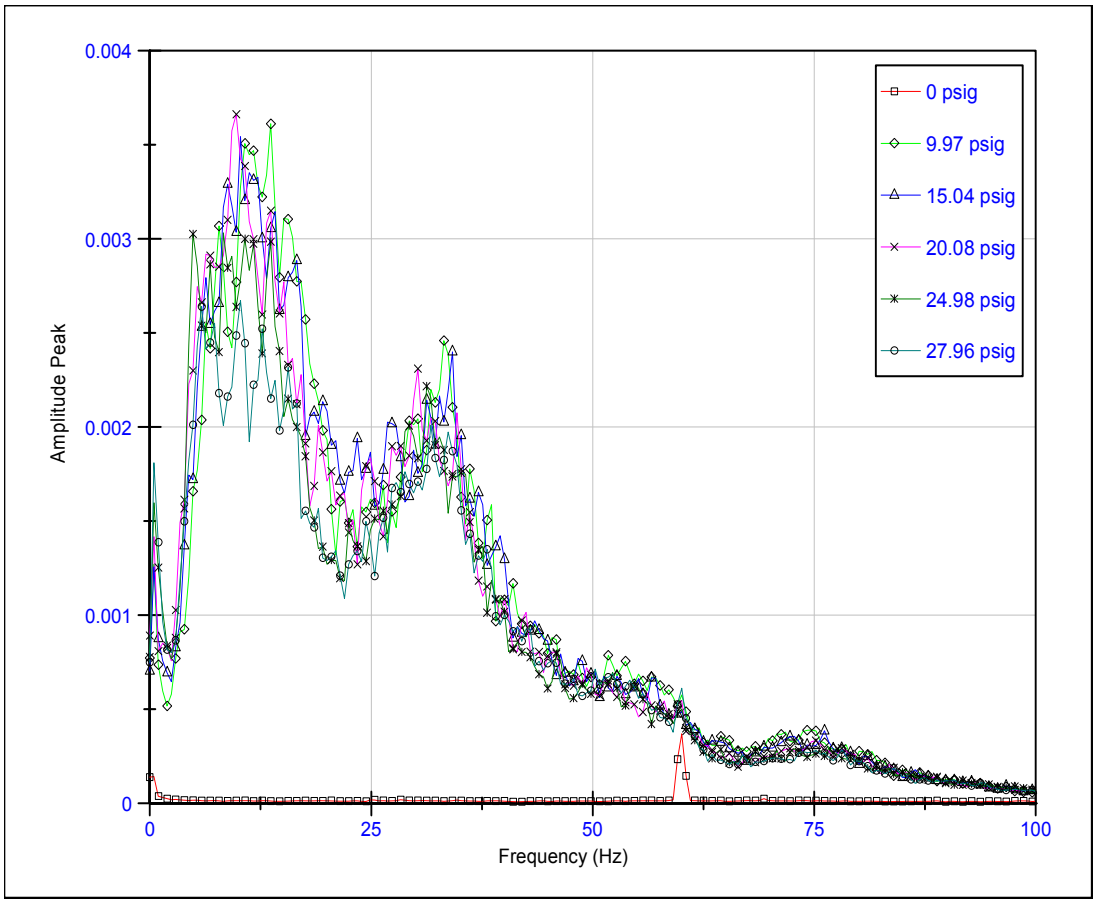


Figure 4.6 FFT plot of differential pressure data collected across tray 3 for reboiler pressure range of 0 to 27.96 psig.

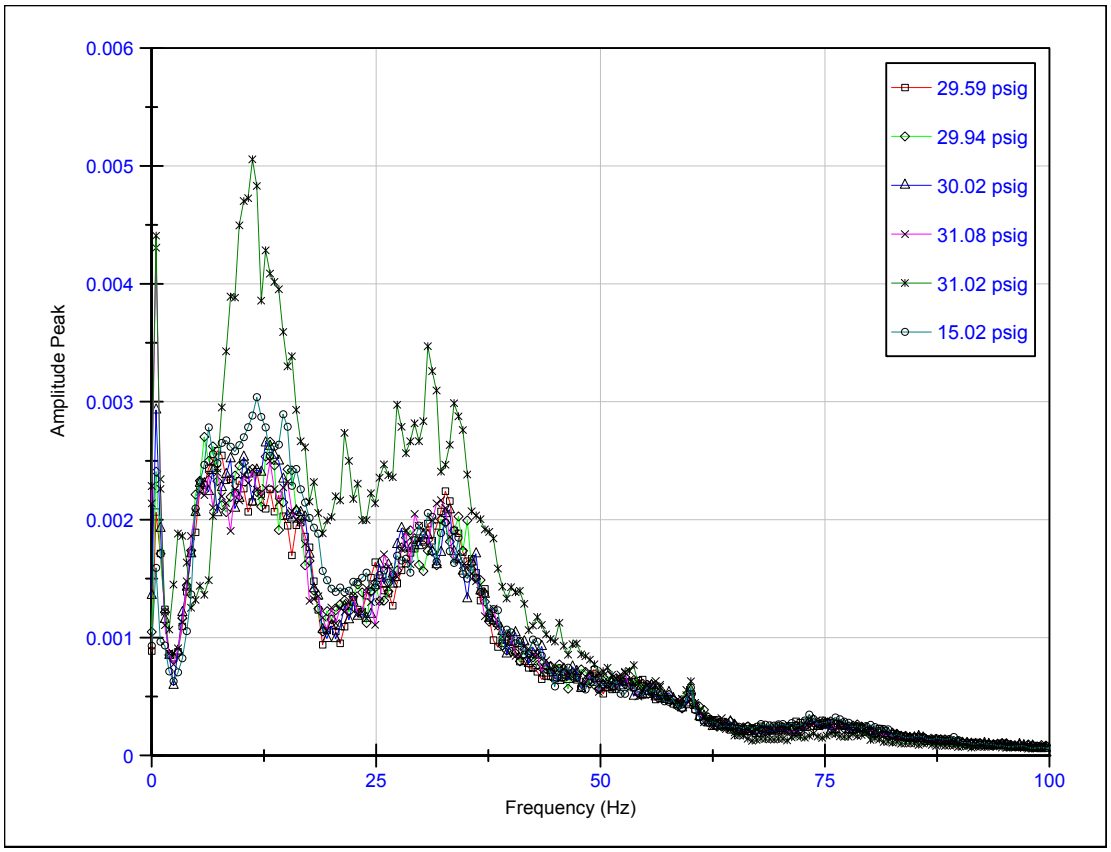


Figure 4.7 FFT plot (frequency 0 to 100 Hz) of differential pressure data collected across tray 3 for reboiler pressure range of 29.59 to 31.02 psig (flooded) and15.02 psig (post flooding).

and 32 Hz. Figure 4.8 shows the broader pictures of peaks between 5 and 15 Hz. A small noise peak at 60 Hz is observed in FFT plot for base data (0 psig) in figure 4.6. The 60 Hz noise causes a peak in all other time series in figure 4.6 and 4.7. In comparison the FFT plots for the sieve tray, tray 4, shown in figure 4.12 is clean at 60 Hz. Figure 4.10 and 4.11 shows the peak at 0.5 Hz. The magnitude of the peak at 0.5 Hz increases as the steam pressure in the reboiler increases. After the column is flooded, the magnitude of the FFT for the post flooding data decreases back to the magnitude of the FFT for the pre flooding data. It is tenuous to identify the hydraulic state from the FFT plots for the bubble cap tray.

Sieve plate, Tray 4

Figure 4.12 through 4.15 shows the FFT plots for ΔP time series collected across tray 4. The magnitude of the 0.5 Hz peak is higher than other peaks in the FFT plots. Figure 4.13 shows the FFT plot for the flooding time series data at 31.02 psig. The magnitude of the frequency curve for the flooding data is higher than pre flooding data and frequency peaks are observed at 0.5, 3

and 10 Hz. Fig. 4.14 of thesis show all of the power is around 5 Hz until the pressure reaches about 20 psig and then some of the power shifts to around 0.5 Hz. There is a broad extending from 5 Hz out to 17 Hz. All signals have a broad peak around 32 Hz of the same magnitude. FFT plots in figures 4.14 and 4.15 shows that the magnitude of the peak at 0.5 Hz increases as the reboiler steam pressure is increased.

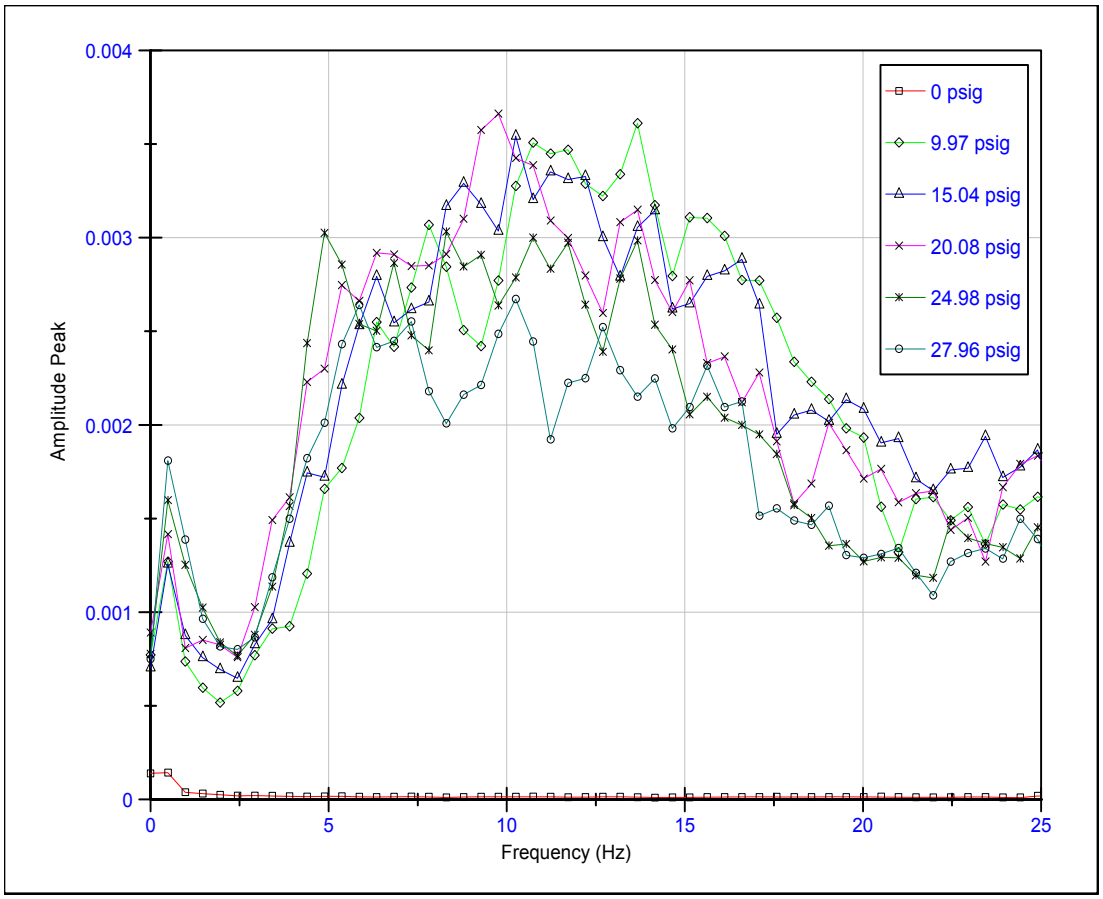


Figure 4.8 FFT plot (frequency 0 to 25 Hz) of differential pressure data collected across tray 3 for reboiler pressure range of 0 to 27.96 psig.

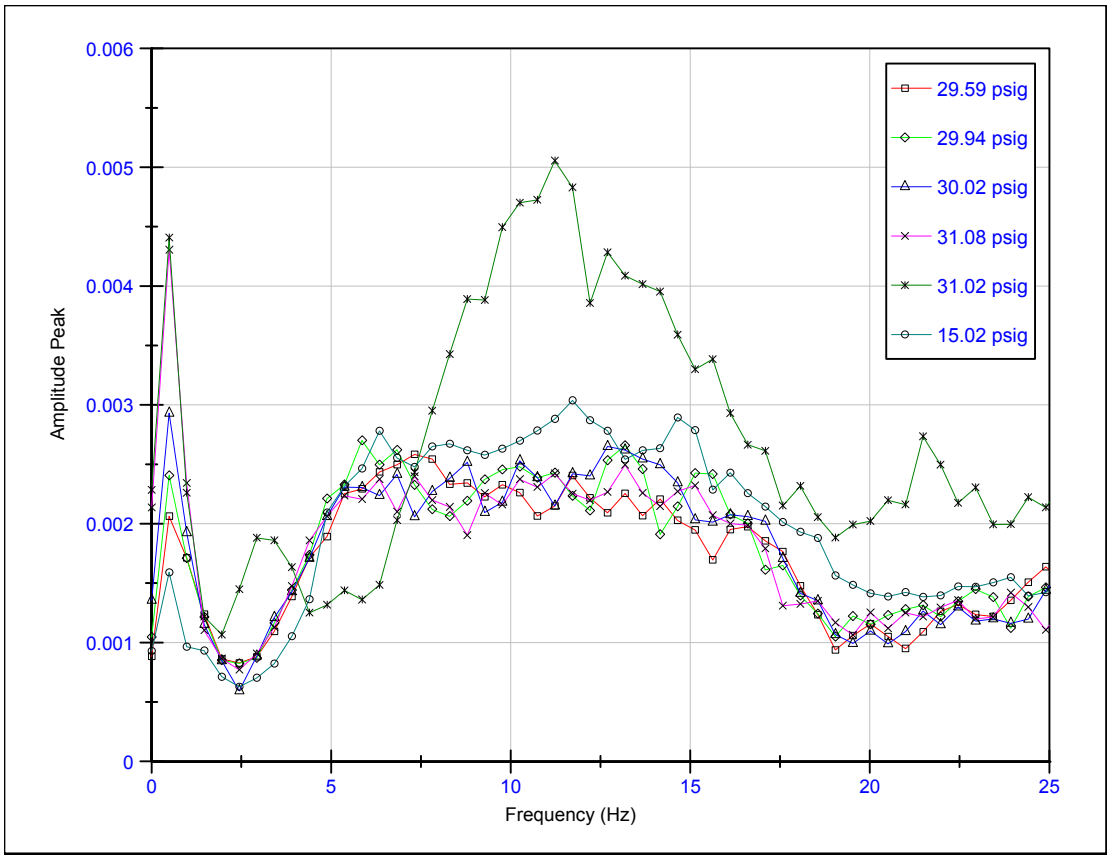


Figure 4.9 FFT plot (frequency 0 to 25 Hz) of differential pressure data collected across tray 3 for reboiler pressure range of 29.59 to 31.02 psig (flooded) and15.02 psig (recovered post flooding).

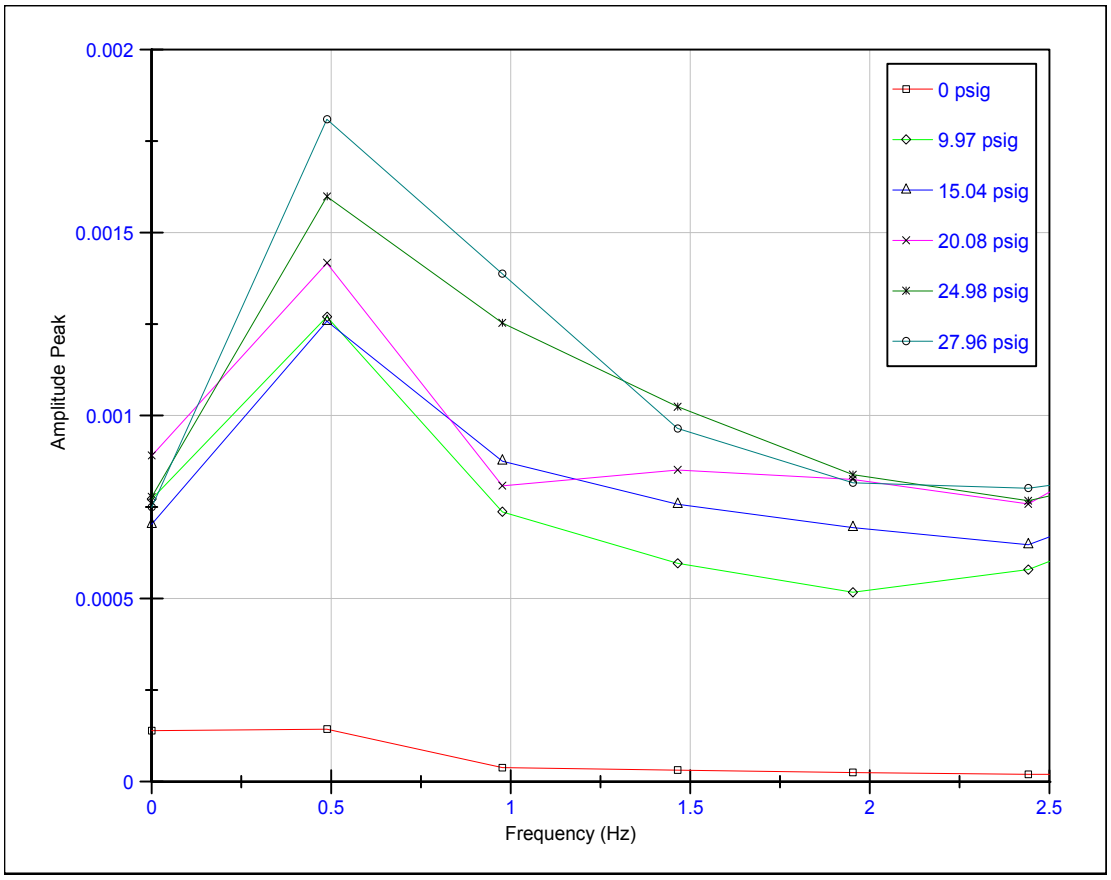


Figure 4.10 FFT plot (frequency 0 to 2.5 Hz) of differential pressure data collected across tray 3 for reboiler pressure range of 0 to 27.96 psig

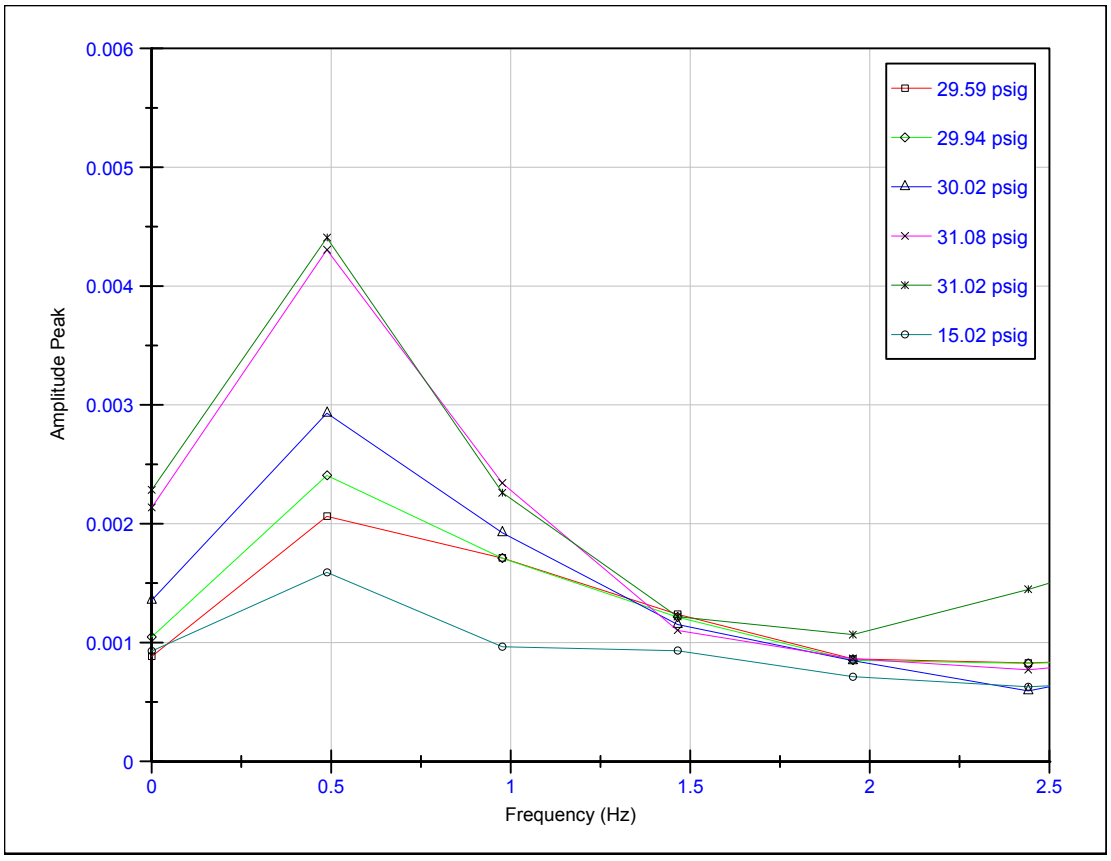


Figure 4.11 FFT plot (frequency 0 to 2.5 Hz) of differential pressure data collected across tray 3 for reboiler pressure range of 29.59 to 31.02 psig (flooded) and15.02 psig (post flooding).

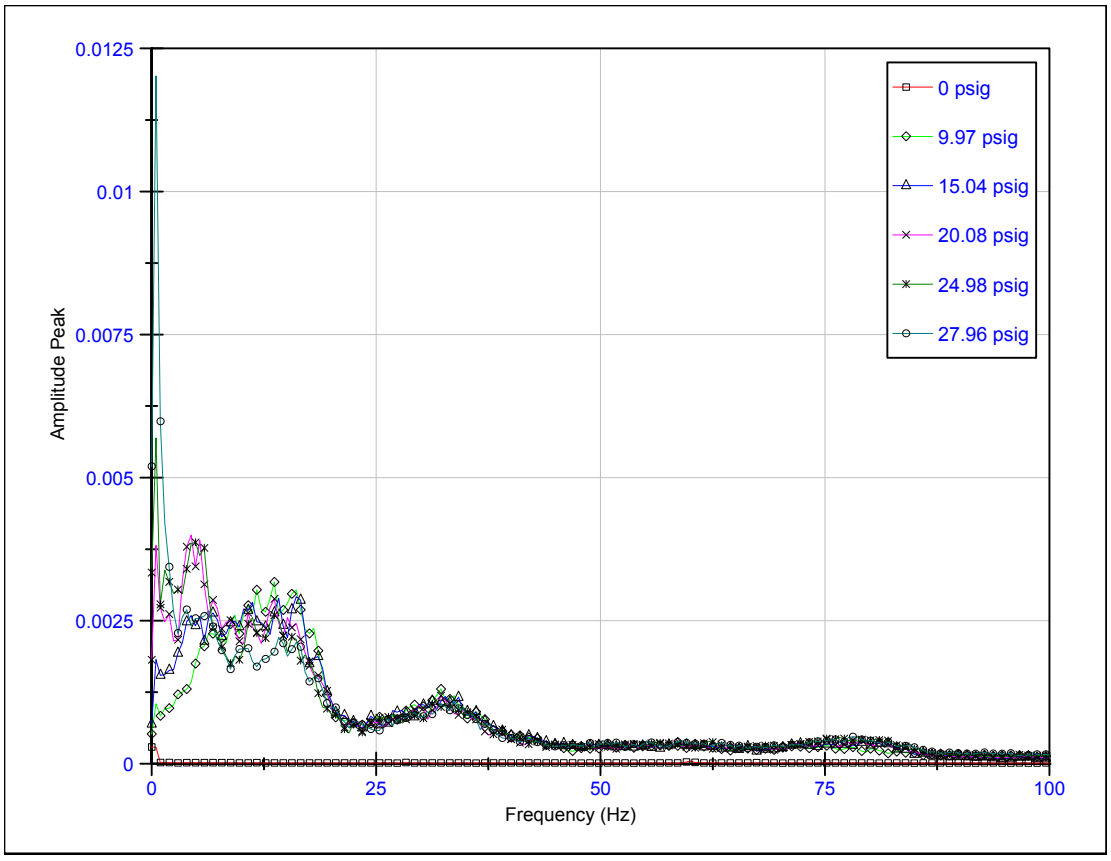


Figure 4.12 FFT plot of differential pressure data collected across tray 4 for reboiler pressure range of 0 to 27.96 psig.

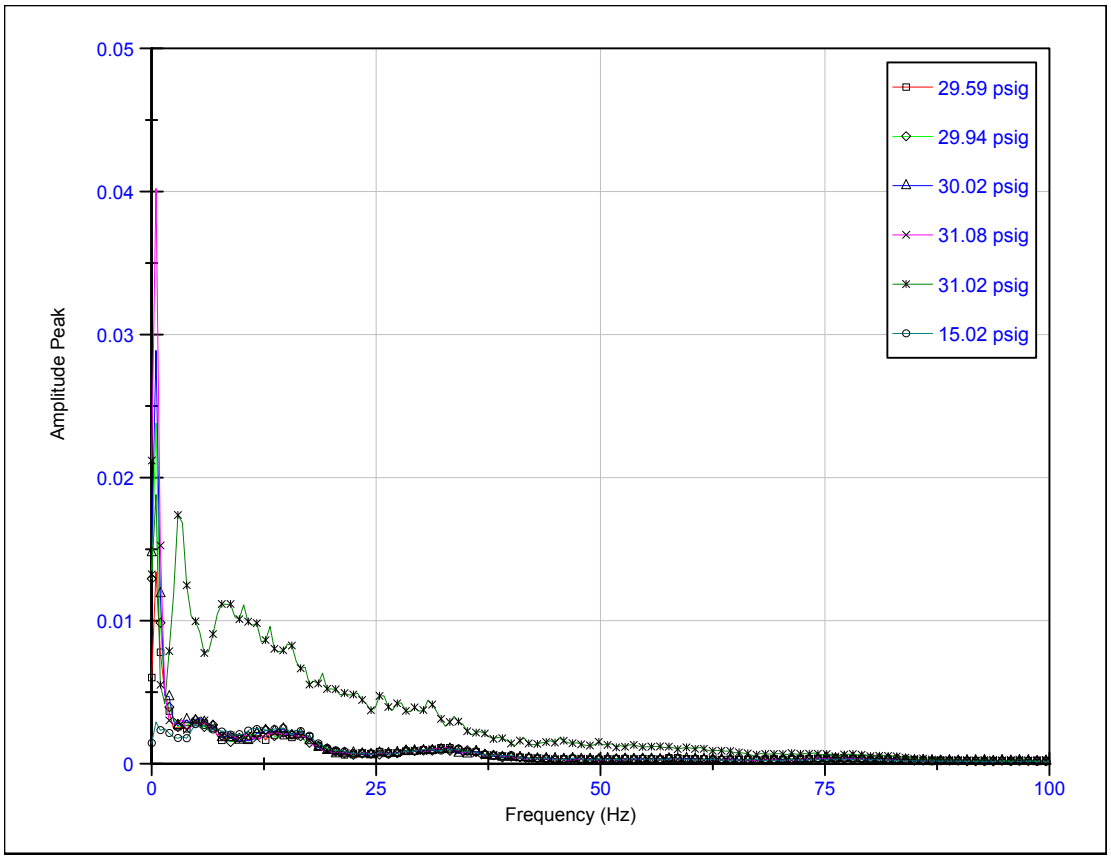


Figure 4.13 FFT plot (frequency 0 to 100 Hz) of differential pressure data collected across tray 4 for reboiler pressure range of 29.59 to 31.02 psig (flooded) and15.02 psig (post flooding).

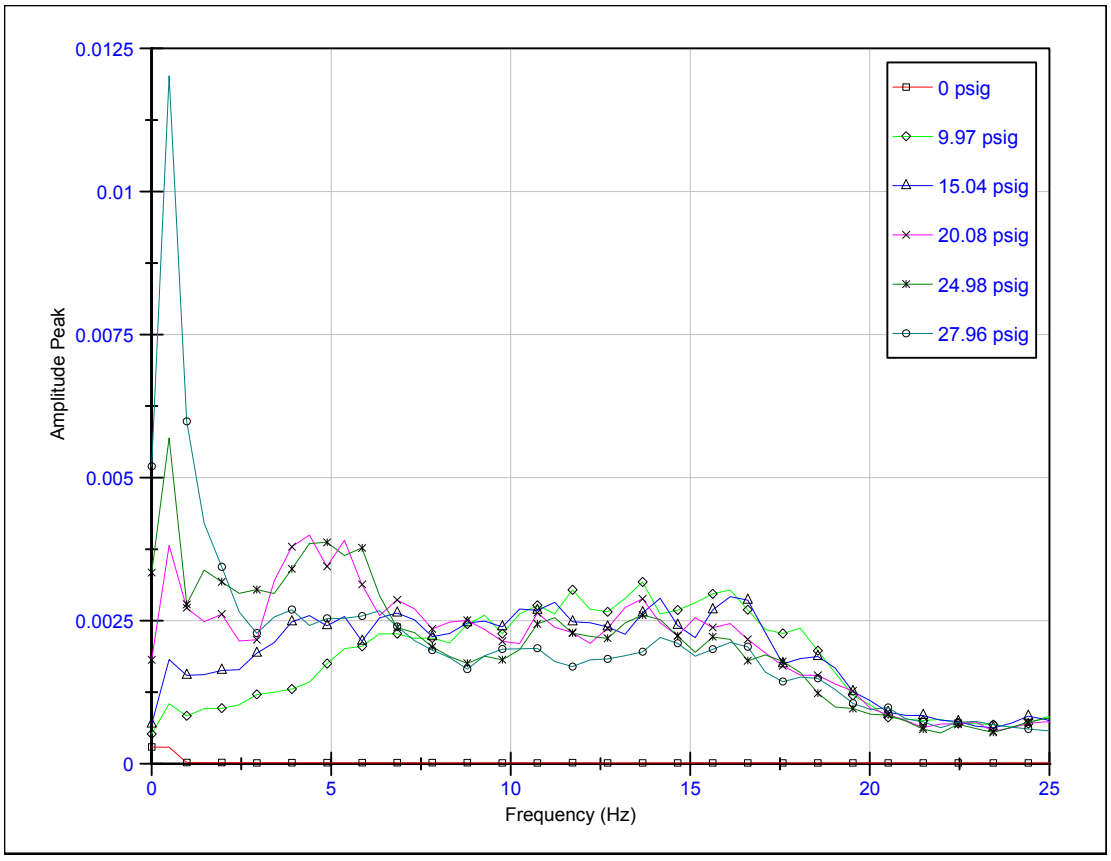


Figure 4.14 FFT plot (frequency 0 to 25 Hz) of differential pressure data collected across tray 4 for reboiler pressure range of 0 to 27.96 psig.

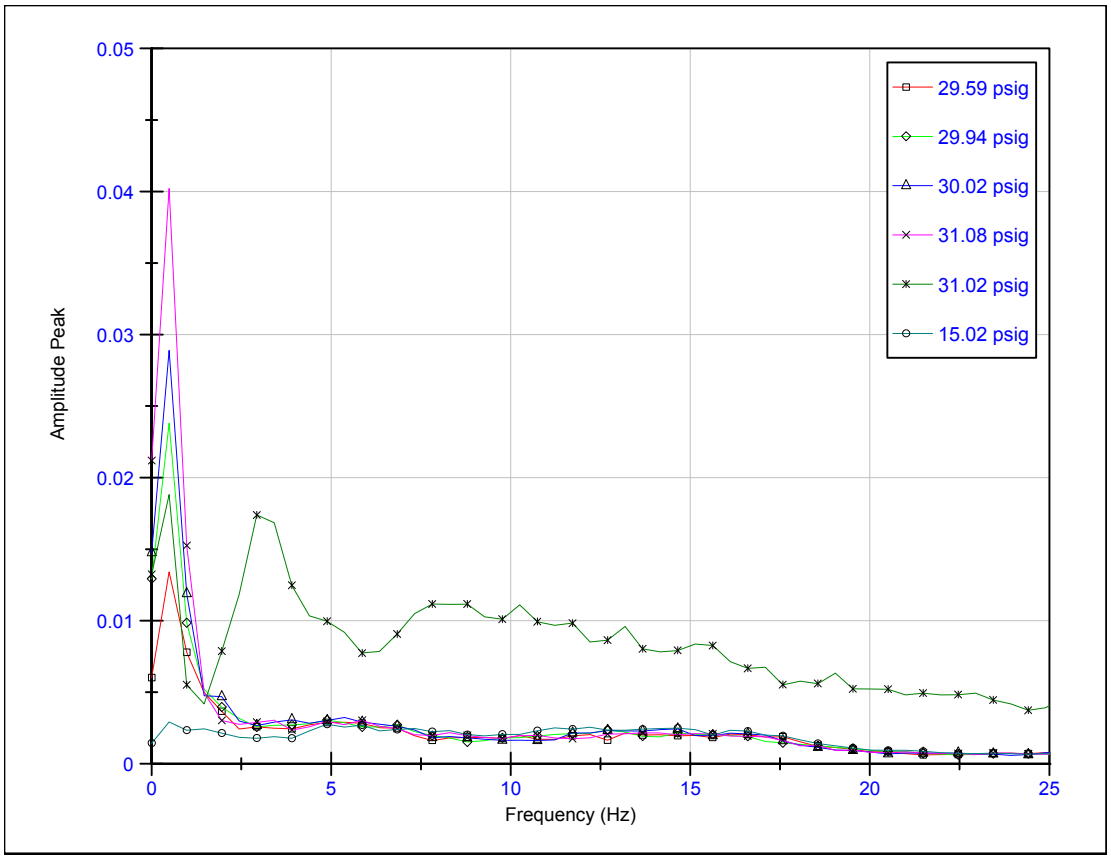


Figure 4.15 FFT plot (frequency 0 to 25 Hz) of differential pressure data collected across tray 4 for reboiler pressure range of 29.59 to 31.02 psig (flooded) and15.02 psig (post flooding).

4.2.1.3 A candidate Flooding Sensor: Autocorrelation function (ACF) analysis – UTK data

The autocorrelation function, mutual information, residual Shannon entropy and symbol sequence histogram were calculated using the NTSAS© software.

Bubble cap, Tray 3

Figure 4.16, 4.17 and 4.18 show the ACF as reboiler steam pressure changes for tray 3. The base data for tray 3 follows a sinusoidal pattern with peaks at lags = multiples of 17. Peak at lag= 17 relates to frequency of 1000/58 = 58.82 Hz. Peaks at lag of 17 indicates 60 Hz noise. This noise was detected in the FFT plots given in figure 4.6 where there is a small peak at 60 Hz. The ACF for other reboiler steam pressures besides the base data indicate a first peak around lag of 29. The ACF for the flooding data (31.02 psig) is similar to the ACF plots for normal runs as shown in Figure 4.17. Figures 4.17 and 4.18 indicate as the reboiler steam pressure in the reboiler is increased, the ACF peak at lag of 29 increases simultaneously. In figure 4.18 the curves for 29.59 and 29.94 psig cluster but there is very little pressure difference for these two data sets. The ACF increases to a maximum at 0.1 at lag of 29 for the last data set (30.08 psig) before flooding.

The value of the AFC minimum between 40 and 50 lags tracks the hydraulics and closeness to flooding fairly well especially as flooding is

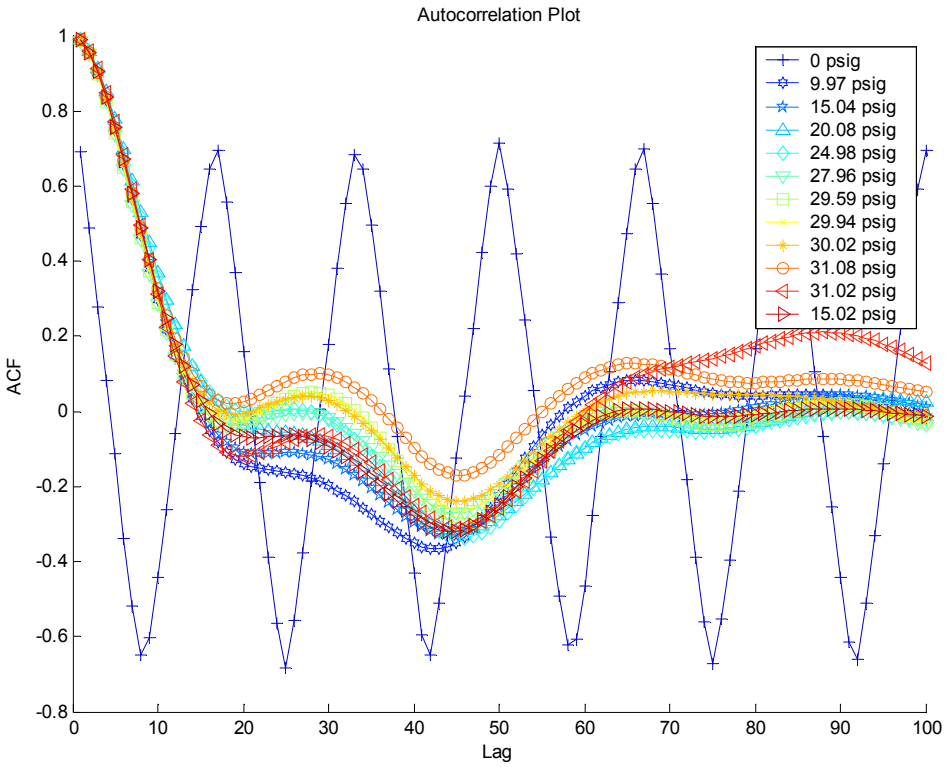


Figure 4.16 Autocorrelation plot for differential pressure data across tray 3.

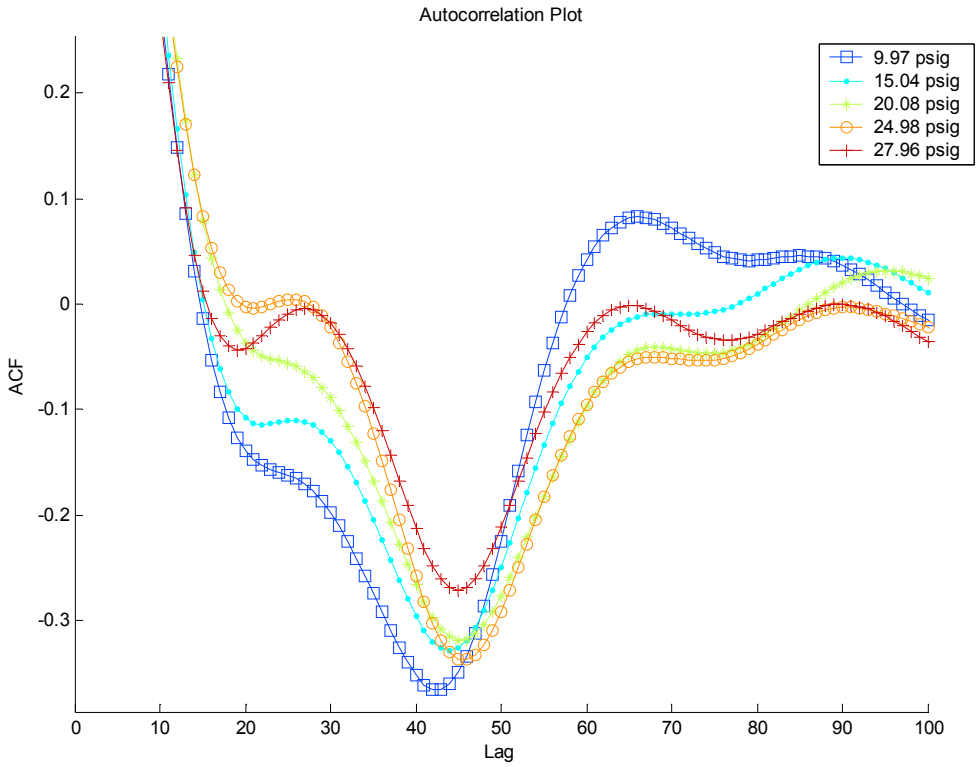


Figure 4.17 Autocorrelation plot for tray 3 data for reboiler pressure range of 9.97 to 27.96 psig

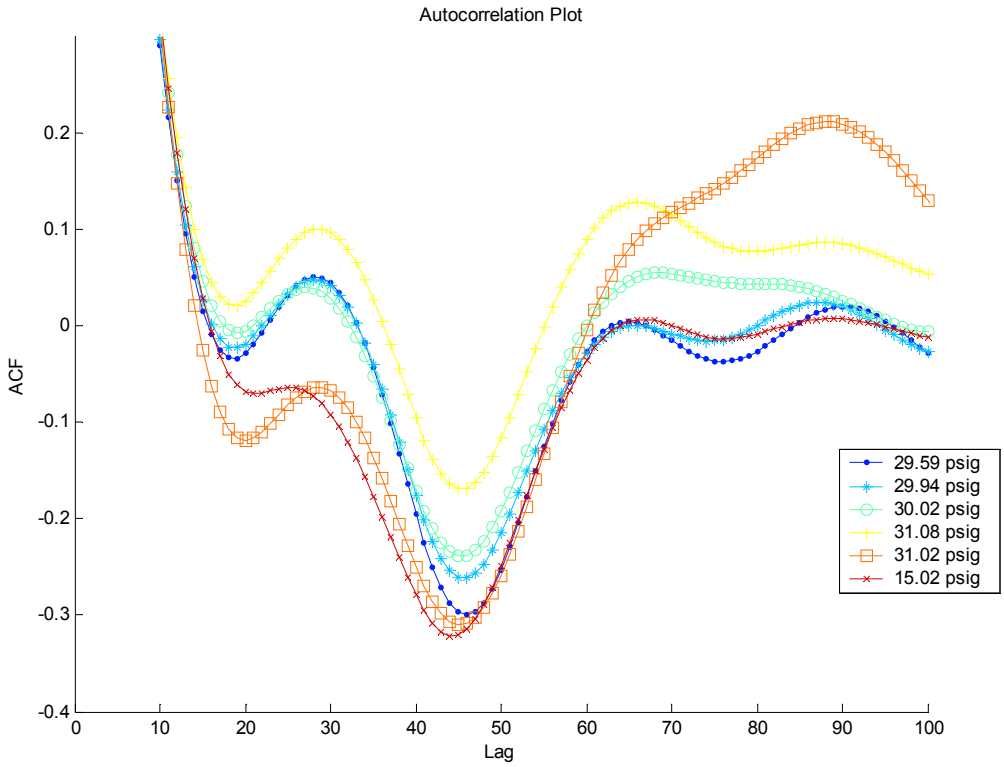


Figure 4.18 Autocorrelation plot for tray 3 differential pressure data for reboiler pressure range of 29.59 to 31.02 psig and15.02 psig (post flooding)

approached. Thus the minimum value of AFC for 40 < lag < 50 is a candidate for a “Flooding Sensor.”

Sieve plate, Tray 4

Figure 4.19a shows the ACF for tray 4 including base, flooded (31.02 psig) and recovered from flooding (15.02 psig) time series. The ACF for flooded data (31.02 psig) has a broad peak around lag of 84 with magnitude of 0.18. The post flooding data has ACF curve similar to the ACF curve for the pre flooding data at the same reboiler steam pressure.

The shape of the ACF curves is very different than those for the bubble cap tray. Figure 4.19b with base, flooded (31.02 psig) and recovered from flooding (15.02 psig) curves removed with the first peak in ACF for different time series data are observed at lag between 62 and 67. The peak tends to shift from lag of 62 to 67. The magnitude of the ACF increases with the increase in reboiler steam pressure. The ACF for the time series data close to flooding takes more time to approach the value of zero. The peak of the ACF at lag of 62-67 varies from 0.07 (9.97 psig) to 9.2 (31.08 psig).

The ACF curves for November 16, 2006 run do not show similarity with the ACF plot for the column runs on September 18, October 2, and October 3, 2005, which show similar ACF curves. The only difference between these column runs was that the ΔP across tray 4 was measured using Validyne sensor on November 16. The MKS sensor was used for measuring the ΔP on the column runs on September 18, October 2, and October 3, 2005.

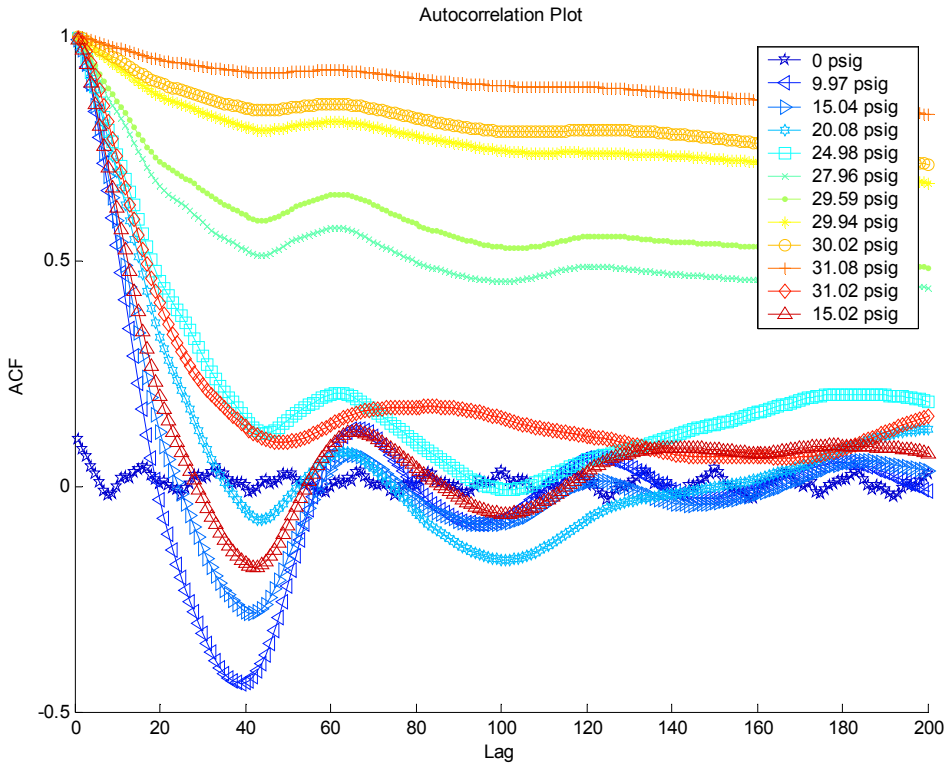


Figure 4.19a Autocorrelation plot for tray 4 differential pressure data.

The red 15.02 psig curve is the recovered from flooding data and the orange circle data is flooded data at 31.02 psig, and are not expected to follow the trend of the other data.

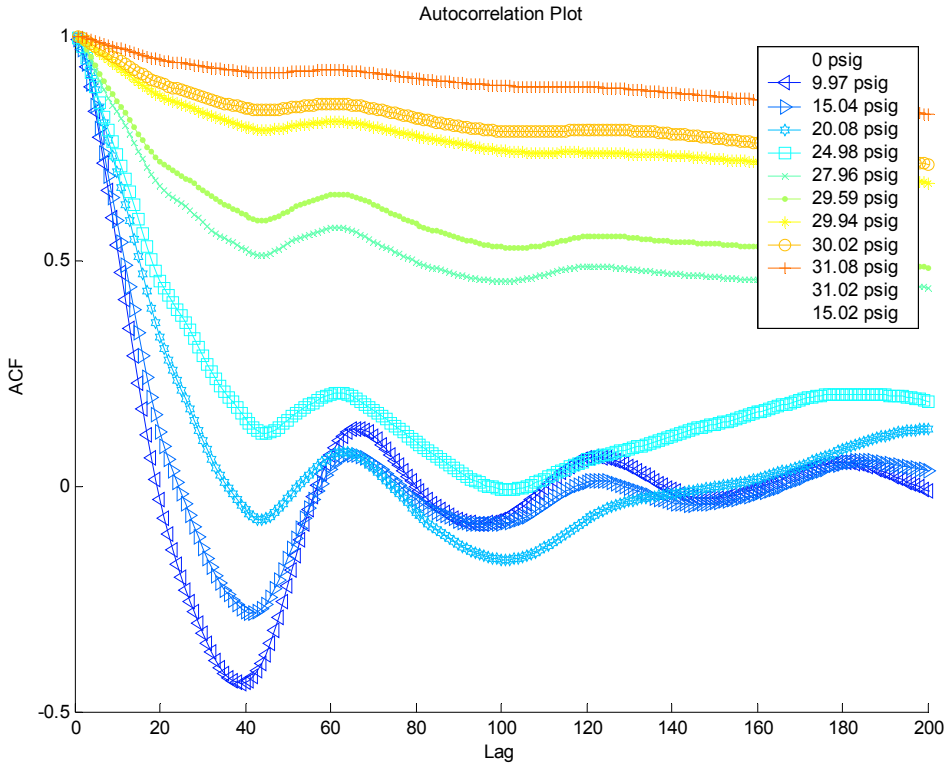


Figure 4.19b Autocorrelation plot for tray 4 differential pressure data without 0, 31.02 (flooding) and 15.02 (post flooding) psig curves.

4.2.1.4 A candidate Flooding Sensor: Mutual Information (MI) analysis – UTK data

Mutual Information is similar to Autocorrelation, but captures both the linear and nonlinear characteristics of the time series. All the plots for Mutual Information are calculated using 4 symbols with sequence length of 3 and interval of 1.

Bubble cap, Tray 3: Figure 4.20 shows the MI plot for ΔP data measured across tray 3. The base data has a wave nature curve similar to ACF plot indicating the presence of low noise signal embedded with the time series during data collection. This noise is identified as 60 Hz in the Fourier transform plot (see figure 4.6). The magnitude of the peak for the flooding data increases back to 0.023, similar magnitude to the MI peaks for normal pre flooding data. The MI curve for the flooding data indicates another peak at a lag of 87 with a magnitude of 0.014.

Figures 4.21 and 4.22 show much clearer plots with the base, flooded (31.02 psig) and recovered from flooding data removed. MI curves covering two different reboiler pressures ranges are split between the two figures. The first peak for each reboiler pressure is observed at lag near 45. The magnitude of the peak decreases from 0.03 to 0.01 with the increase in reboiler pressure from 9.97 psig to 31.08 psig.

The magnitude of MI values at this peak clearly separate and can be associated with hydraulic changes on tray 3 and more globally changes in the

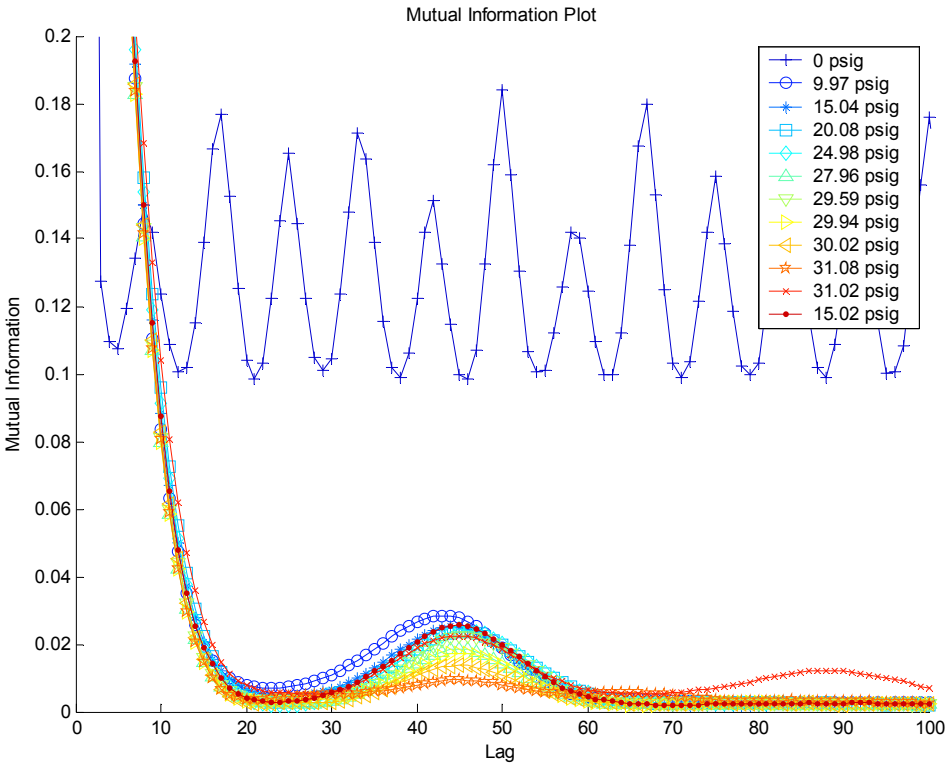


Figure 4.20 Mutual Information plot for tray 3 data.

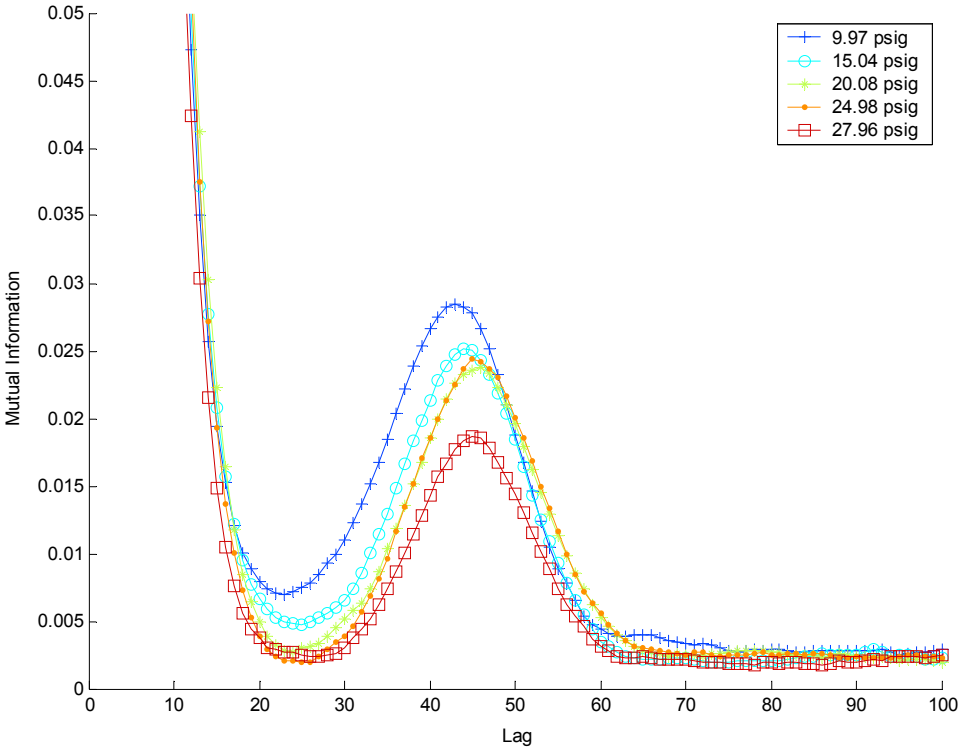


Figure 4.21 Mutual Information plot for tray 3 data for reboiler pressure range of 9.97 to 27.96 psig.

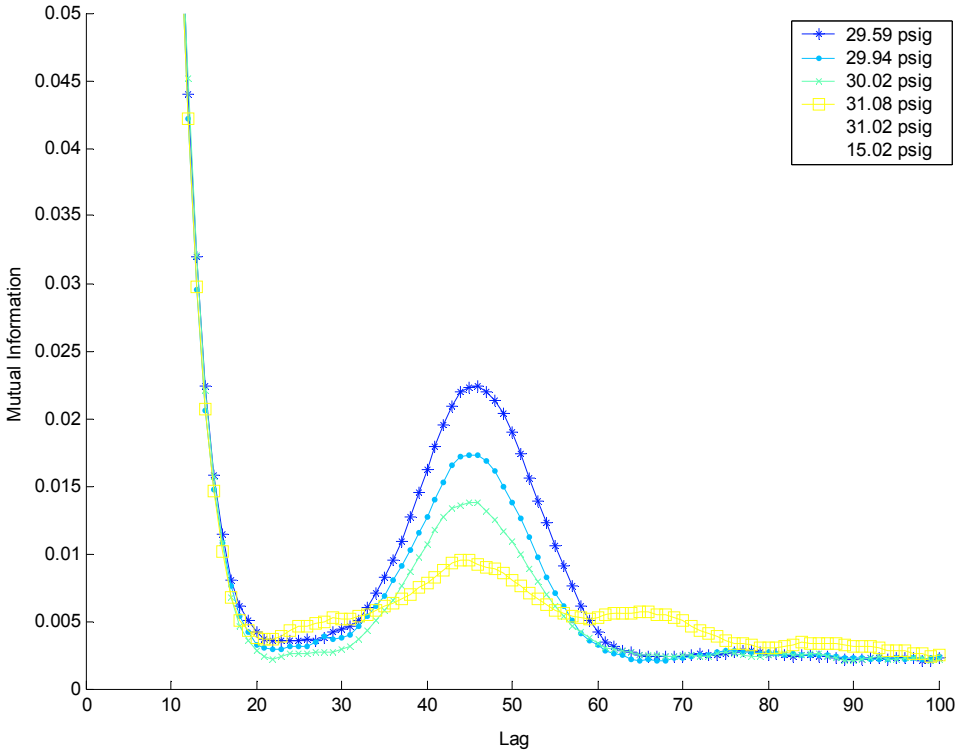


Figure 4.22 Mutual Information plot for tray 3 data for reboiler pressure range of 29.59 to 31.08 psig without 0, 31.02 (flooding) and 15.02 (post flooding) psig curves.

column. A ‘Flooding Sensor’ could be based on this targeted MI value. This information could be used to push the column toward maximum throughput but avoid flooding by limiting the value of this MI peak.

Sieve plate, Tray 4: Figure 4.23a shows the MI plot for all tray 4 data. There is no sharp peak in the MI plot observed for pressures below 27.96 psig. A broad peak is observed at lag of 63 for pressure equal and above 27.96 psig. Figure 4.23b is the same plot with base (0 psig), flooded (30.02 psig) and recovered from flooding (15.02 psig) curves removed to clearly show the trend in the MI curve with reboiler pressure. The MI increases from 0 to 0.4 as the reboiler pressure is increased from 9.97 psig to 31.08 psig. MI curves for normal operation pressure fall steeply to their minimum value whereas the MI for data close to flooding takes longer time to settle down. Mutual information plot for tray 4 indicates that as the column approaches’ flooding, the liquid on the tray becomes more chaotic (review figure 2.1) [1]. The MI value monotonically increases as the reboiler steam pressure increases over nearly all lags. A suggested MI value to monitor closeness to flooding and thus form the basis for a “Flooding Sensor” is the magnitude of the first peak between 55 and 75 lags.

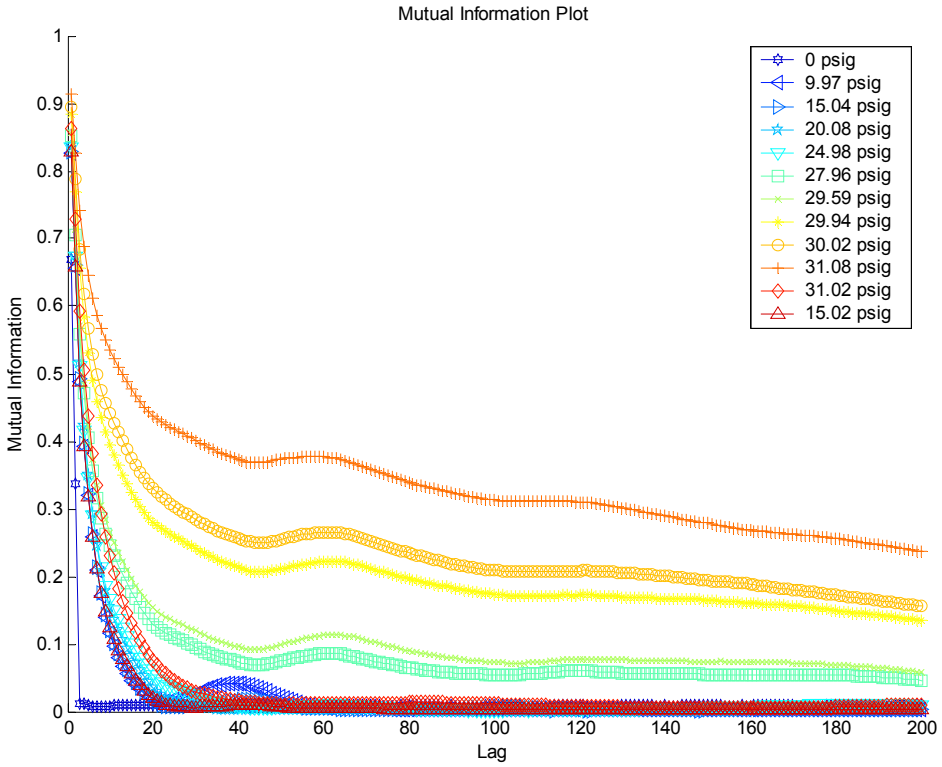


Figure 4.23a Mutual Information plot for tray 4 data.

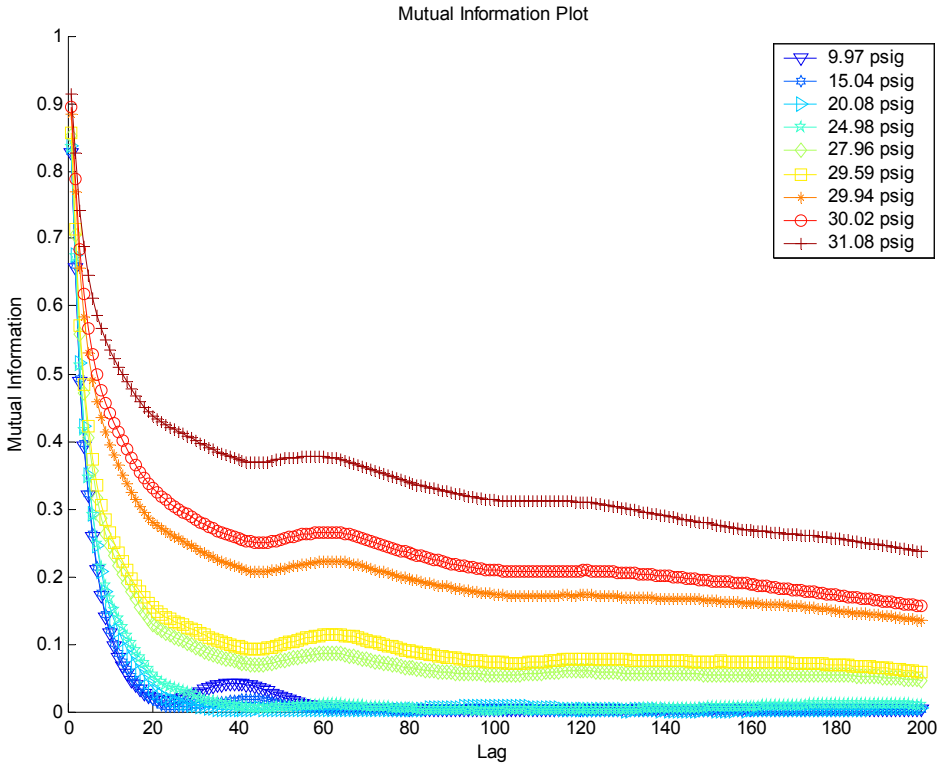


Figure 4.23b Mutual Information plot for tray 4 differential pressure data without 0, 31.02 (flooding) and 15.02 (post flooding) psig curves.

4.2.1.5 Residual Shannon Entropy (RSE) – UTK data

Bubble cap, Tray 3: Figure 4.24 and 4.25 are the RSE plots for differential pressure time series data collected across tray 3. All the plots for RSE are calculated using 4 symbols with sequence length of 3 and interval of 1. The RSE plots show similar characteristics as the mutual information plots for tray 3 and tray 4 because mutual information is calculated using joint Shannon entropy. The RSE plots are not as smooth as the mutual information plots because Shannon entropy is more sensitive to noise and other disturbances than mutual information. There are peaks observed at lag of 22 and between lag of 40-48 in figure 4.24 and 4.25. The peaks appearing at lag of 22 for different time series follows a certain pattern. As the reboiler pressure is increased the magnitude of the peak decreases from 0.022 to 0.006. The magnitude of peak for the time series collected during the flooding of the column increases to 0.018 which is close to the peak for normal runs.

Sieve plate, Tray 4: Figure 4.26 shows the RSE plot for differential pressure data collected across tray 4. The normal run time series (lower reboiler pressure from 9.97 psig to 24.98 psig) settle to a lower RSE value approximately equal to 0.01. A small broad peak is observed at lag of 40 for reboiler pressures 9.97 psig and 15.04 psig. As the reboiler pressure increases above 24.98 psig, the RSE curves for the time series take longer lag to settle. The RSE value increases from 0.01 to 0.25 at lag of 40 as the reboiler pressure is increased from 9.97 psig to 31.08 psig. While the RSE

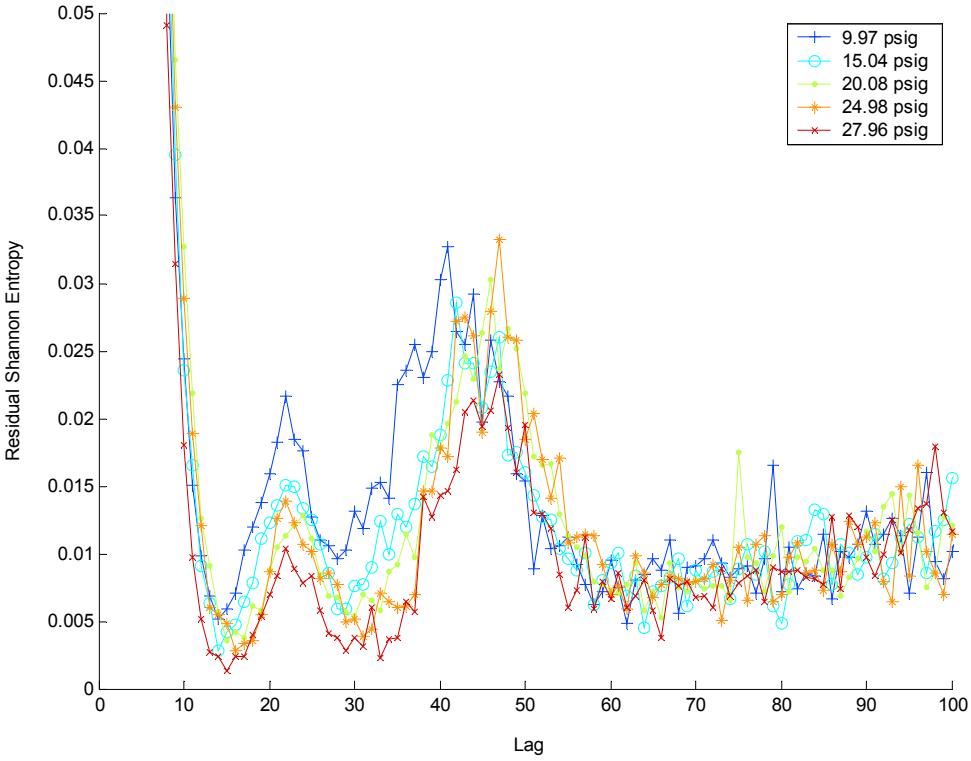


Figure 4.24 Residual Shannon Entropy plot for tray 3 data for reboiler pressure range of 9.97 to 27.96 psig.

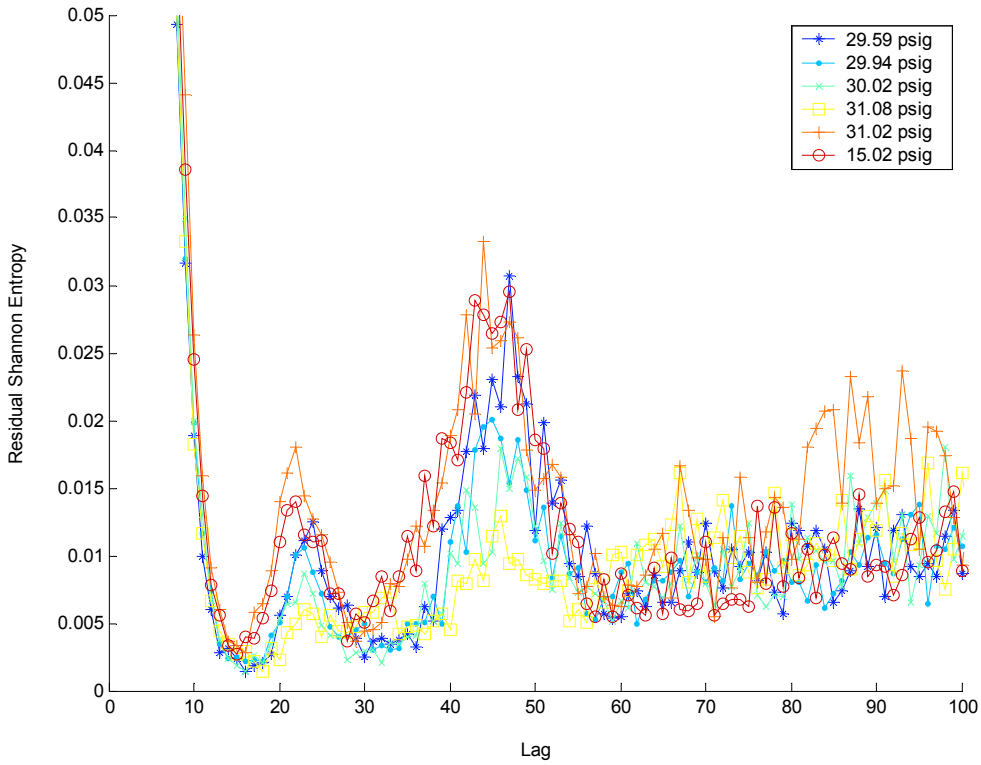


Figure 4.25 Residual Shannon entropy plot for tray 3 data for reboiler pressure range of 29.59 to 31.02 psig and 15.02 psig (post flooding).

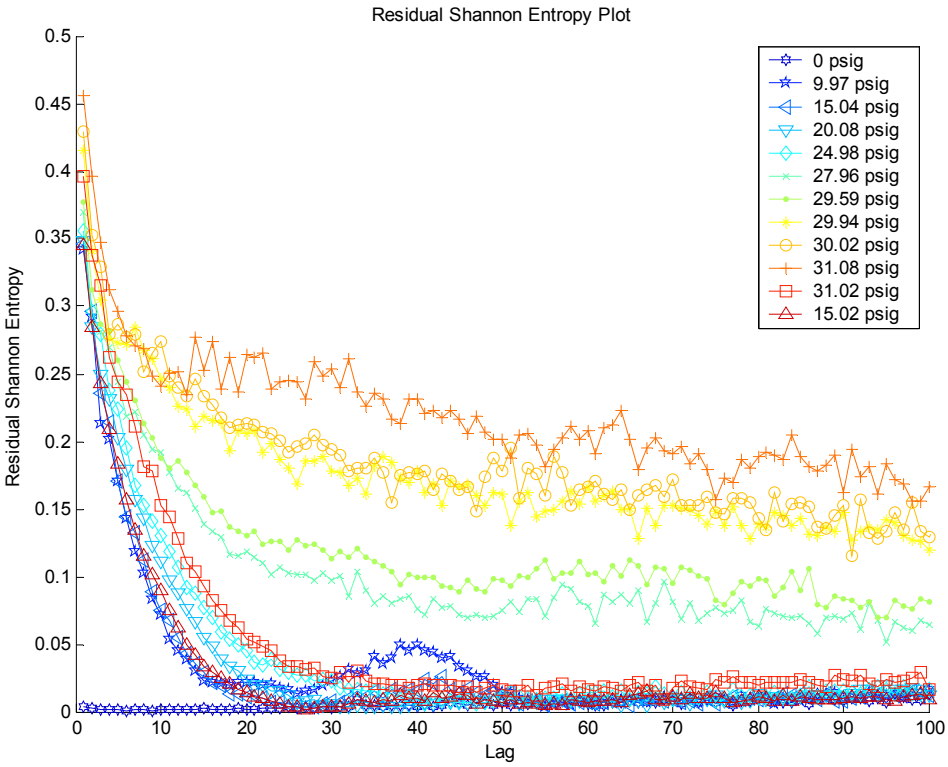


Figure 4.26 Residual Shannon entropy plot for tray 4 data for all reboiler pressures.

plots provide a similar tracking ability to MI plots, calculating the MI is the favored technique for quantifying the hydraulic state on a distillation tray as the MI plots are much smoother.

4.2.2 FRI DISTILLATION COLUMN DATA

The FRI data was collected on a low pressure (150 psig) distillation column with proprietary trays at a pilot plant located in Stillwater, OK. Few details are available, however, it is known that the operating pressure was 150 psig, and the differential pressure is measured across 4 trays. There is a nitrogen purge through the pressure taps but the flow is not sonic. It is difficult to judge the effect of the purge system flow rate responding to the instantaneous pressure in the column at each tap port. The length of the pressure taps is about 120 feet and contains some tubing size changes and several elbows. The length of the taps assures that some signal distortion due to resonance will be encountered according to the simple model presented by Validyne [ref]. The changing tube size and direction changes within the tap run likely introduces several resonance frequencies. The Validyne sensor is used to acquire the data. The following subsections discuss the analysis of the differential pressure data collected across 4 trays on December 15, 2005.

4.2.2.1 Mean and Standard deviation

Figure 4.27 shows the mean and the standard deviation of the differential pressure data collected at different times during the run. The mean differential

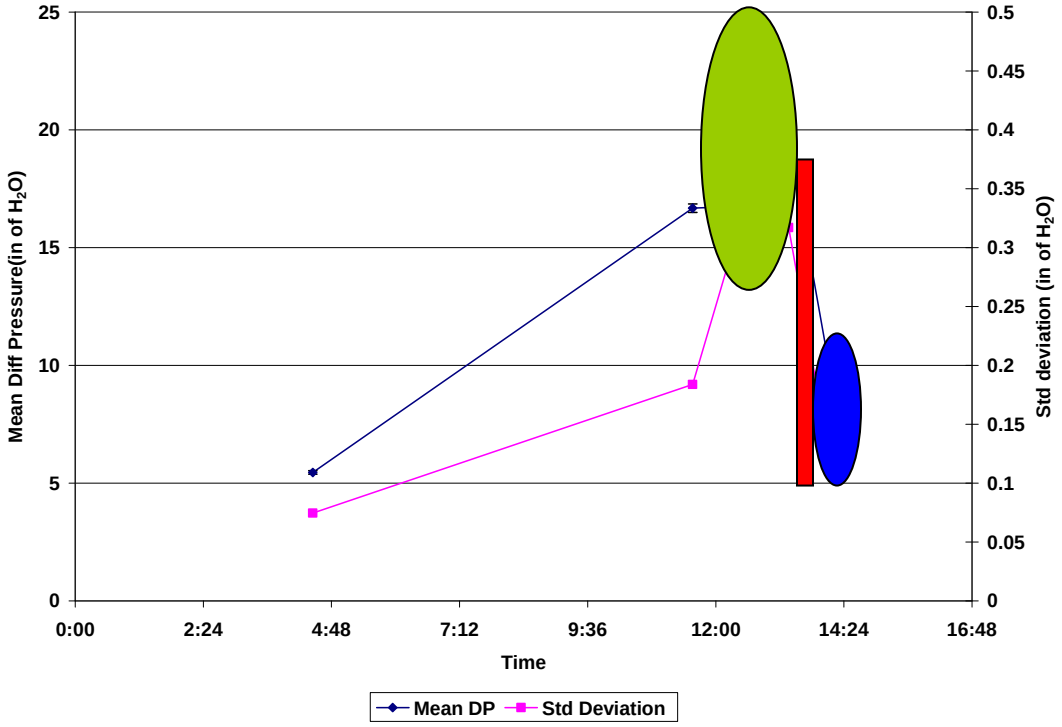


Figure 4.27 Mean and standard deviation vs. time graphs for FRI data.

pressure across 4 trays increases as the run progresses. The reboiler steam pressure is not available for this data set. Therefore, the average pressure drop across the trays is used as the indicator of the column load. All the points in the light green circle in figure 4.27 represent the mean and standard deviation for the time series collected in the 20 minutes range before the column was flooded. The mean pressure across the tray increases but the standard deviation increases and then decreases. There was no flooding data available due to the saturation of the differential pressure sensor.

However figure 4.27 illustrates that data was collected very close to flooding and after flooding. The flooding of the column occurred in the time period represented as a red rectangle. The points in the blue oval in figure 4.27 represent the mean and the standard deviation for the post flooding data. The mean differential pressure across the trays decreases because the trays have less liquid on them after returning to normal pressures. The shape of the mean and standard deviation contains a similar finger print as obtained from the UTK column for 4 replicate campaigns shown in figures A.1 to A.4 located in Appendix A.

4.2.2.2 FFT analysis – FRI data

The FFT plots were created using the same criteria used for analyzing the UTK data. Due to the unavailability of reboiler pressure data, the time series are referenced with their respective mean differential pressure measurement. Figure 4.28 shows the FFT plot for the differential pressure data collected across 4 trays at FRI. These time series are digital band pass filter with the high pass set to 0.1 Hz and the low pass set to 100 Hz. Small 60 Hz noise peak shown in figure 4.28 for the base data. Fig 4.29 shows some frequency content in the base data from 0.5 to 4 Hz.

Frequency peaks with comparatively higher magnitude are observed at lower frequencies equal to 0.5 and around 2.5 Hz. Smaller magnitude peaks are observed at 12.5, 28, 32, 38, 48 and 52 Hz. The peaks at 0.5 Hz and around 2.5 Hz are clearly visible in Figure 4.29. The magnitude of the peaks at 0.5 Hz and around 2.5 Hz does not follow any kind of trend. The only observation that we can makes is that the magnitude of the peaks in the FFT plot for the time series closer to the flooding point (mean ΔP of 16.67 inches of H_2O and higher) is higher than the time series that have a lower mean ΔP (mean ΔP of 16.67 inches of H_2O and lower).

Both UTK and FRI data shows peaks around 0.5 Hz and 30 Hz. FRI data when compared to UTK data has greater power at frequency of 0.5 Hz. FFT for FRI data (figure 4.28) shows a peak at 16 Hz which is close to the 14

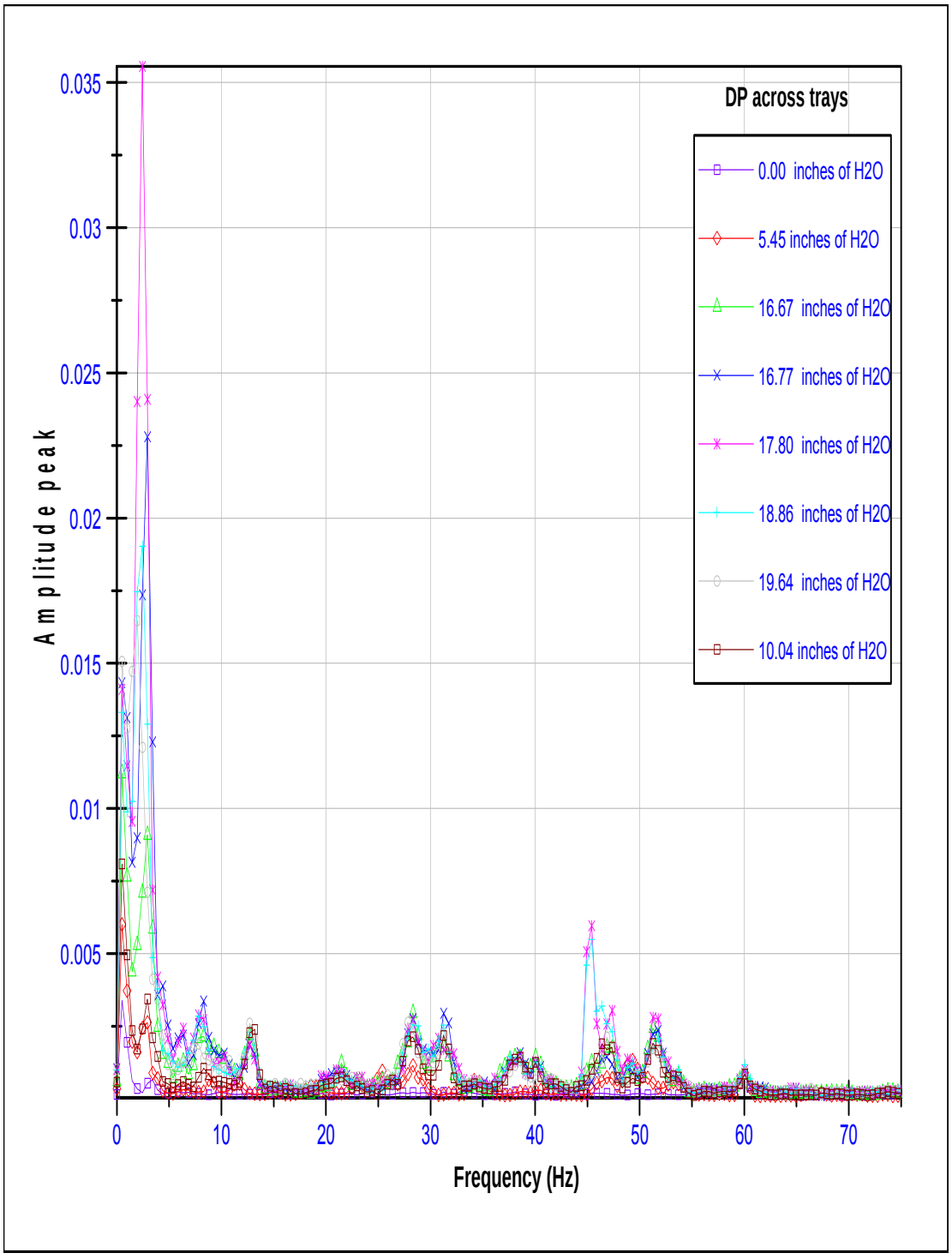


Figure 4.28 FFT plot (frequency 0 to 100 Hz) for FRI differential pressure data.

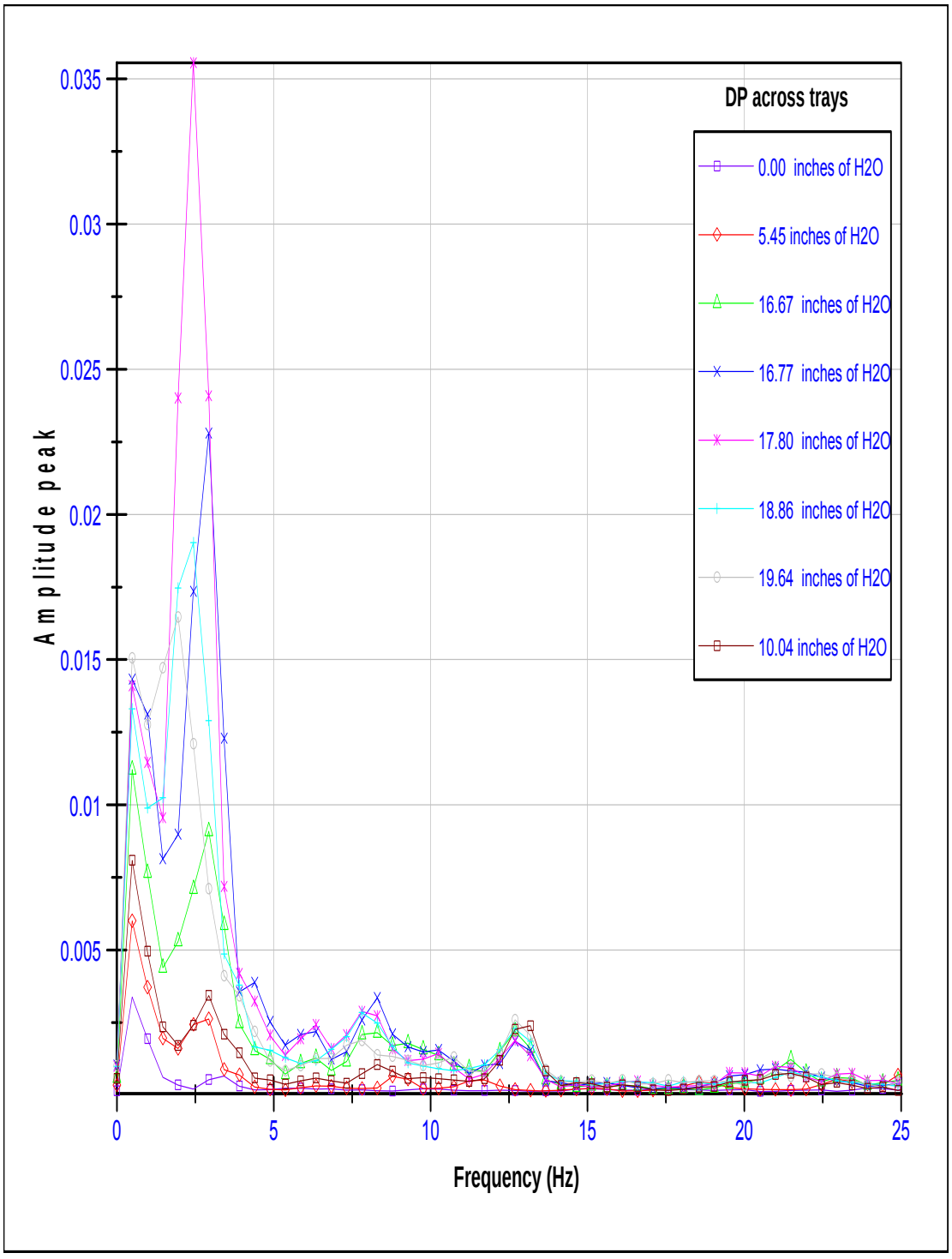


Figure 4.29 FFT plot (frequency 0 to 25 Hz) for FRI differential pressure data.

Hz natural frequency of plumbing calculated using equation 2.7. The FRI data shows more activity at higher frequencies between 40 and 60 Hz.

4.2.2.3 Autocorrelation function (ACF) analysis – FRI data

Figure 4.30 and 4.31 shows the ACF plot for the FRI data. The high frequency waves in the autocorrelation plot are due to noise present in the time series. Figure 4.30 shows a modulated low frequency wave. There is once cycle of the low frequency wave. The low frequency wave is modulated with a higher frequency wave. The high frequency periodicity in the base (column not operating) AFC can be observed in all operating data especially at lower average ΔP. The autocorrelation curves for the time series with higher differential pressure across the trays have their maxima between lag of 350 and 450 which represents the presence of lower frequencies between 2.5 and 3 Hz in the FFT plots. Figure 4.30 indicates that as the column trays get loaded and the column moves towards flooding, the autocorrelation curves take longer time to settle down to zero. This feature is similar to the observations made with the UTK data. The FRI data has greater noise component in the data compared to UTK data.

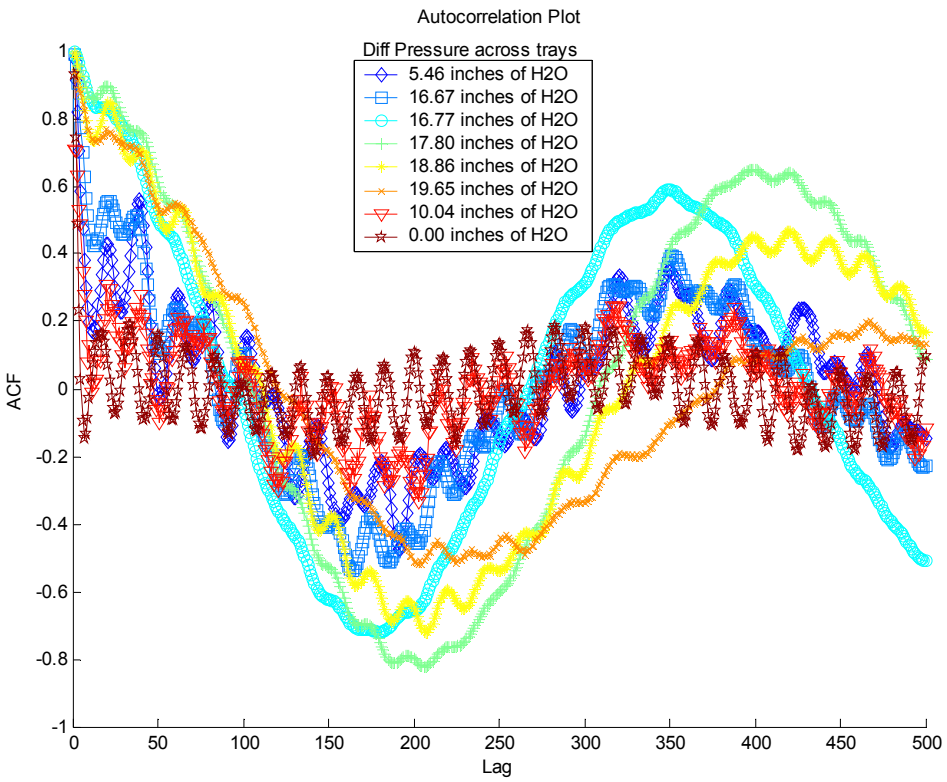


Figure 4.30 Autocorrelation plot for FRI differential pressure data (Lag 0-500).

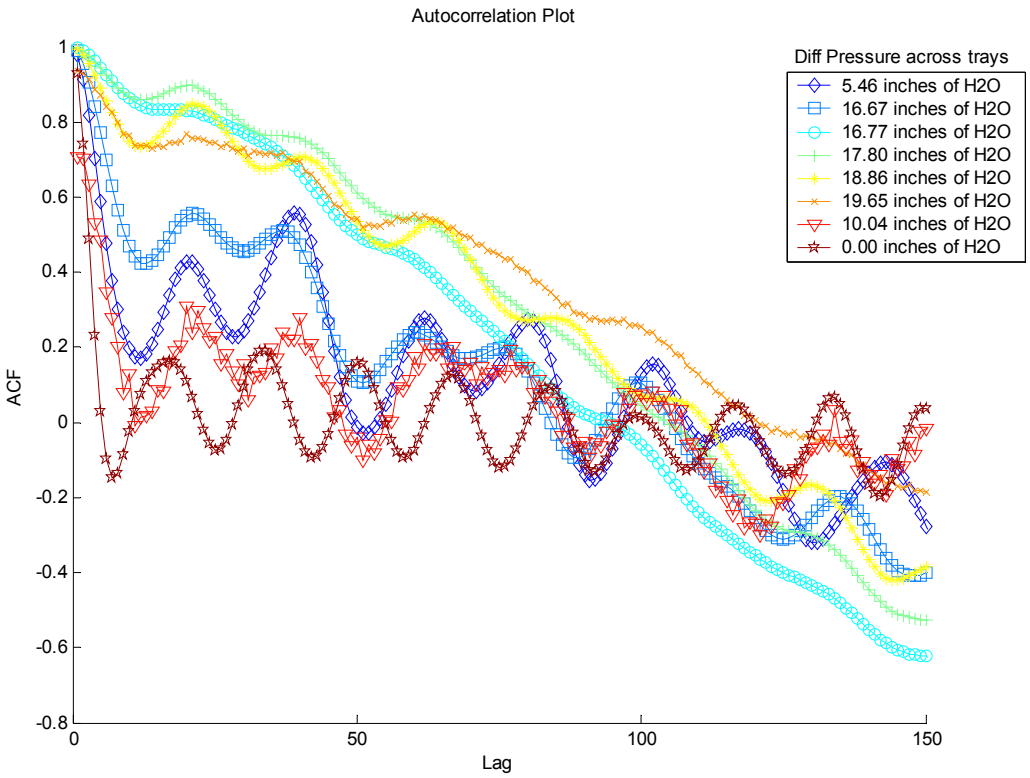


Figure 4.31 Autocorrelation plot for FRI differential pressure data (Lag 0-150).

4.2.2.4 Mutual Information (MI) analysis – FRI data

Figures 4.32 and 4.33 show the mutual information plots for FRI data. The MI plots for the FRI data were calculated using 4 symbols with sequence length of 3 and interval of 1. The MI for the time series with mean differential pressure below 16.67 inches of H_2O settle down to a MI value approximately to 0.5, whereas the MI curves for the time series with mean differential pressure greater than 16.67 inches of H_2O have their first trough around lag of 100 and take longer time to settle to a constant MI value. FRI data in contrast with UTK data does not show clear trend of increasing values for MI at a particular lag.

4.2.2.5 Residual Shannon Entropy (RSE) – FRI data

The RSE plot for FRI data is shown in figure 4.34. Four symbols, sequence length of 3 and interval of 1 were used for calculating RSE. The RSE curves follow similar patterns as the MI curves. The peaks in the RSE curves at or around lag of 20 indicate some level of predictability for time series with mean differential pressure below 16.67 inches of H_2O. The RSE curves for time series with higher mean differential pressure take longer time to settle down to a constant RSE value. There are no major peaks observed in figure 4.34.

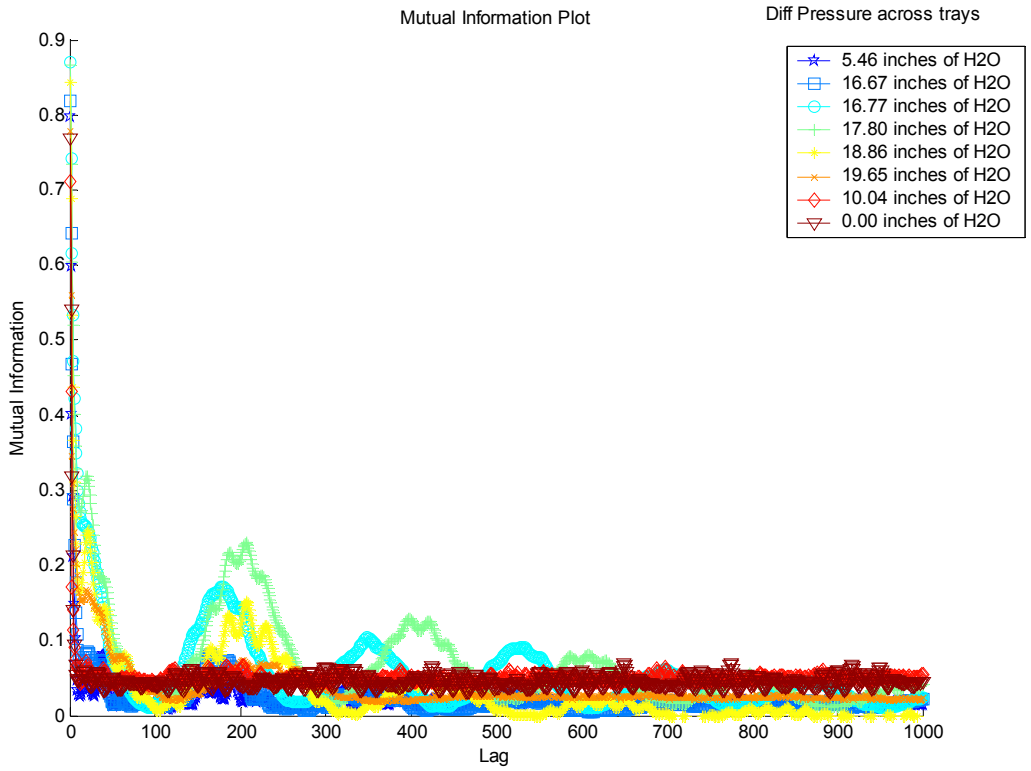


Figure 4.32 Mutual information plot for FRI differential pressure data (Lag 0 to 1000)

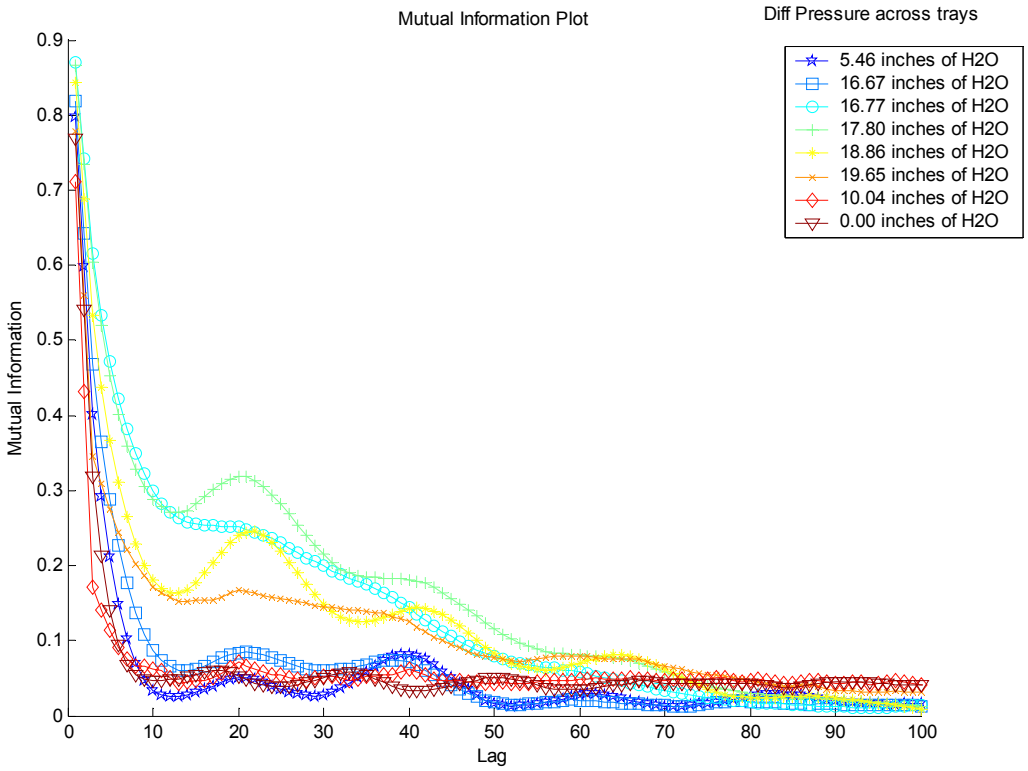


Figure 4.33 Mutual information plot for FRI differential pressure data (Lag 0 to 100).

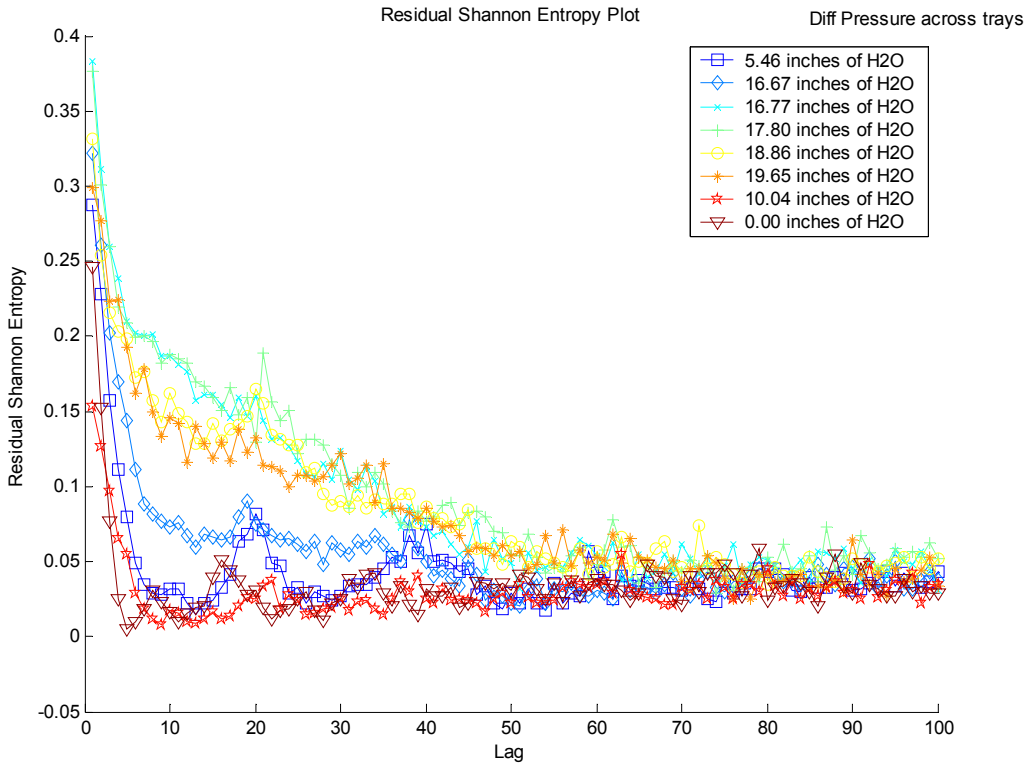


Figure 4.34 Shannon Entropy plot for FRI differential pressure data (Lag 0 to 100).

CHAPTER 5 CONCLUSIONS AND FUTURE WORK

5.1 CONCLUSIONS

A hydraulic flooding sensor has been developed in a laboratory setting. This research shows that the best calculations to identify the hydraulic state on a distillation tray and define an operational constraint are:

1. Autocorrelation Function maximum or minimum value in a carefully selected range of lags
2. Mutual Information maximum or minimum value in a carefully selected range of lags
3. monitor both the AFC and MI

Figures 4.17 through 4.19b confirm AFC as a linear technique to characterize the hydraulic state on a sieve tray and bubble cap tray. Figures 4.21 through 4.23b validate MI as a nonlinear methodology to track the hydraulic state on a sieve tray and bubble cap tray.

The implementation procedure would be to run a feedback controller with the flooding sensor as the supervisor to the column control variable that has been chosen to regulate the column throughput. The column throughput would be slowly increased until the target hydraulic value is reached. Then the flooding controller would control the throughput so the column rides on the constraint. With experience operating at a higher throughput and learning the sensitivity

of the hydraulic value has for various disturbances the hydraulic value is most sensitive the constraint could be moved to allow more throughputs.

Results from an industrial column are very encouraging as the ACF and MI analysis has several characteristics to the UTK 9-in diameter column. This is even more encouraging as the measurements were taken across 4 trays. There is a hypothesis that by characterizing small time scales phenomena the sensor can be applied to different kinds of trays and columns with different diameter. Issues identified in the study of FRI column time series are the interference in the time series due to resonance in the long taps used to connect the ΔP sensor. This could be resolved by placing a ΔP sensor at each port into the column with both sensors referenced to atmosphere. The difference between the two ΔP sensors across the tray or trays would be the tray or section ΔP. Another approach, perhaps more clever, would be to use analog filtering to remove the resonance frequencies if the hydraulic information is not near the resonance frequencies.

The study used high speed (1000 Hz) differential pressure data sets were collected across distillation trays. The distillation column at University of Tennessee, Knoxville (UTK) was the main research and demonstration site. The UTK column is 9 inches inside diameter, has 4 trays each of a different type not counting the reboiler. Many data sets were collected synchronously across the top tray (sieve tray) and across the next tray (bubble cap) from the top. Flooding always occurred on the sieve tray. To prove the application of this ‘flooding sensor’ in the field, data available from a pilot plant distillation

column (low pressure, 4 foot diameter) located at Fractionation Research Inc. (FRI), Stillwater, OK was also analyzed. These time series were analyzed using linear and nonlinear methods such as autocorrelation, frequency analysis, mutual information and residual Shannon entropy. There was no separation of material carried out in the distillation column at UTK as it ran with water at total reflux. For the sieve tray, the magnitude of the first maxima peak in the autocorrelation, frequency analysis, mutual information and residual Shannon entropy plots increases, as the column moves towards the flooding. The behavior of the plots for the bubble cap tray also showed clear trends with increasing column throughput. Online monitoring of the chosen peak or peaks allows tracking of the hydraulic state and to predicting flooding.

The experiments were carried out on distillation column in the Unit Operations Laboratory at University of Tennessee, Knoxville (UTK) and also at Fractional Research Inc. (FRI) located in Stillwater, OK. The experiments involved measuring differential pressure time series data at high frequency (1000 Hz) across a tray or trays in the distillation column.

The distillation column at UTK flooded at reboiler steam pressure of 30-31 psig. During all the runs at UTK, flooding occurred on tray 4 as expected. The mean differential pressure across trays increases as the column reboiler pressure is increased. This is due to the increased liquid and vapor flow rates and increased amount of liquid build up on the trays. The standard deviation of the differential pressure time series increases as the column approaches flooding point. The FFT plots for the UTK data indicated

peaks at 0.5 Hz, 5-15 Hz and 32 Hz. The magnitude of the peak at 0.5 Hz increased as the reboiler steam pressure was increased. The magnitude of the first peak in the autocorrelation plots for tray 3 and tray 4 data increased as the column moved towards flooding. Similarly, the magnitude of the first peak in the mutual information and residual Shannon entropy plots for tray 4 increased as the column moved towards flooding, whereas the peaks decreased for tray 3 data. The peaks for time series at different pressures in the Mutual information and residual Shannon entropy plot for tray 4 were more distinguishable than tray 3 data. Incipient flooding is more recognizable by observing tray 4 data. The patterns in the differential pressure data collected at UTK are repeatable. The figures in appendix A, B and C prove the repeatability of the UTK data. The Mutual information plot for tray 3 provides a better discrimination than the autocorrelation function whereas for tray 4, both Mutual information and autocorrelation provide similar differentiation between the incipient flooding and the normal pressure data.

The mean differential pressure increases as the FRI column moves towards flooding. The standard deviation of the time series increased and then decreased as the column approached flooding. FFT plots for the FRI data show peaks at 0.5 Hz and around 2.5 Hz. The magnitude of the peaks in the autocorrelation, mutual information and residual Shannon entropy plots for the time series data close to flooding (pressures from 16.77 to 19.65 psig) was higher than time series collected at the start up (low pressures from 5-16.67 psig) of the column. There was no increasing pattern for the time series

data with mean ΔP higher than 16.67 inches of H_2O across the tray in the FRI column.

This research shows that besides observing the mean and the standard deviation values across the trays or columns, analysis of high speed differential pressure measurements helps in detecting incipient flooding. If this analysis can be done online during the collection of the data, incipient flooding can be detected by observing the values of autocorrelation, mutual information and residual Shannon entropy at a predetermined lag. Further experimentation is required on pilot size distillation columns (FRI) to determine the lag and the maximum allowable values for autocorrelation, mutual information and residual Shannon entropy.

5.2 FUTURE WORK

The experiments at FRI pilot plant were run according the requirements of the member companies which were testing their respective trays. For the future runs at FRI or any other pilot plant, the runs need to be specially designed for this type of data collection. More information should be available regarding the packing or the trays used in the column.

All the runs on the column at UTK were done with the same tray configuration with tray 4 being the sieve tray. The configuration of the trays should be changed to all sieve trays or a different kind of tray. This will

provide a better idea whether similar patterns in the ACF, MI and RSE plots are observed or not for a different tray configuration.

During the runs at UTK column, the steam pressure fluctuated when the reboiler pressure was increased above 30 psig. This results in more fluctuations on the steam valve while trying the control the steam pressure at a constant pressure. The steam pressure supply should be constant when the column is run at higher reboiler steam pressures.

There is no concrete evidence to identify the origin of the frequencies in the FFT plots for FRI and UTK data. High speed video cameras can be used to collect and study the bubbling and movement of liquid waves on the tray. The high speed videos can then be related to the time series data and the origin of the frequencies in the FFT plot can be quantified.

All the analysis on the UTK and FRI columns was done after the experiments were complete. A code written in Matlab or LabVIEW will help in doing the analysis online and detect incipient flooding while the column is running. The effect of transients on the linear and non-linear analysis can also be studies with the online analysis tool.

BIBLIOGRAPHY

Bibliography

[1] C. S. Daw, C. E. A. Finney, E. R. Tracy, “A review of symbolic analysis of experimental data”, *American Institute of Physics*, Vol. 74, No. 2(2003), 915-930.

[2] C. E. A. Finney, K. Nguyen, C. S. Daw, J. S. Halow, “Symbol-Sequence Statistics for monitoring fluidization”.

[3] C. E. A. Finney, “MCEC Nonlinear Time Series Analysis Toolbox for MATLAB – Reference Manual and Tutorial”, Release 2+, 1999.

[4] C. S. Daw, M. B. Kennel, C. E. A. Finney, F. T. Connolly, “Observing and modeling nonlinear dynamics in an internal combustion engine”, Physical Review E57 (1998), 2811–2819.

[5] Distillation column flooding predictor
http://www.eere.energy.gov/inventions/pdfs/2ndpoint.pdf#search=%22fact%20sheets%20about%20distillation%22

[6] New Energy-Efficient Cocurrent Distillation Technology Is a Major Step Forward for Industry
http://es.epa.gov/techinfo/facts/distlatn.html

[7] A. M. Fraser, H. L. Swinney, “Independent coordinates for strange attractors from mutual information”, Physical Review A, Vol. 33, No.2 (1986), 1134-1140.

[8] H. Z. Kister, “Distillation operation”, McGraw-Hill Publishing Company, 1990.

[9] A. I. Karamavruc, N. N. Clark, J. S. Halow, “Application of mutual information theory to fluid bed temperature and differential pressure signal analysis”, Elsevier Science, Powder Technology 84 (1995), 247-257.

[10] “LabVIEW Analysis Concepts”, National Instruments, March 2004.

[11] J. Yang and L. A. Glasgow, “Chaos Analysis of bubble formation transition phenomena on a multi-hole sieve plate”, Chem. Eng. Comm., 2000, Vol. 177, 49-64.

[12] C.E. Shannon, "A Mathematical Theory of Communication", *Bell System Technical Journal*, vol. 27, 379-423, 623-656, July, 1948.

[13] S. Rajput (2003), “Detecting Changes in Global Dynamics with Principal Curves and Information Theory”, Thesis, University of Tennessee, 2003.

[14] Q. Guo, G. Yue, and J. Werther, “Dynamics of Pressure Fluctuation in a Bubbling Fluidized Bed at High Temperature”, Ind. Eng. Chem. Res. 2002, 41, 3482-3488.

[15] X. Tang and E. Tracy, “Data compression and information retrieval vai symbolization”, American Institute of Physics, vol. 8, 688-700, September 1998

[16] Crutchfield, J. P. and Packard, N. H. (1983), Symbolic dynamics of noisy chaos, Physica D, 7, 201.

[17] C. S. Daw, C. E. A. Finney, M. B. Kennel, “Symbolic approach for measuring temporal “irreversibility””, The American Physical Society, vol. 62 (2), 1912-1921, August 2000.

[18] Fractional Research Inc. website (www.fri.org)

[19] H. Kantz and T. Schreiber (1997), “Nonlinear Time Series Analysis”, Cambridge University Press.

[20] S. Rajput and D. Bruns, “Nonlinear time series analysis of pressure measurements on structured –packing column”, Presentation at AICHE 2003 Annual meeting, San Francisco.

[21] Department of Energy, Office of Information Technology, DE-PS36-03GO93015 31, Appendix F, 2004.

[22] Stober, Bernie, Exxon Mobil, Private Communication, Chief Technologist, 2005

[23] Schwanke, Carl O., ExxonMobil, Private Communication, Measurement and Control Engineering Center, Industrial Advisory Board Meeting, Oct. 2-3, 2003, Knoxville, TN.

[24] Lewis, J. Christopher, Seibert, A. Frank, Fair, James R., Performance Evaluation of the Pattern Recognition Flooding Predictor, Report presented to George E. Dzyacky, University of Texas at Austin (2001).

[25] Nguyen, K. , Daw, C. S., Chakka, P. , Cheng, M. , Bruns, D. D., Finney, C .E .A. & Kennel, M. .B., “Spatio-temporal dynamics in a train of rising bubbles,” *Chem. Eng. J.*, Vol**.** 64. No. 1, pp. 191-197 (1996).

[26] Sarnobat, Sachin U., Rajput, Sandeep, Bruns, Duane D., DePaoli, David W., Daw, C. Stuart, Nguyen, Ke, “The impact of external electrostatic fields on gas-liquid bubbling dynamics,” *Chemical Engineering Science*, Vol. 59, pp. 247-258 (2004).

[27] Daw, Fuller, Flynn, Finney, “Application of symbol sequence analysis and temporal irreversibility to monitoring and controlling boiler flames,” Pennie & Edmonds, LLP

- United States Patent Application 20030093246, May 15, 2003
- United States Patent Application 20040039551, Feburary 26, 2004

[28] Dzacky, George E. Distillation Column Predictor. U. S. Patent 5,784,538 (1999).

[29] Jaroslav Stark and Kate Hardy, “Chaos: Useful at Last,” *Science*, Vol. 301, No. 29, pp. 1193-1194 (2003).

[30] G. Chen, FRI, OCAST Proposal, Distillation Column Flooding Sensor, April 19, 2005

[31] Mulhe, Finney, Nguyen, Daw, “Method of applying non-linear dynamics to control a gas-phase polyethylene reactor operability,” U.S. Patent Application 20030121330, July 3, 2003, Univation Technologies, LLC.

[32] Davis, Daw, Feldkamp, Hoard, Yuan, Connolly, “Methods of controlling cyclic variation in engine combustion”

- United States Patent number: 5,921,221, July 13, 1999

[33] www.validyne.com “Estimating the Frequency Response of Variable Reluctance Sensors in Gas”.

APPENDICES

APPENDICES

APPENDIX A: LINEAR ANALYSIS FOR DIFFERENT RUNS

This appendix shows mean, standard deviation, FFT plots and autocorrelation plots in order for UTK distillation column data collected across tray 4 (sieve tray) using MKS sensor on September 18, 2006, May 2, 2007 and May 3, 2007. The same quantities for UTK distillation column data collected across tray 4 (sieve tray) using the Validyne sensor on November 16, 2006 that is presented in the thesis body are repeated here for easy comparison.

A.1 Mean and Standard Deviation

The figures for each campaign for mean and standard deviation show similarities in patterns over all four experimental runs.

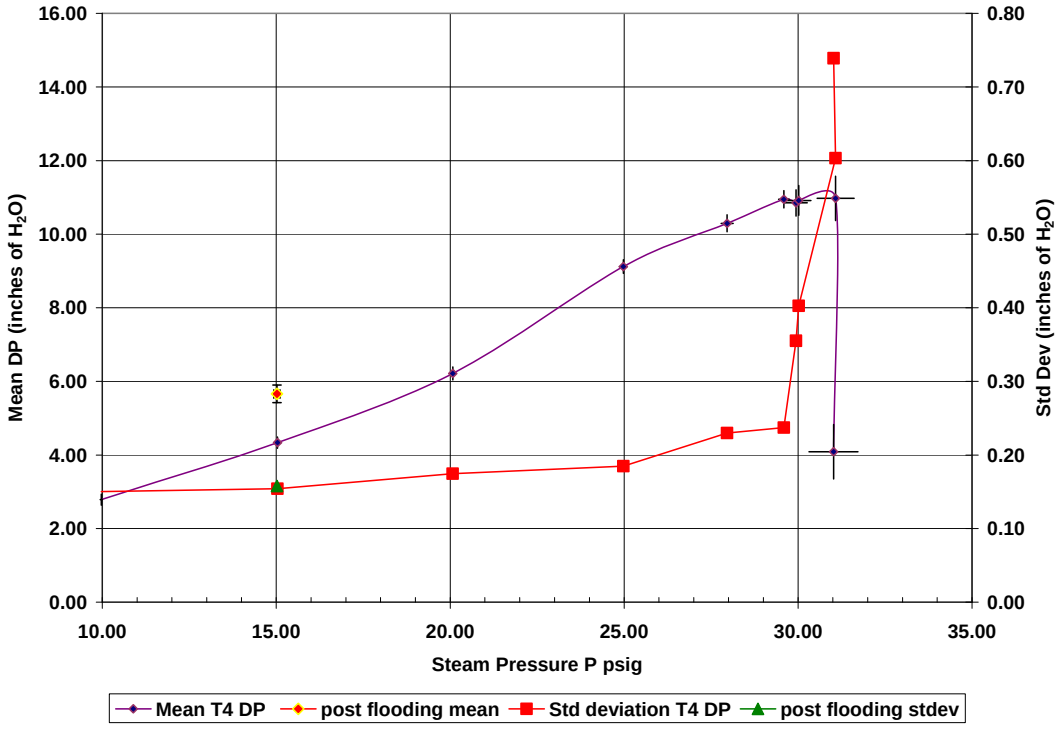


Figure A.1 Mean and standard deviation vs. reboiler steam pressure plot for tray 4 differential pressure data (UTK column, tray 4 data, November 16, 2006). Figure 4.5 repeated from section 4.

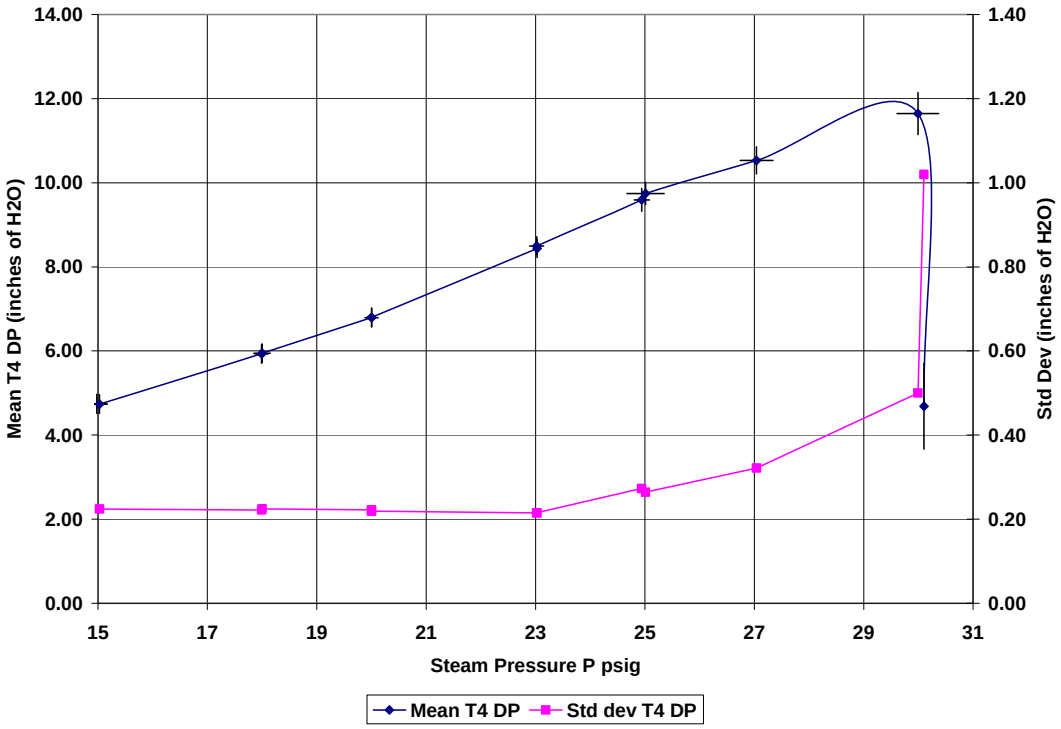


Figure A.2 Mean and standard deviation vs. reboiler steam pressure plot (UTK column, tray 4 data, September 18, 2006)

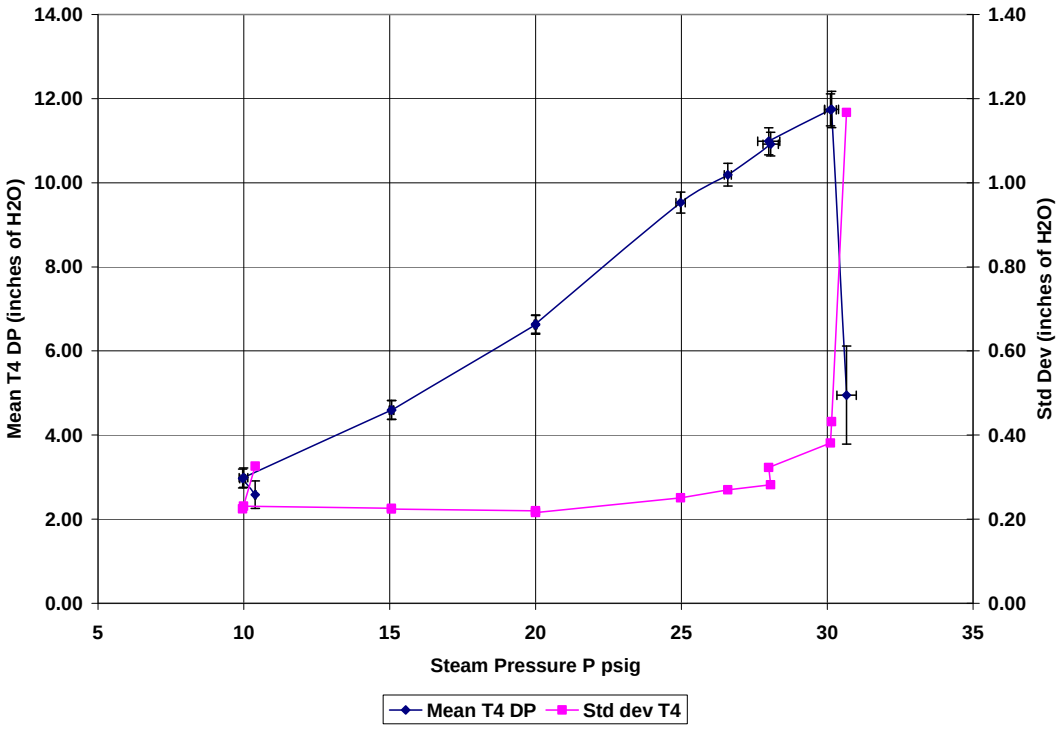


Figure A.3 Mean and standard deviation vs. reboiler steam pressure plot (UTK column, tray 4 data, October 2, 2006)

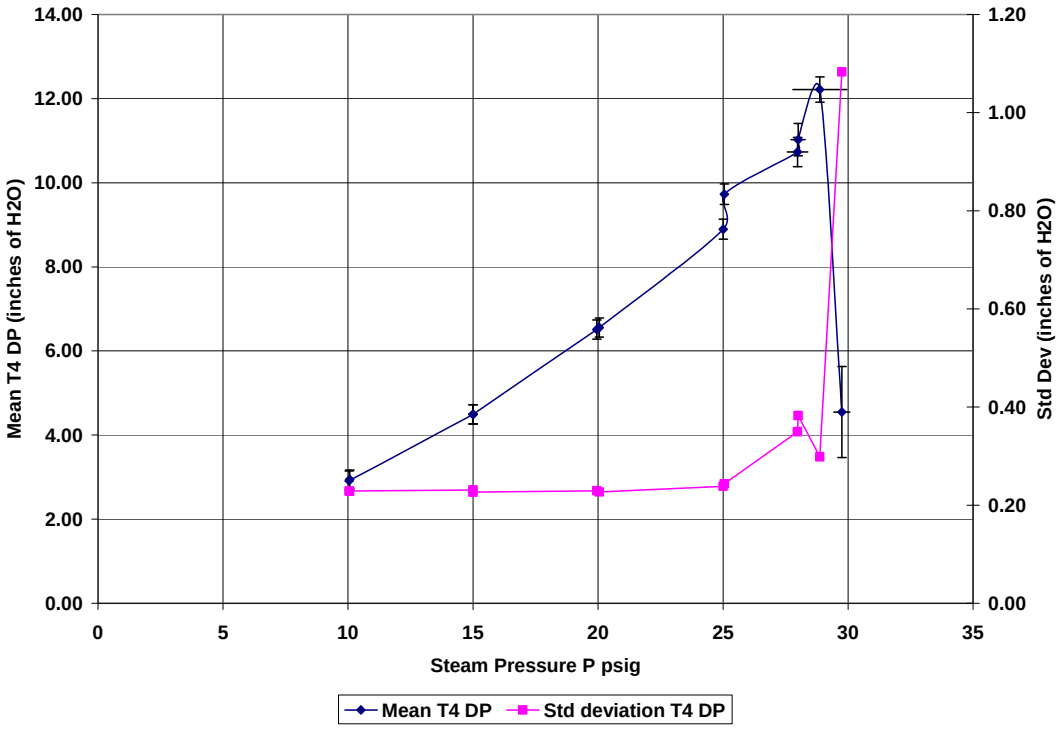


Figure A.4 Mean and standard deviation vs. reboiler steam pressure plot (UTK column, tray 4 data, October 3, 2006)

A.2 Frequency analysis

The figures for each campaign for frequency analysis show similarities in patterns over all four experimental runs. It is hard to see any reliable trends to us to track hydraulic state.

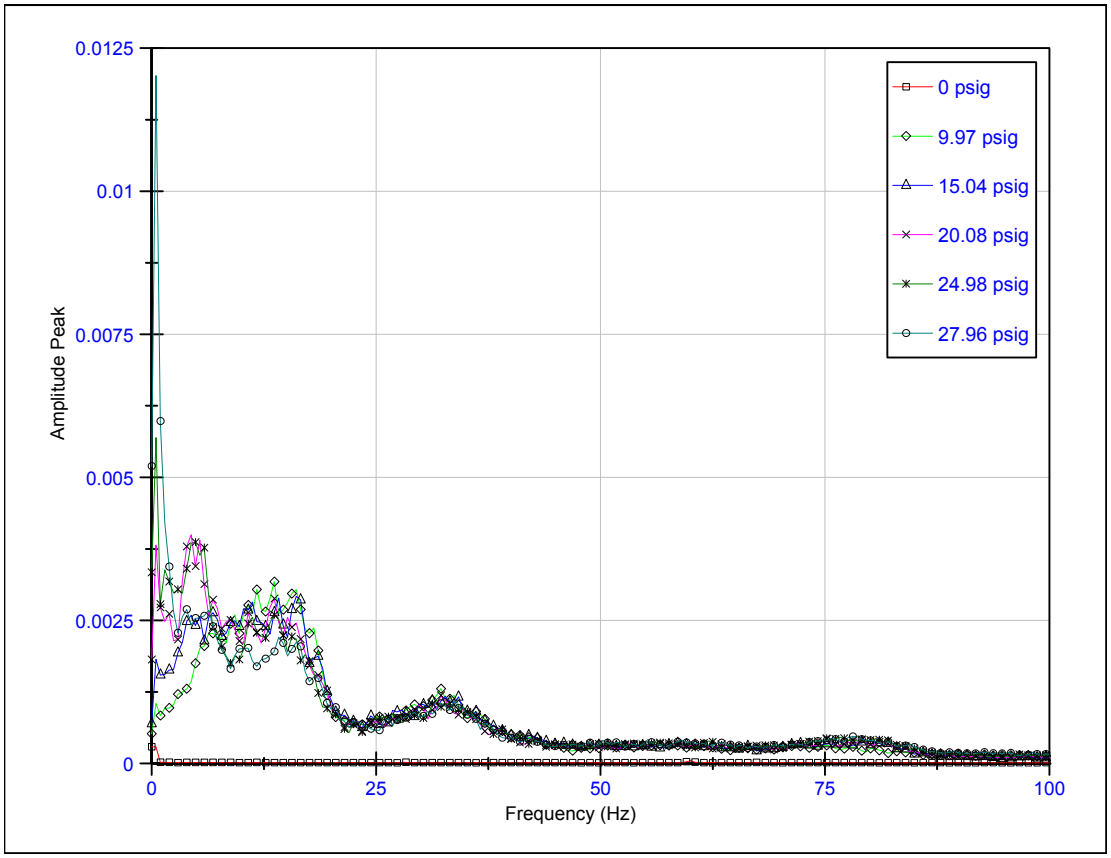


Figure A.5 FFT plot of differential pressure data collected across tray 4 for reboiler pressure range of 0 to 27.96 psig. (UTK column, tray 4 data, November 16, 2006). Figure 4.12 repeated from section 4.

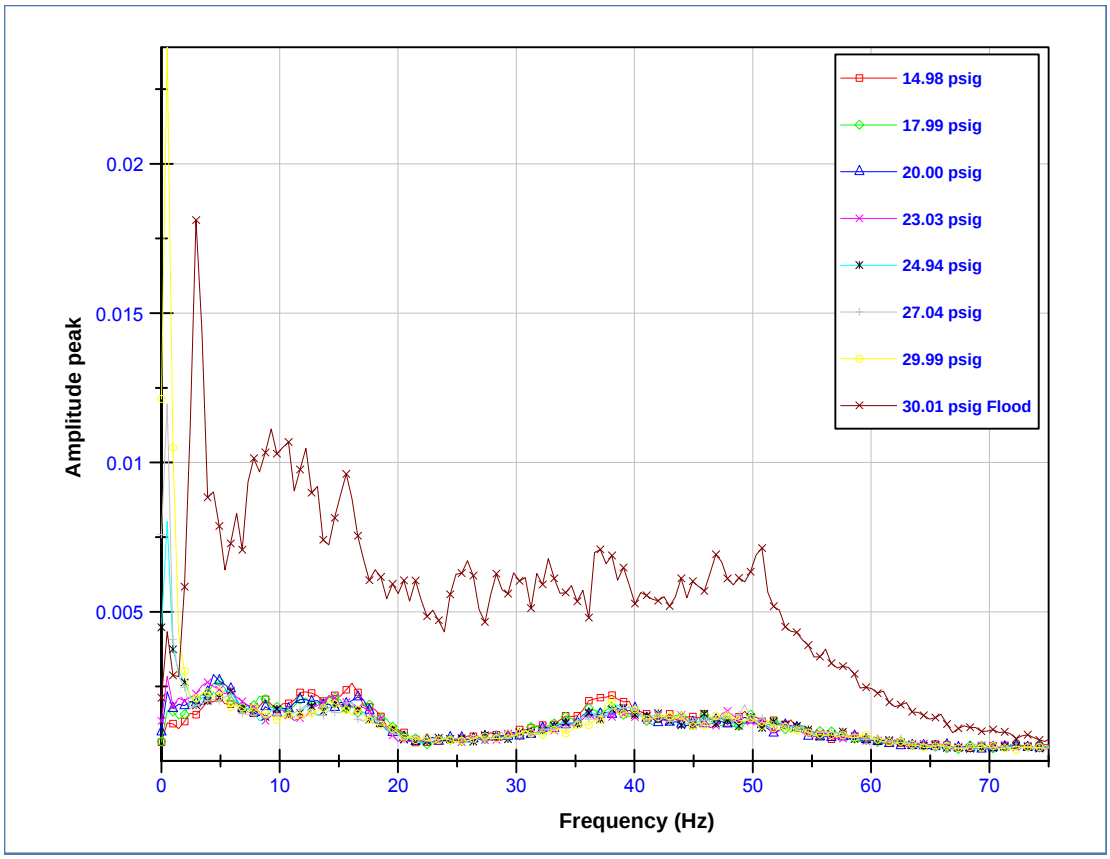


Figure A.6 FFT plot (UTK column, tray 4 data, September 18, 2006)

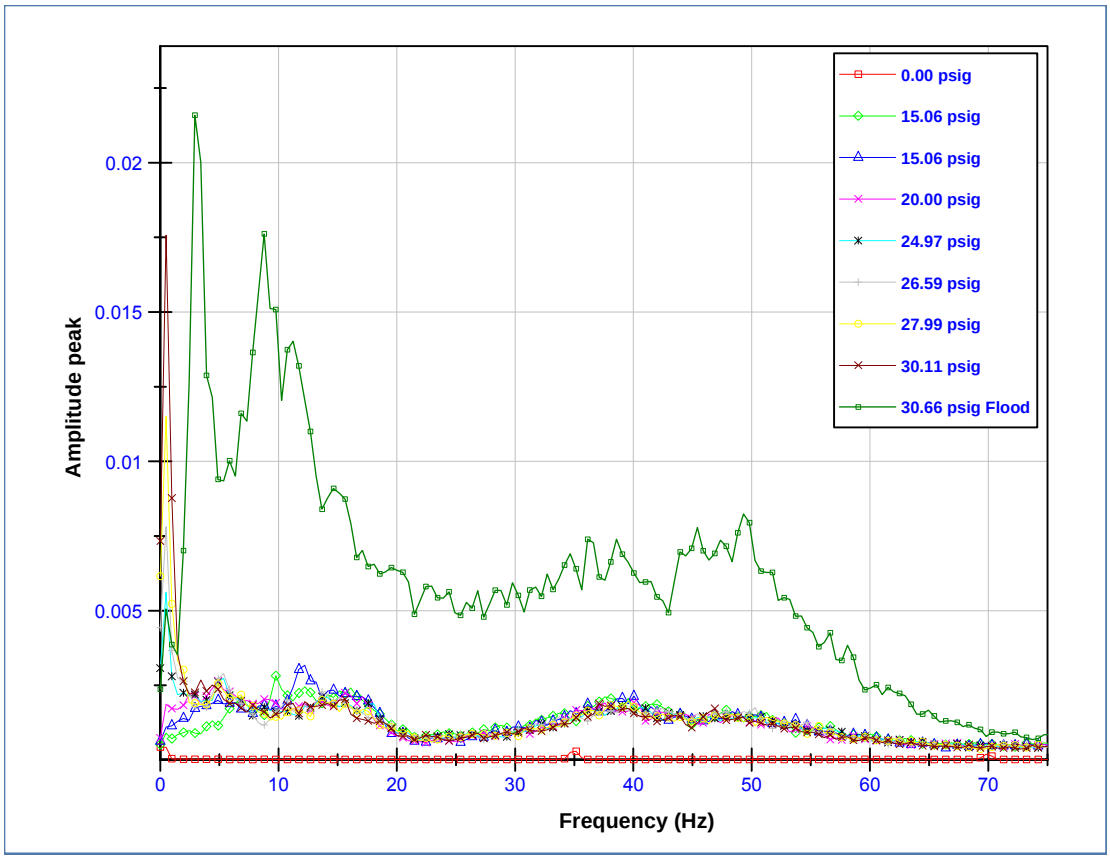


Figure A.7 FFT plot (UTK column, tray 4 data, October 2, 2006)

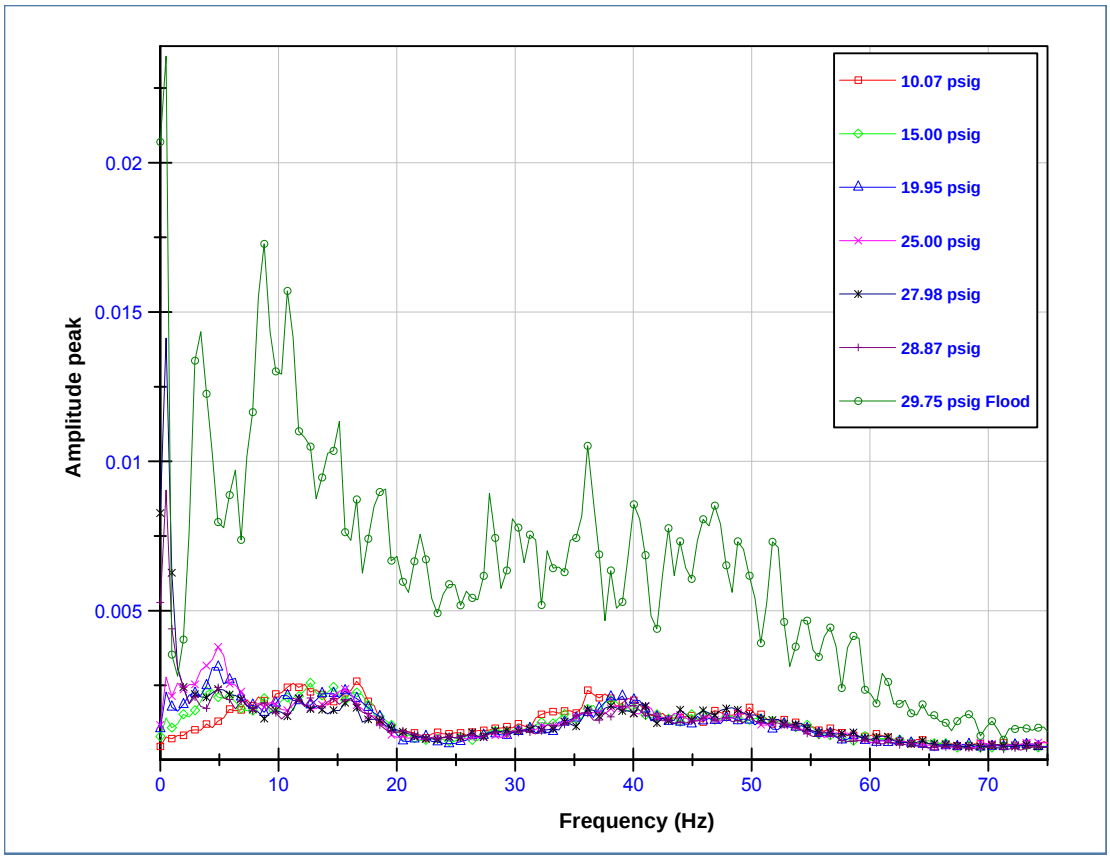


Figure A.8 FFT plot (UTK column, tray 4 data, October 3, 2006)

A.2 Autocorrelation Function analysis

The ACF curves for November 16, 2006 run do not show similarity with the ACF curves for the column runs on September 18, October 2, and October 3, 2005, which show similar ACF curves. The only difference between these column runs was that the ΔP across tray 4 was measured using Validyne sensor on November 16. The MKS sensor was used for measuring the ΔP on the column runs on September 18, October 2, and October 3, 2005.

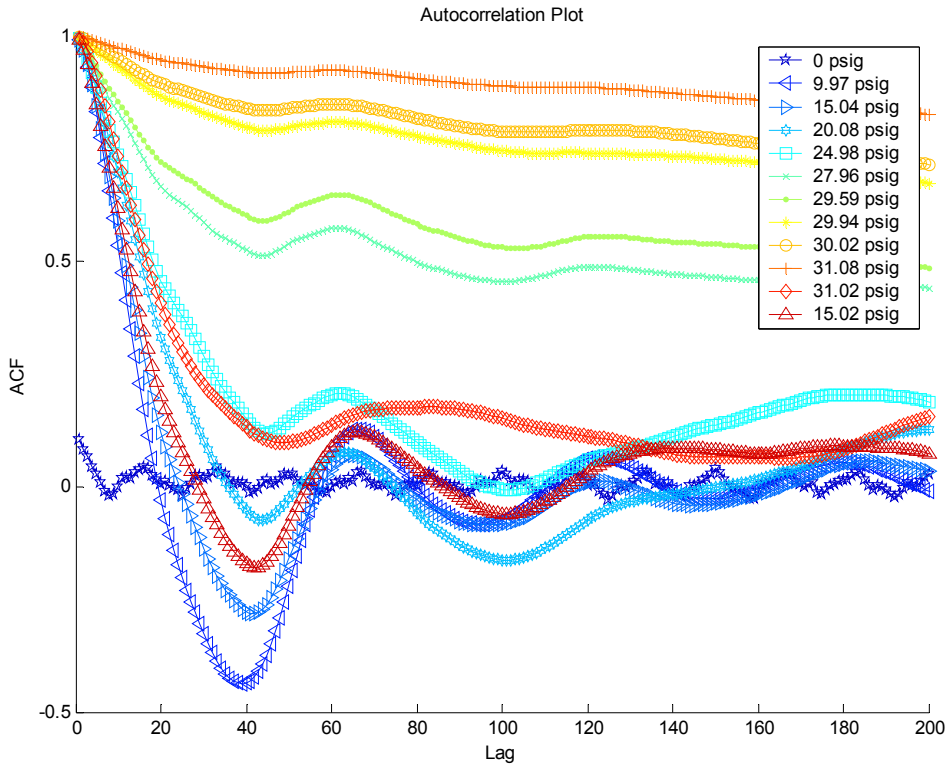


Figure A.9 Autocorrelation plot for tray 4 differential pressure data. (UTK column, tray 4 data, November 16, 2006). Figure 4.19 repeated from section 4.

The red 15.02 psig curve is the recovered from flooding data and the orange circle data is flooded data at 31.02 psig, and are not expected to follow the trend of the other data.

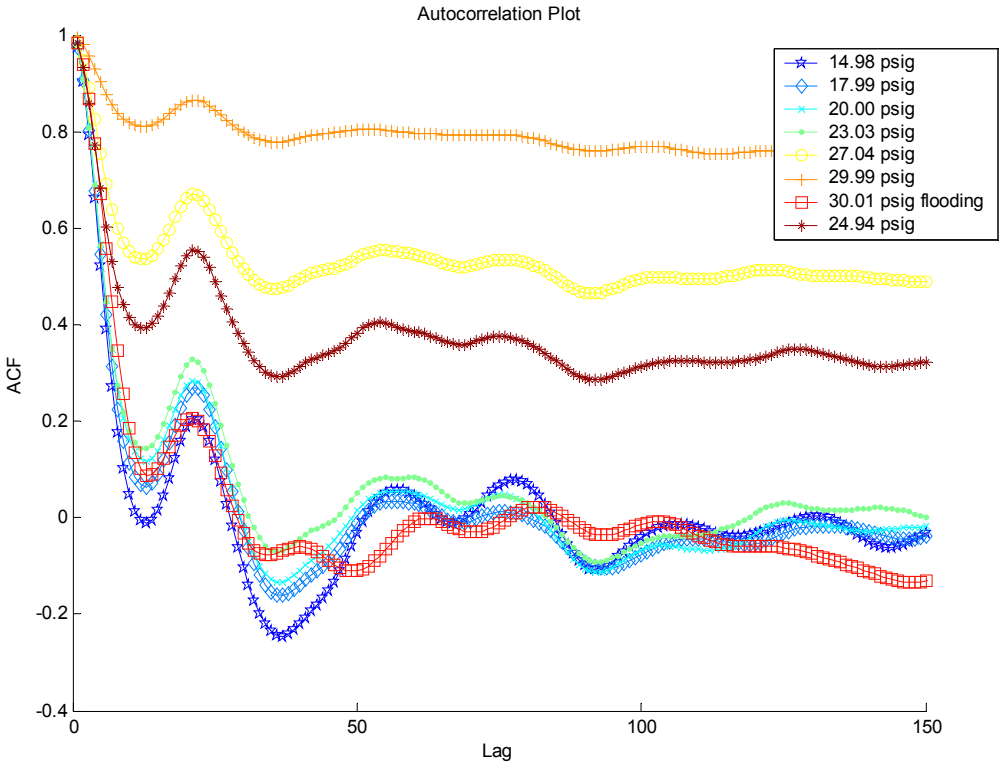


Figure A.10 Autocorrelation plot (UTK column, tray 4 data, September 18, 2006)

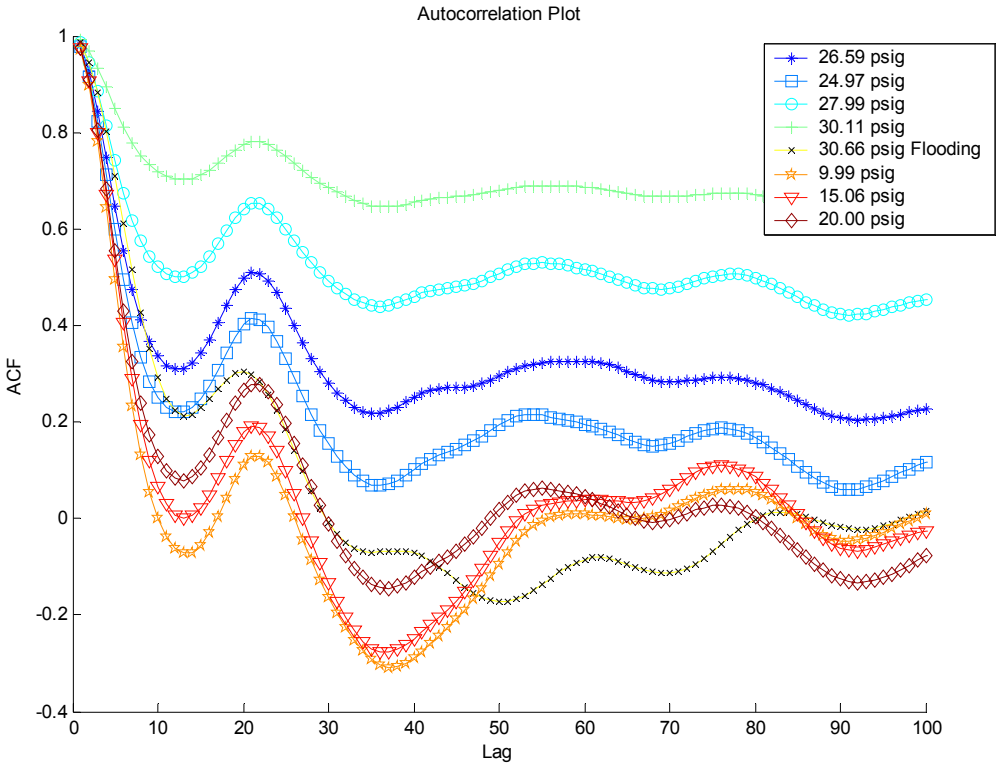


Figure A.11 Autocorrelation plot (UTK column, tray 4 data, October 2, 2006)

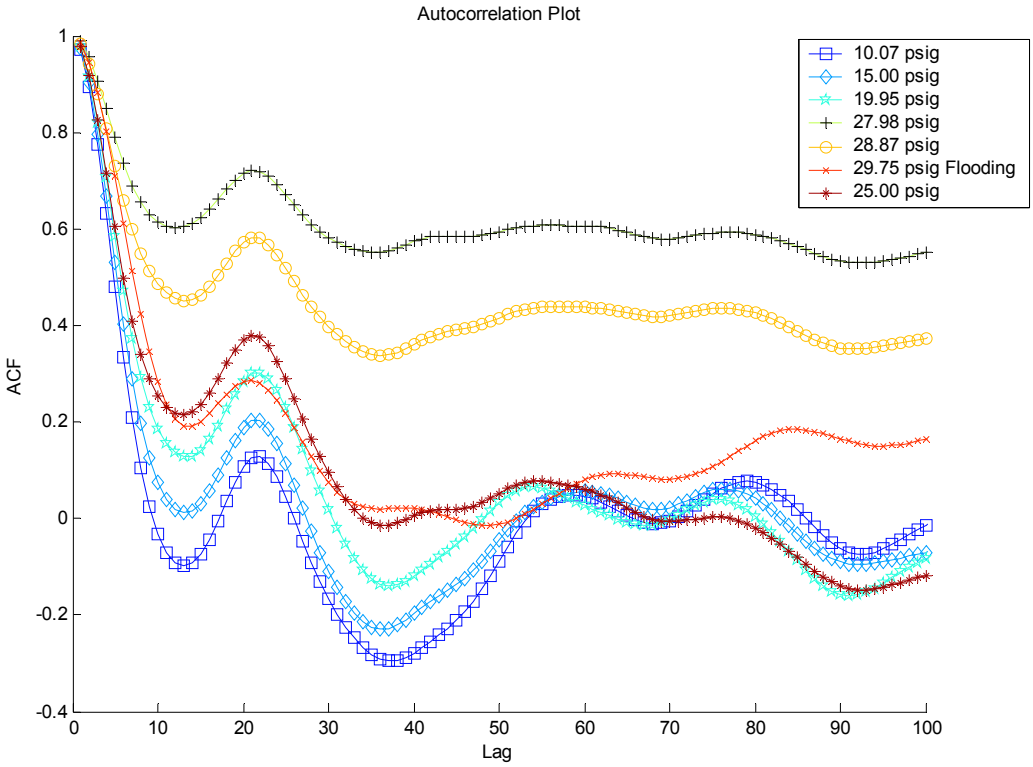


Figure A.12 Autocorrelation plot (UTK column, tray 4 data, October 3, 2006)

APPENDIX B: NON-LINEAR ANALYSIS FOR DIFFERENT RUNS

The MI and RSE plots for November 16, 2006 run do not show similarity with the MI and RSE plot for the column runs on September 18, October 2, and October 3, 2005, which show similar MI and RSE curves. The only difference between these column runs was that the ΔP across tray 4 was measured using Validyne sensor on November 16. The MKS sensor was used for measuring the ΔP on the column runs on September 18, October 2, and October 3, 2005.

Figures in appendix B shows the Mutual information and Shannon entropy plots for distillation column data collected across tray 4 using MKS sensor on September 18, 2006, May 2, 2007 and May 3, 2007. The figures show similarities in patterns on all the three experimental runs.

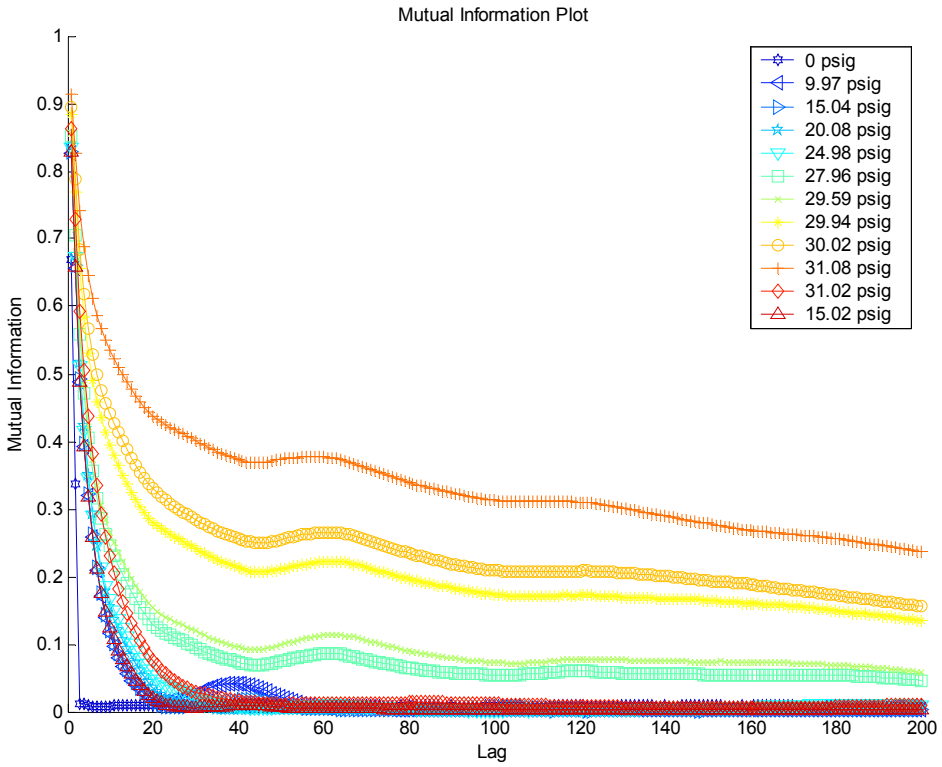


Figure B.1 Mutual Information plot for tray 4 with all differential pressure data. (UTK column, tray 4 data, November 16, 2006). Figure 4.23 repeated from section 4.

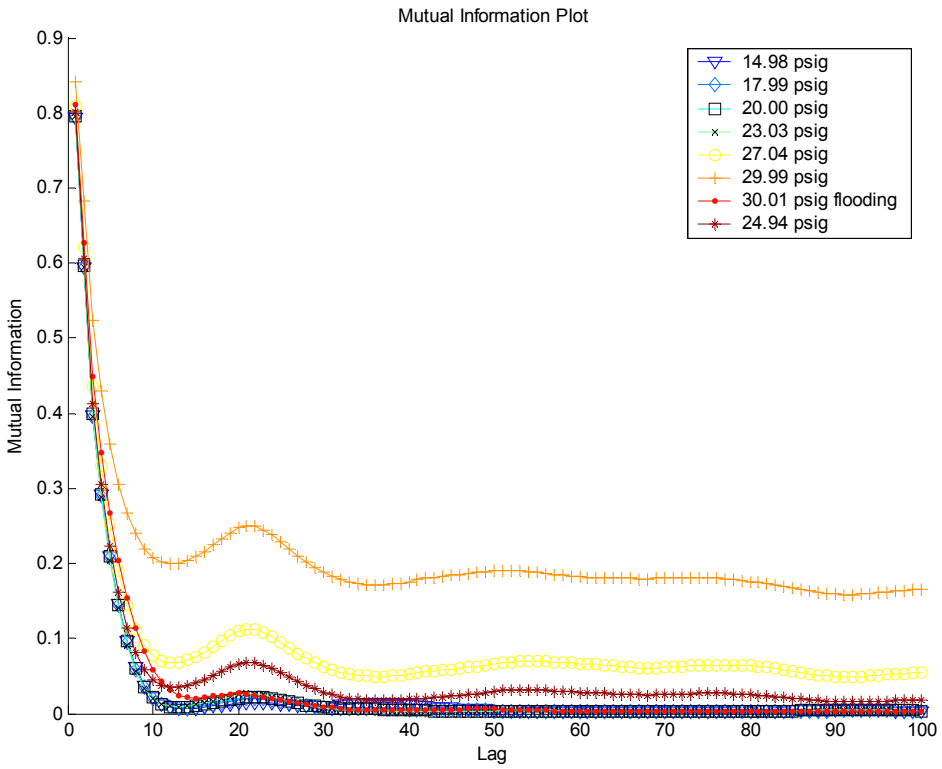


Figure B.2 Mutual information plot (UTK column, tray 4 data, September 18, 2006)

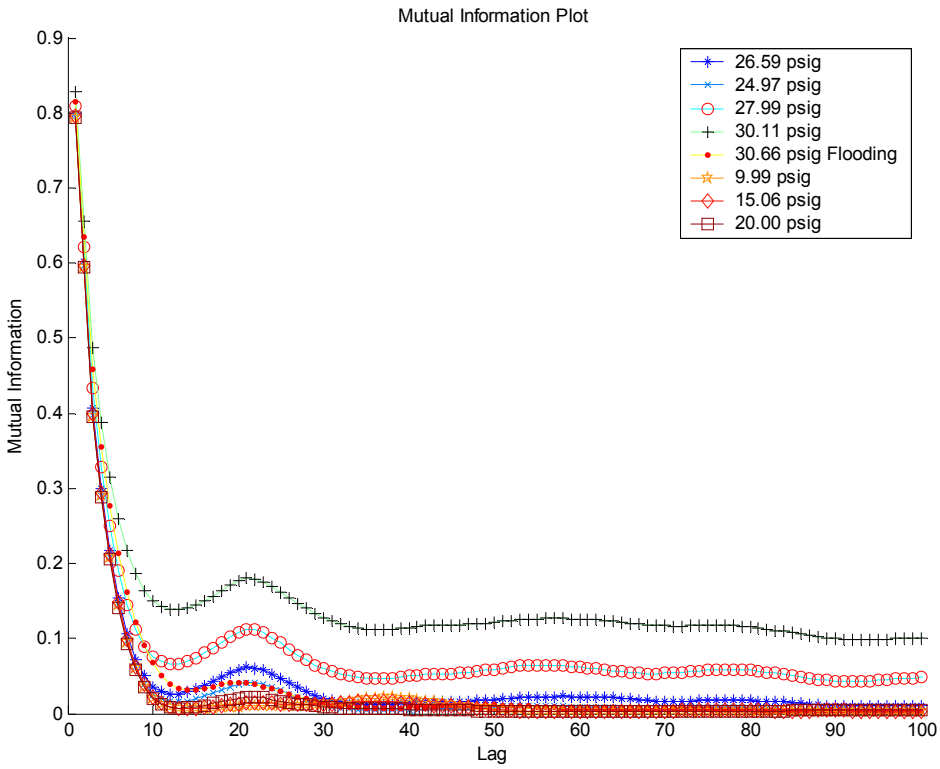


Figure B.3 Mutual information plot (UTK column, tray 4 data, October 2, 2006)

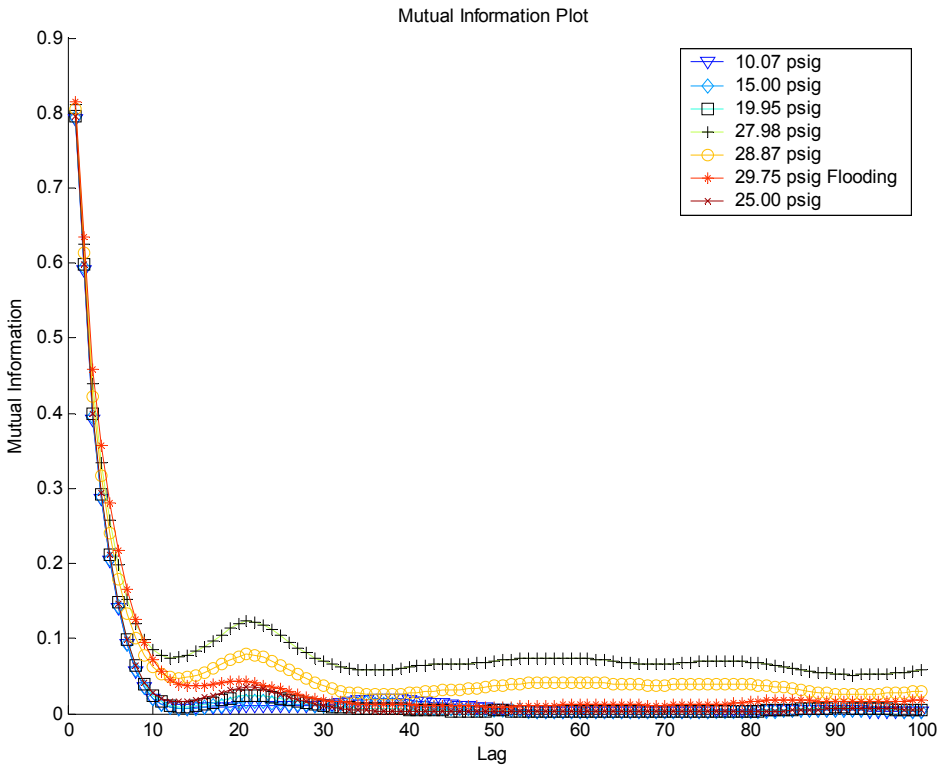


Figure B.4 Mutual information plot (UTK column, tray 4 data, October 3, 2006)

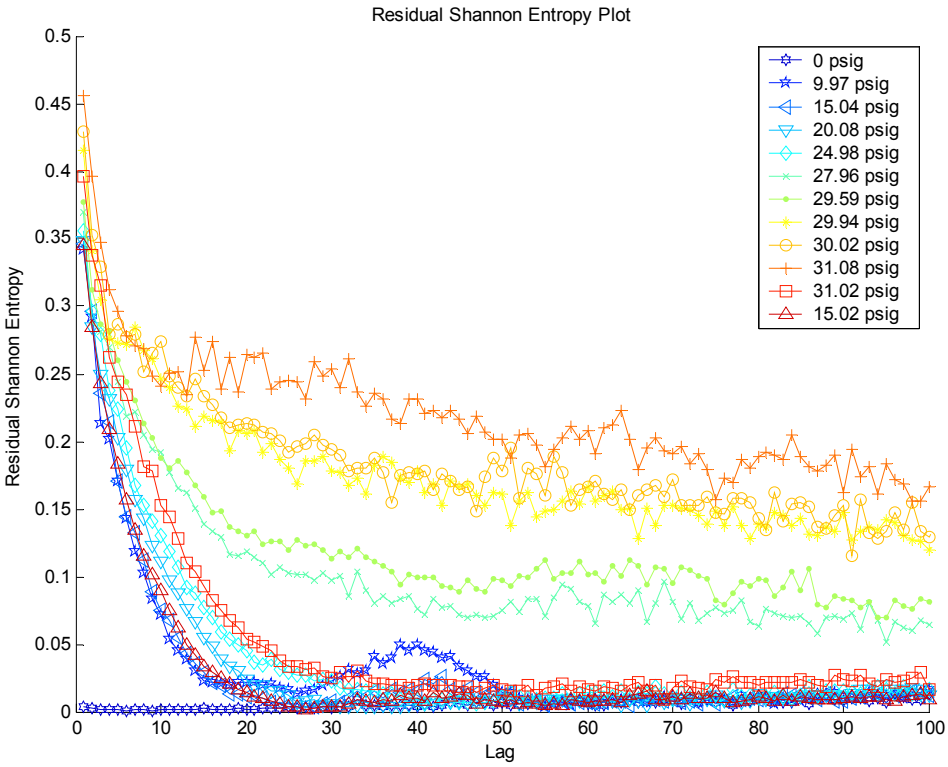


Figure B.5 Residual Shannon entropy plot for tray 4 data for all reboiler pressures. (UTK column, tray 4 data, November 16, 2006). Figure 4.26 repeated from section 4.

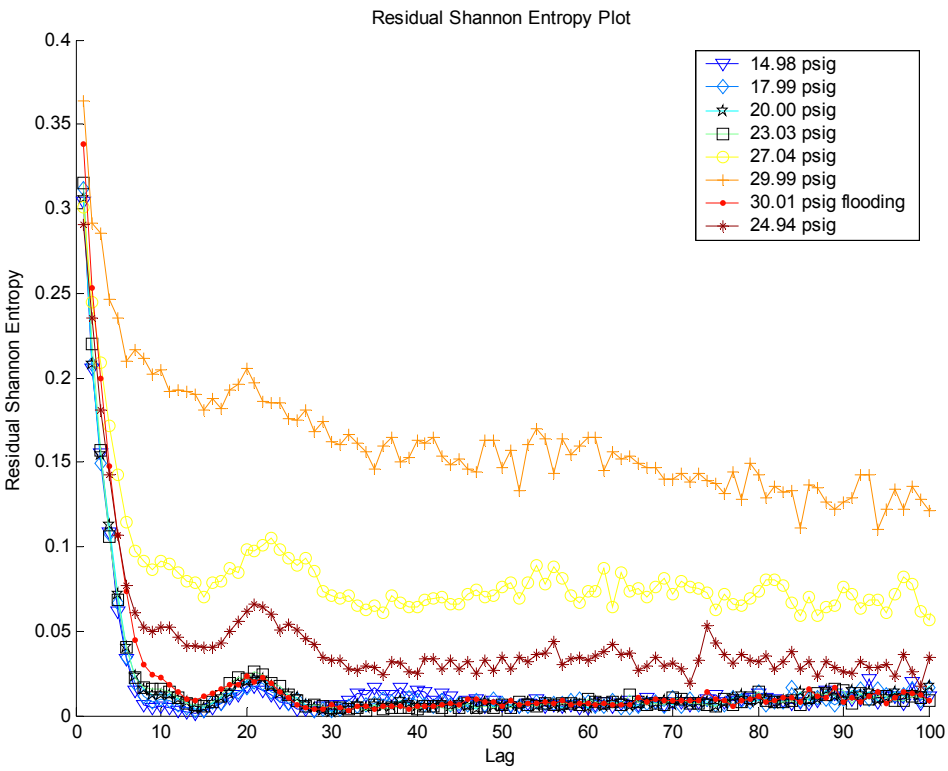


Figure B.6 Residual Shannon entropy plot (UTK column, tray 4 data, September 18, 2006)

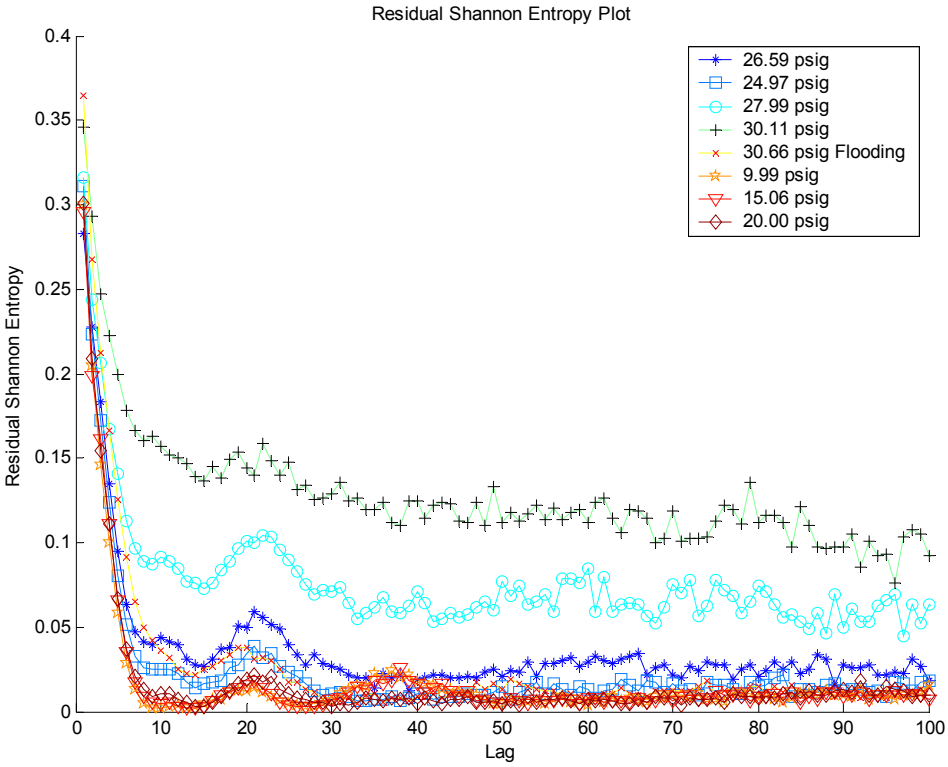


Figure B.7 Residual Shannon entropy plot (UTK column, tray 4 data, October 2, 2006)

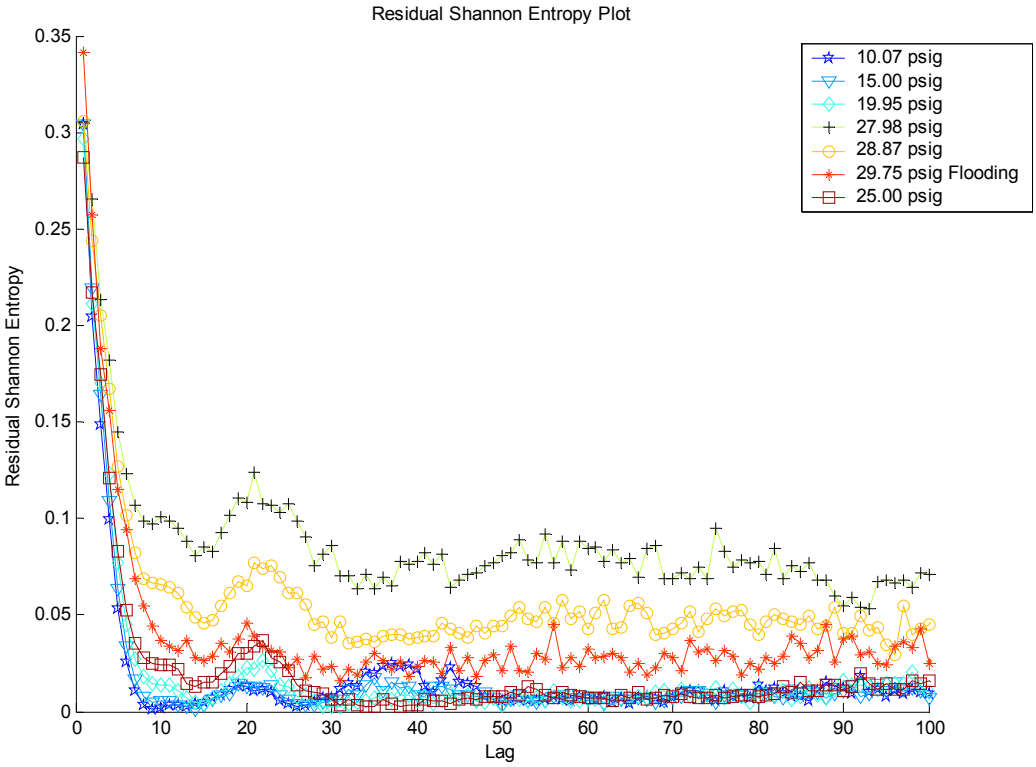


Figure B.8 Residual Shannon entropy plot (UTK column, tray 4 data, October 3, 2006)

APPENDIX C: RUNNING MEAN AND VARIANCE FOR UTK DATA

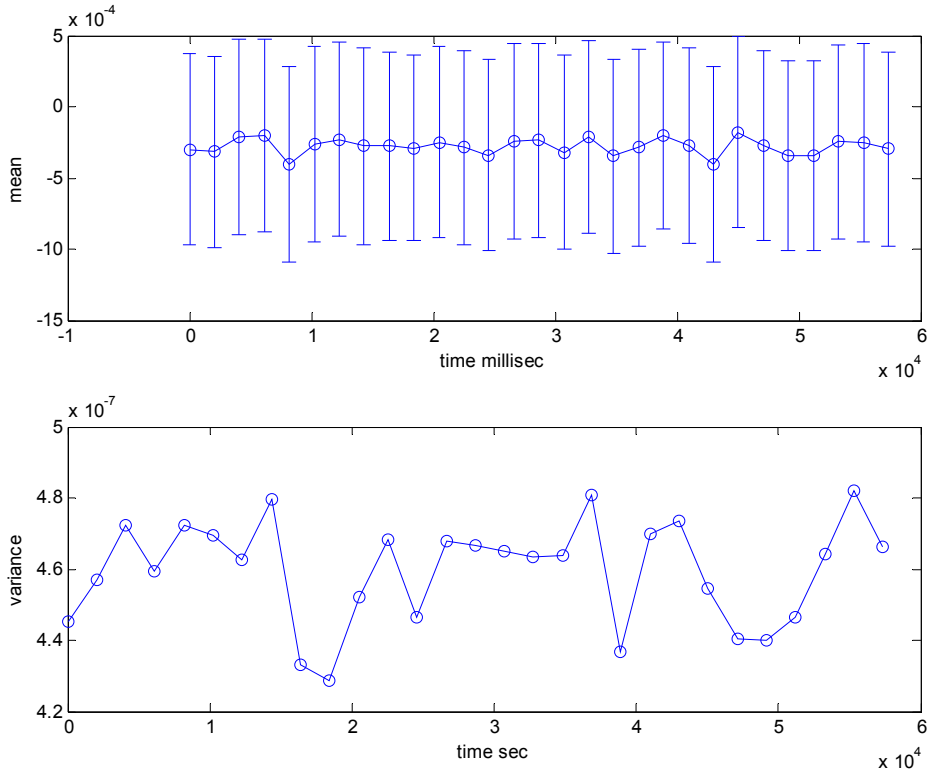


Figure C.1 Running mean and variance for tray 3 time series at reboiler pressure = 0 psig

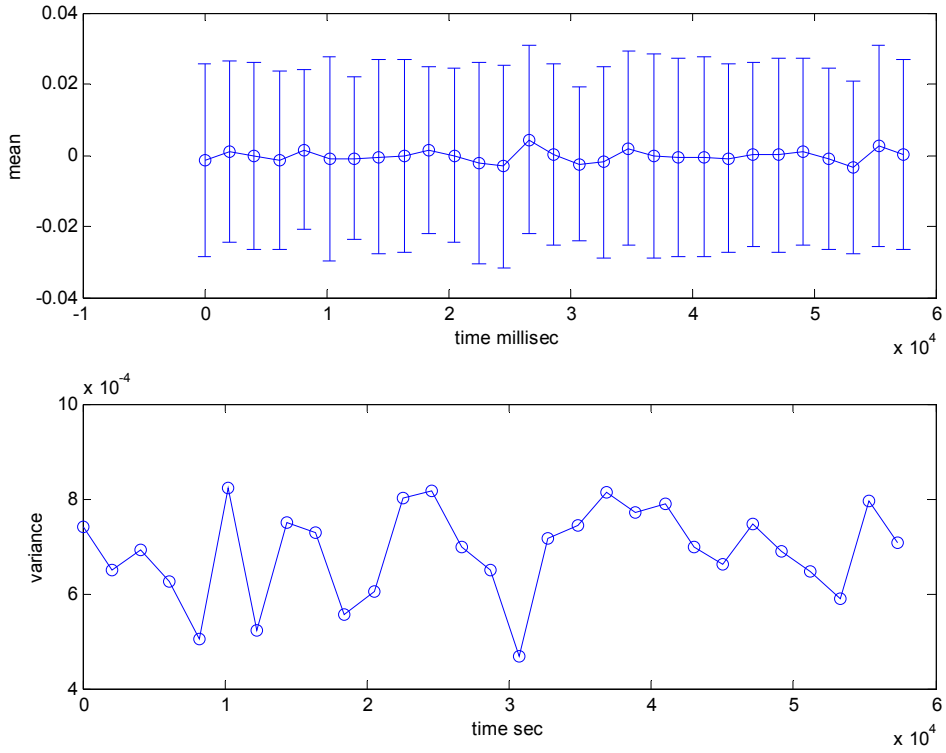


Figure C.2 Running mean and variance for tray 3 time series at reboiler pressure = 9.97 psig

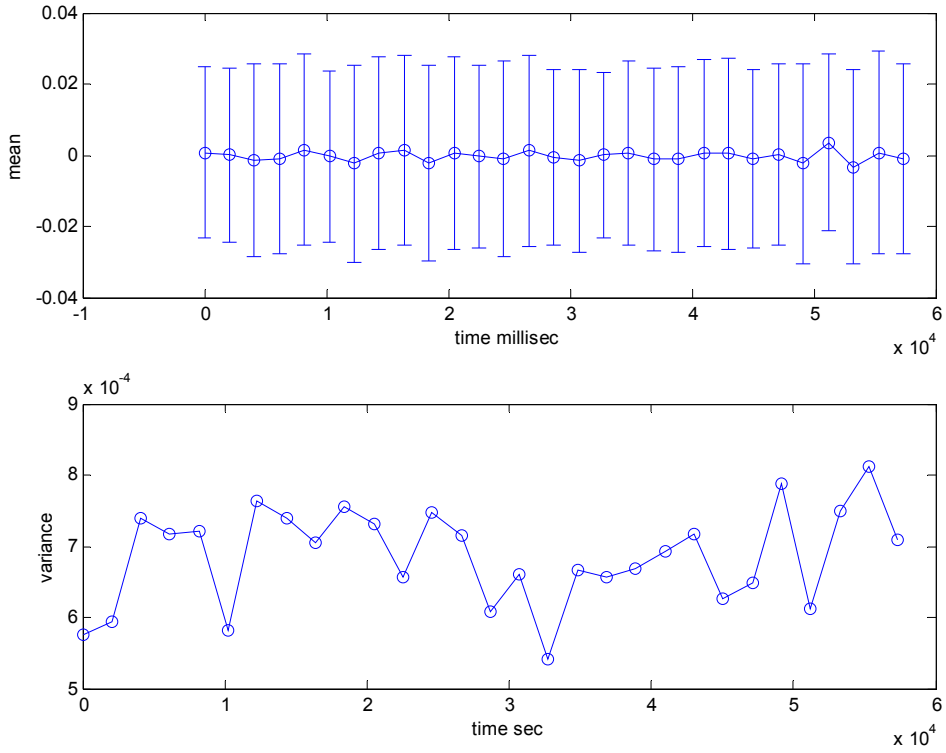


Figure C.3 Running mean and variance for tray 3 time series at reboiler pressure = 15.04 psig

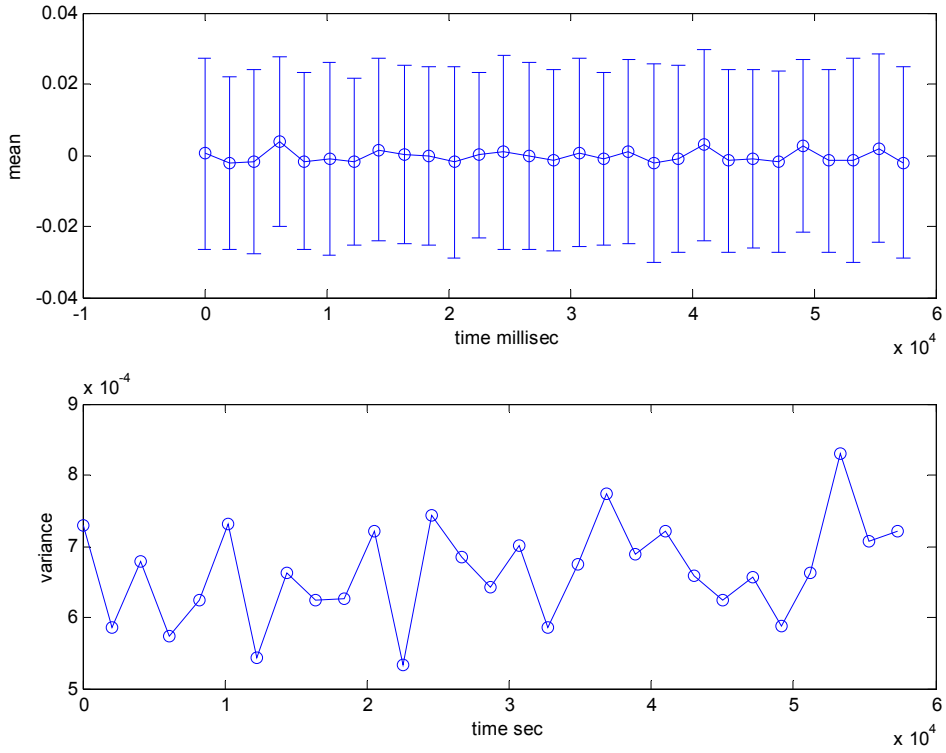


Figure C.4 Running mean and variance for tray 3 time series at reboiler pressure = 20.08 psig

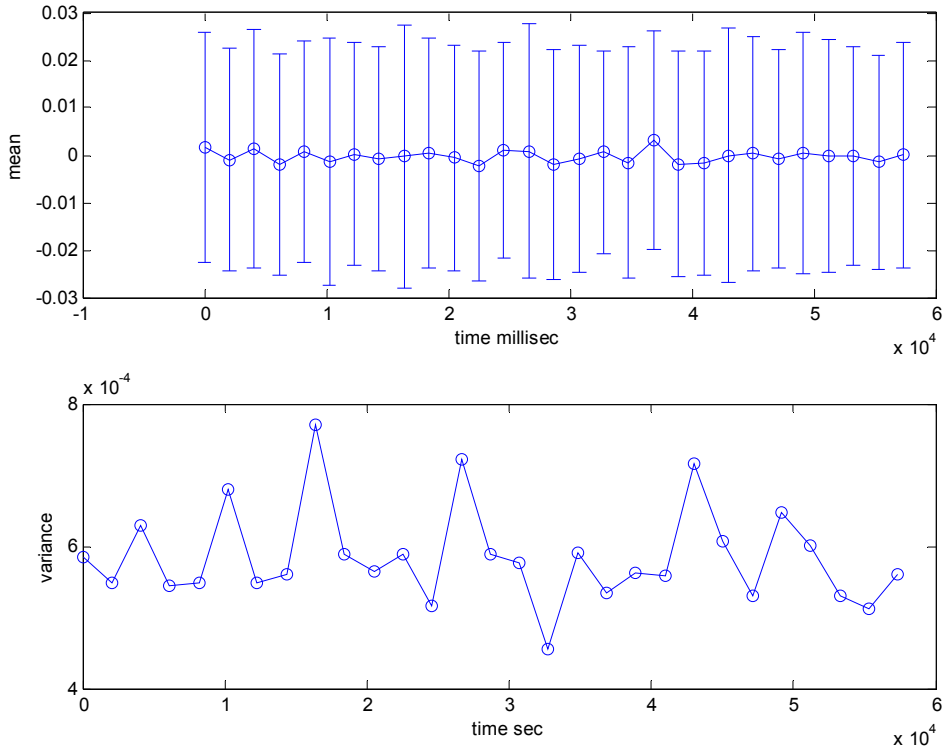


Figure C.5 Running mean and variance for tray 3 time series at reboiler pressure = 24.98 psig

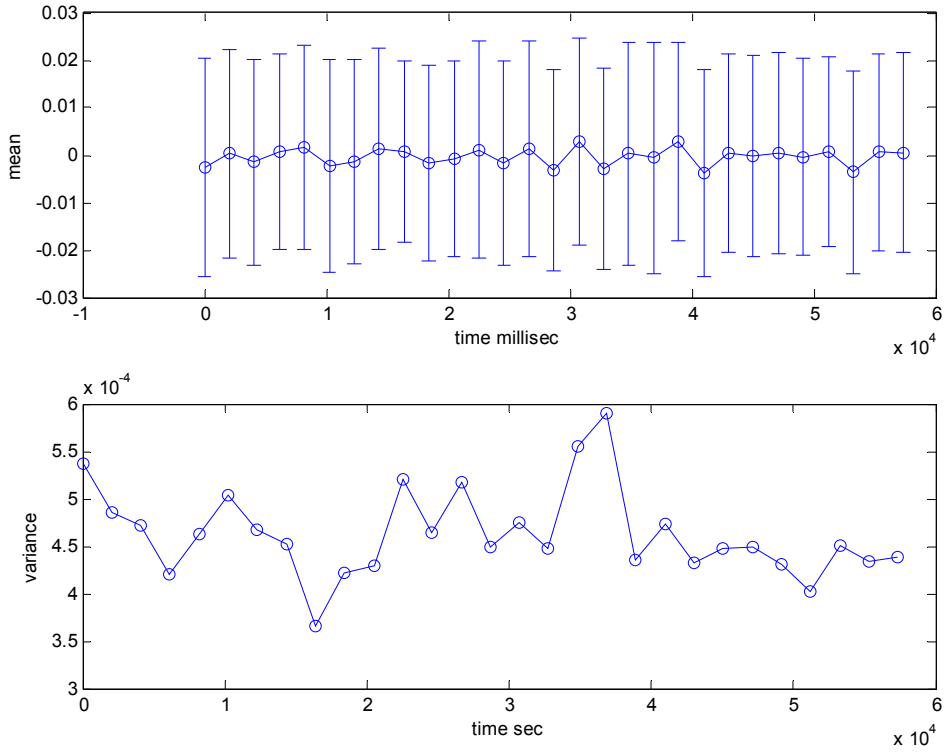


Figure C.6 Running mean and variance for tray 3 time series at reboiler pressure = 27.96 psig

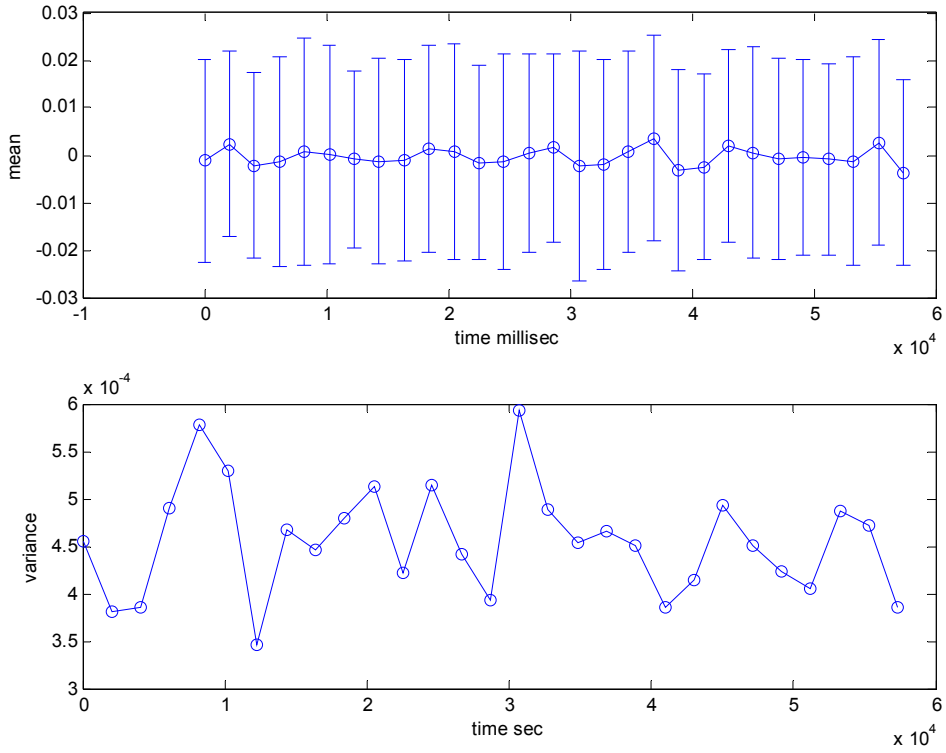


Figure C.7 Running mean and variance for tray 3 time series at reboiler pressure = 29.59 psig

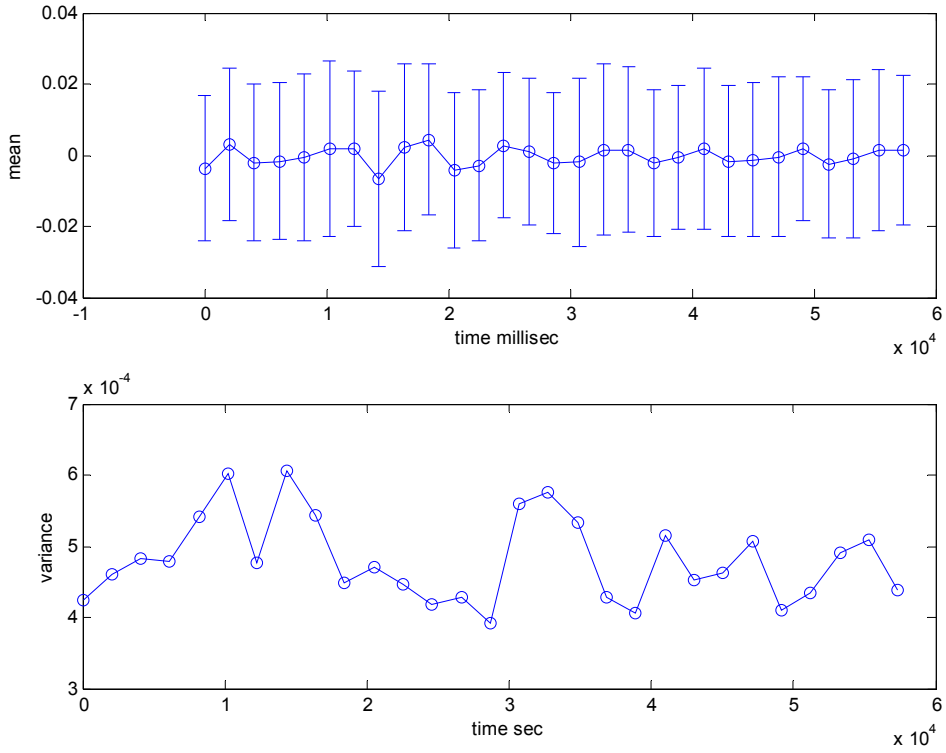


Figure C.8 Running mean and variance for tray 3 time series at reboiler pressure = 29.94 psig

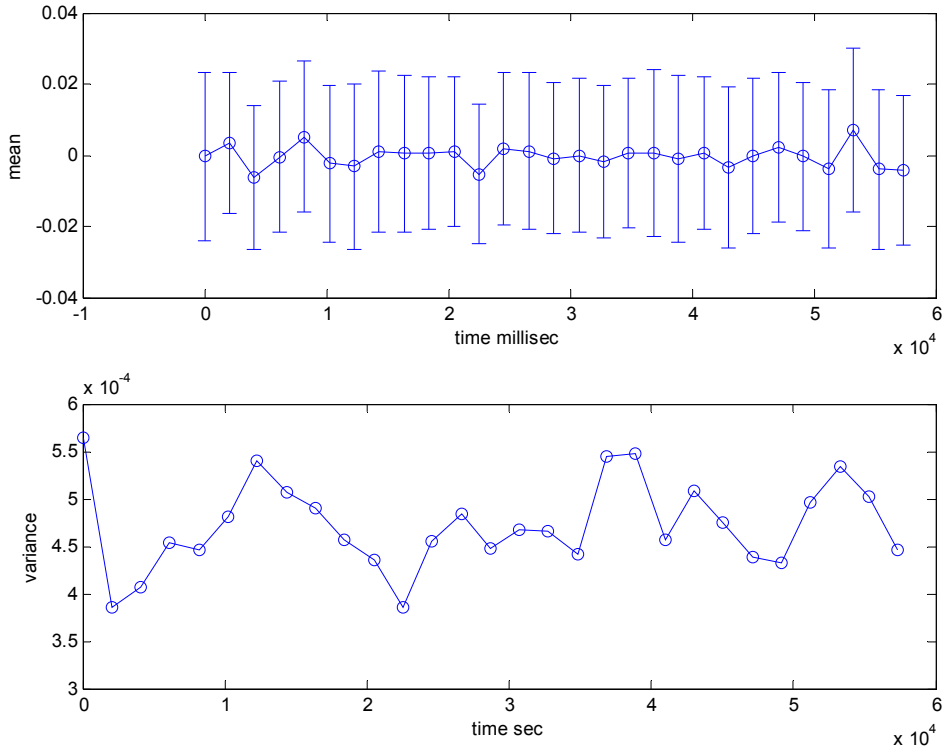


Figure C.9 Running mean and variance for tray 3 time series at reboiler pressure = 30.02 psig

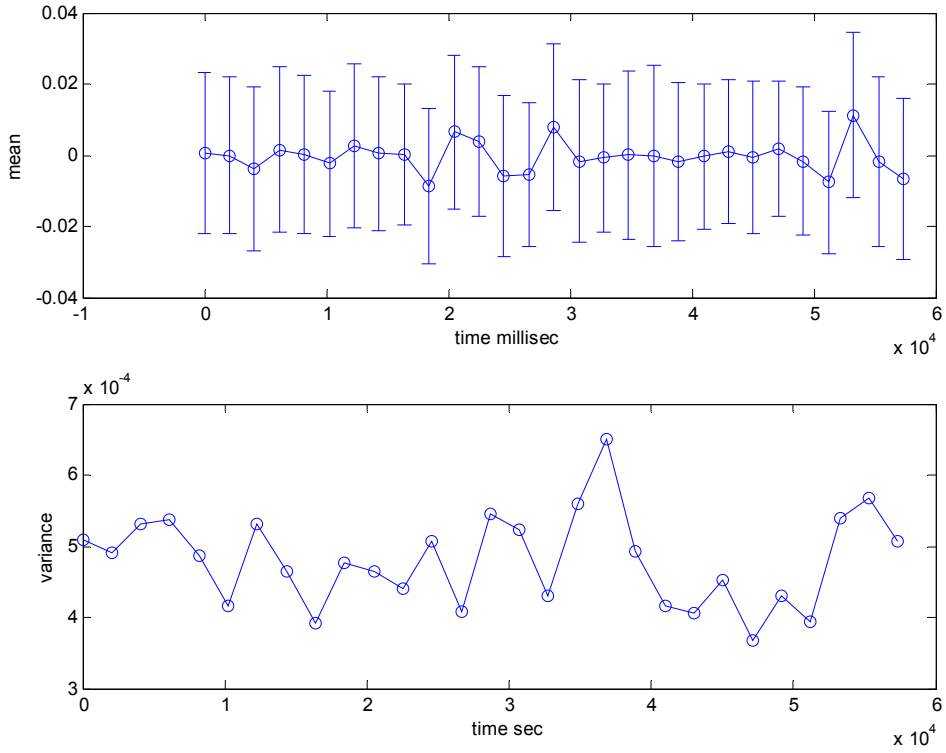


Figure C.10 Running mean and variance for tray 3 time series at reboiler pressure = 31.08 psig

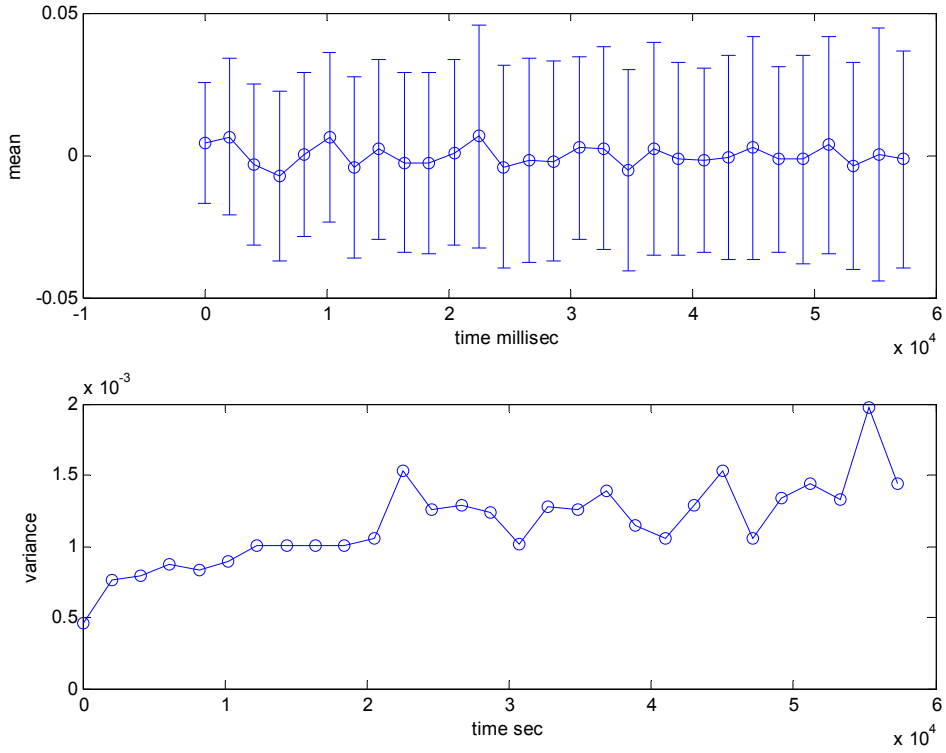


Figure C.11 Running mean and variance for tray 3 time series at reboiler pressure = 31.02 psig

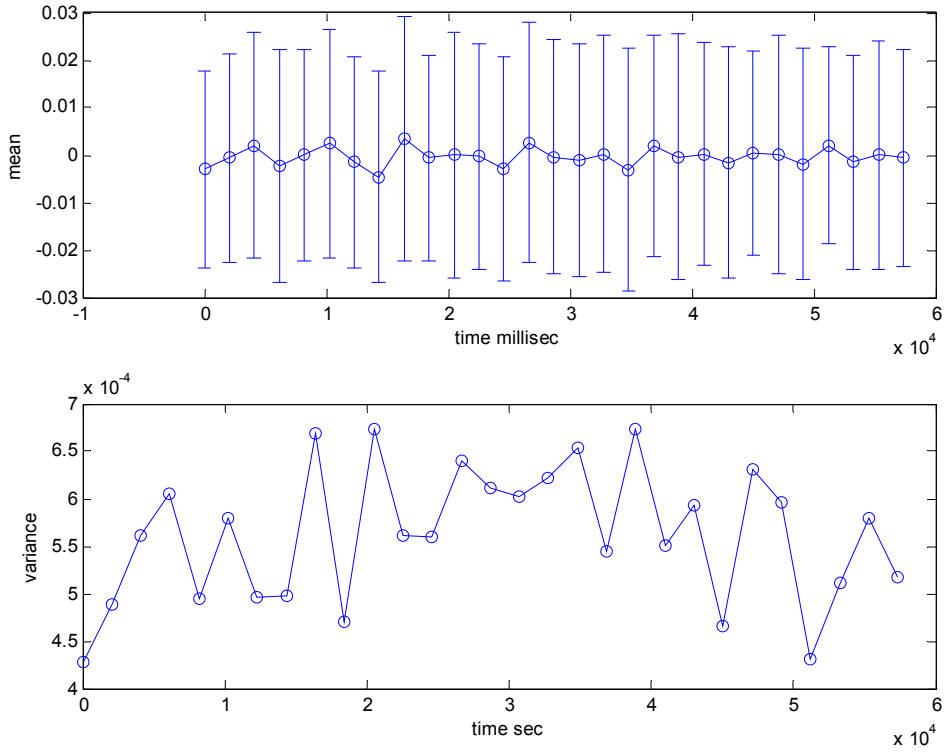


Figure C.12 Running mean and variance for tray 3 time series at reboiler pressure = 15.02 psig

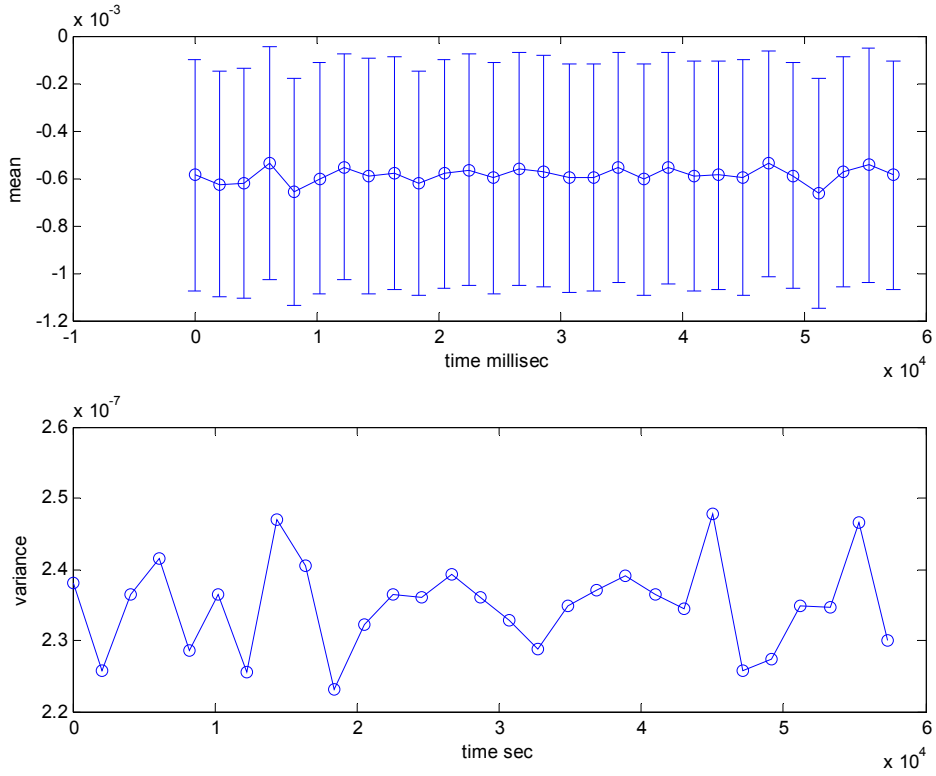


Figure C.13 Running mean and variance for tray 4 time series at reboiler pressure = 0 psig

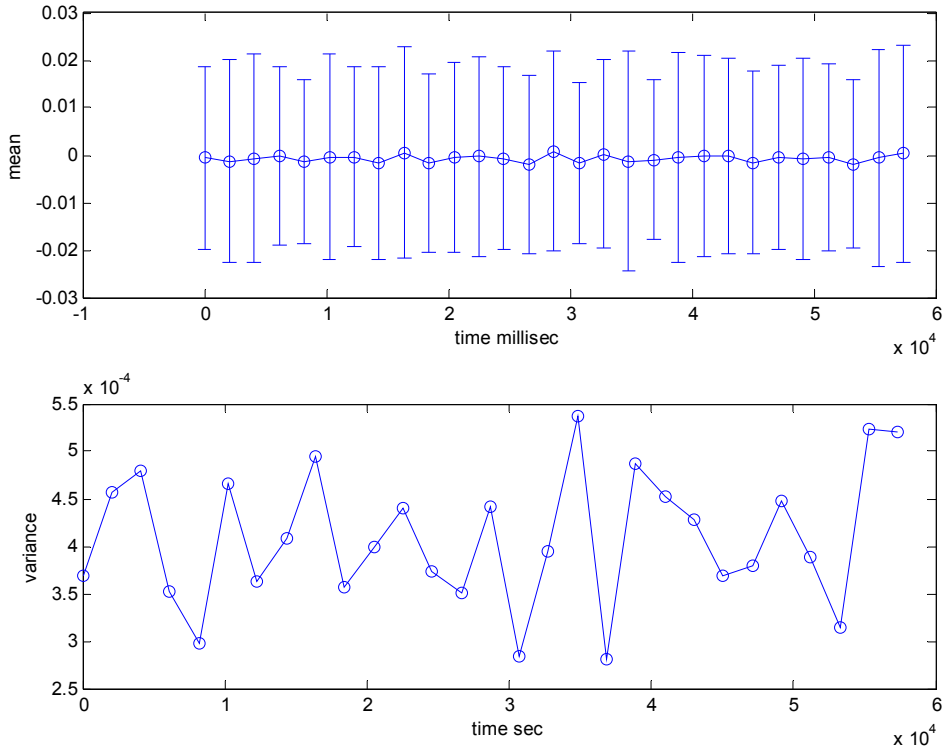


Figure C.14 Running mean and variance for tray 4 time series at reboiler pressure = 9.97 psig

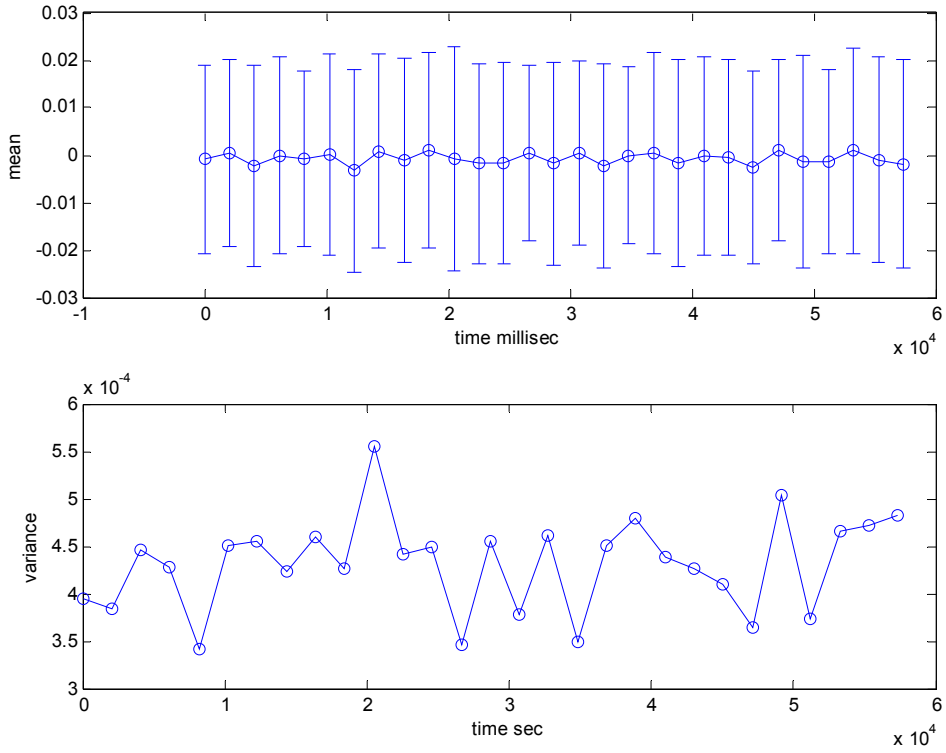


Figure C.15 Running mean and variance for tray 4 time series at reboiler pressure = 15.04 psig

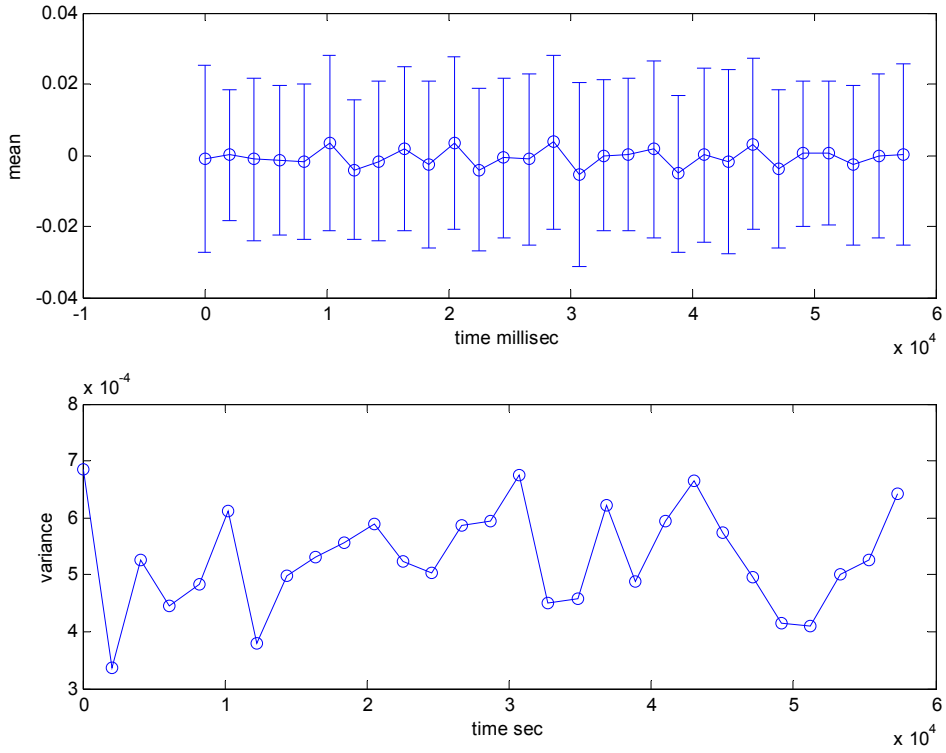


Figure C.16 Running mean and variance for tray 4 time series at reboiler pressure = 20.08 psig

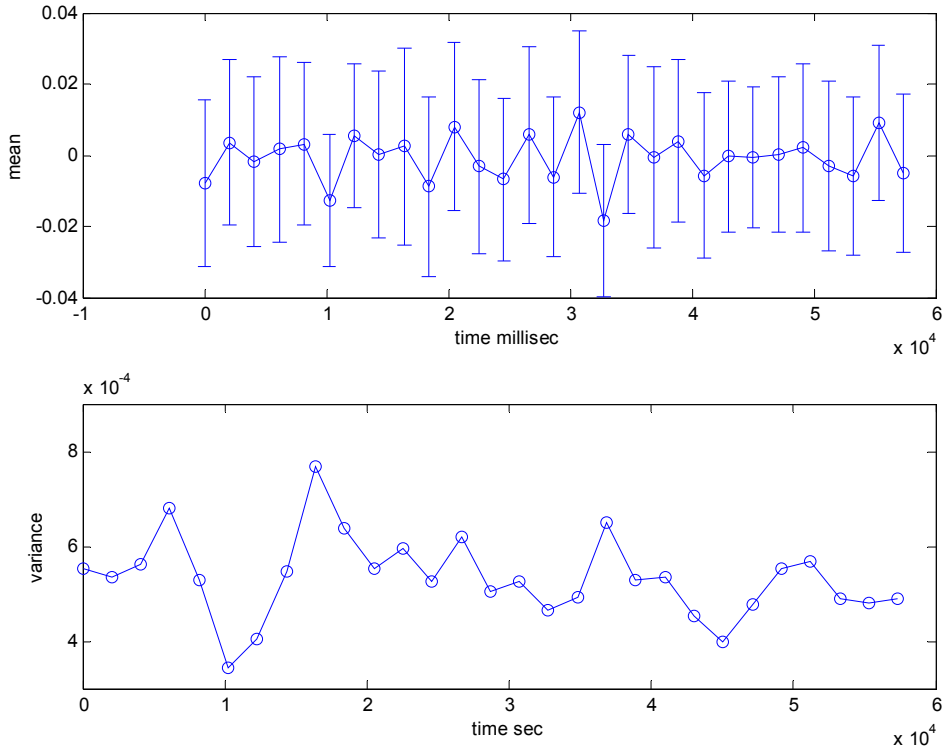


Figure C.17 Running mean and variance for tray 4 time series at reboiler pressure = 24.98 psig

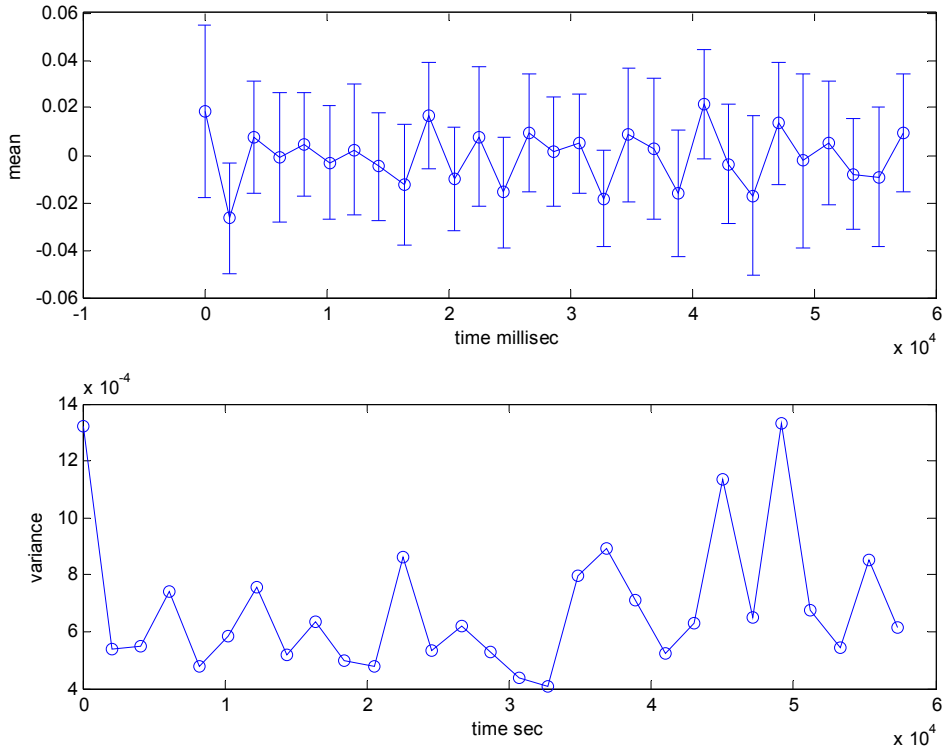


Figure C.18 Running mean and variance for tray 4 time series at reboiler pressure = 27.96 psig

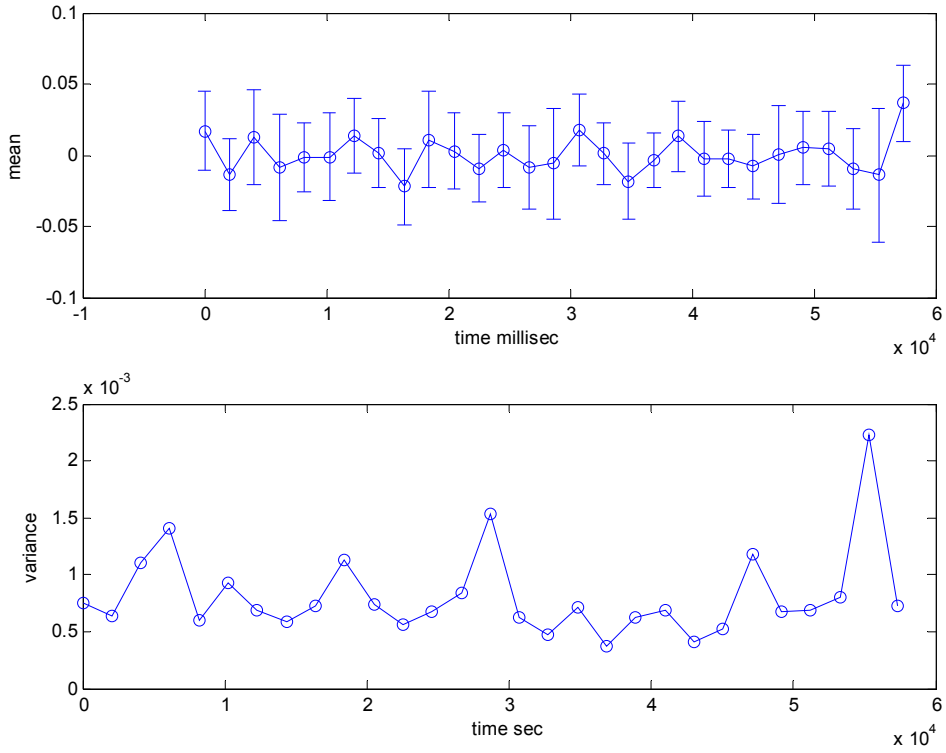


Figure C.19 Running mean and variance for tray 4 time series at reboiler pressure = 29.59 psig

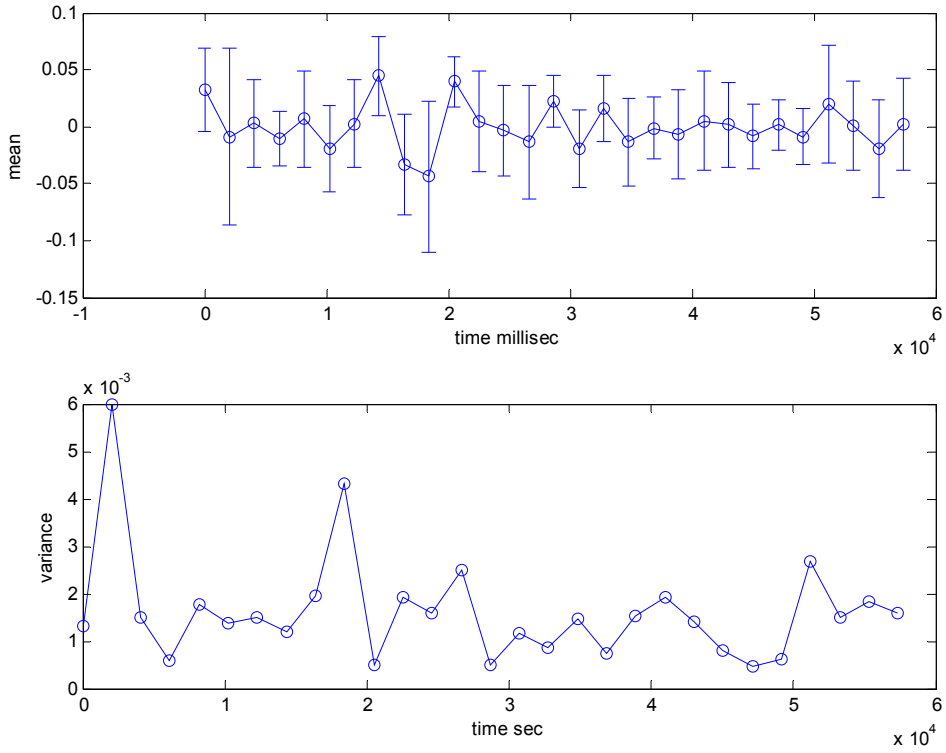


Figure C.20 Running mean and variance for tray 4 time series at reboiler pressure = 29.94 psig

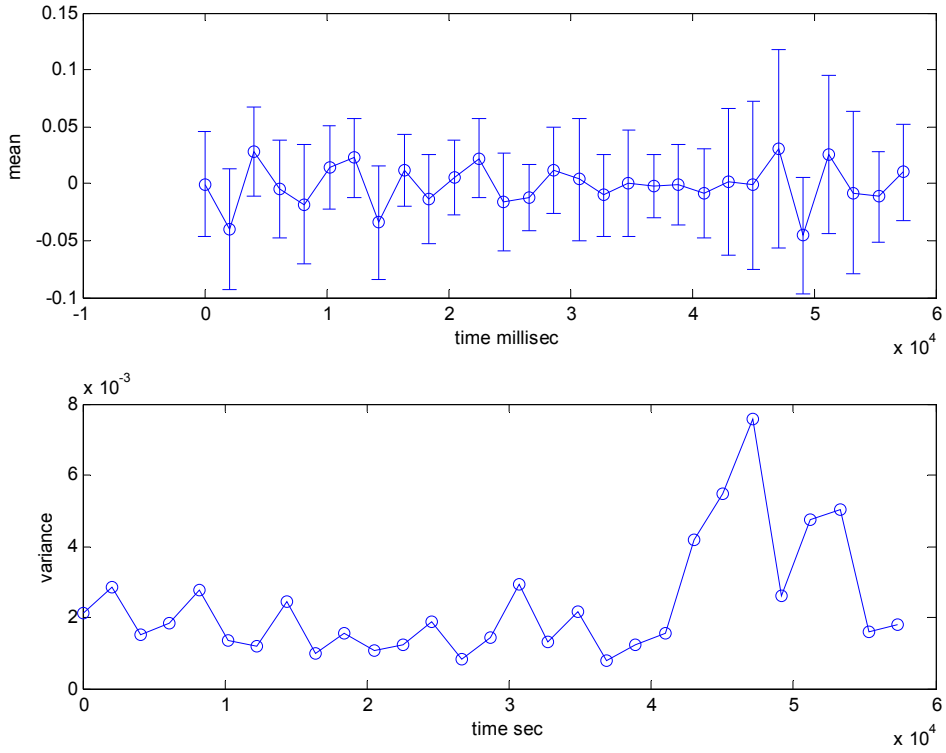


Figure C.21 Running mean and variance for tray 4 time series at reboiler pressure = 30.02 psig

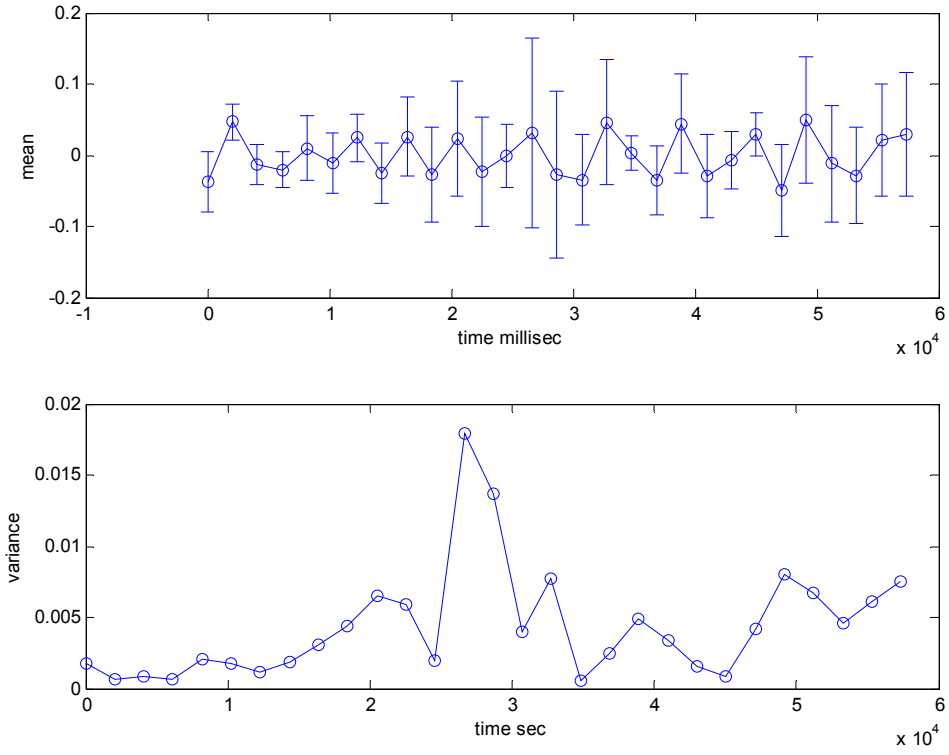


Figure C.22 Running mean and variance for tray 4 time series at reboiler pressure = 31.08 psig

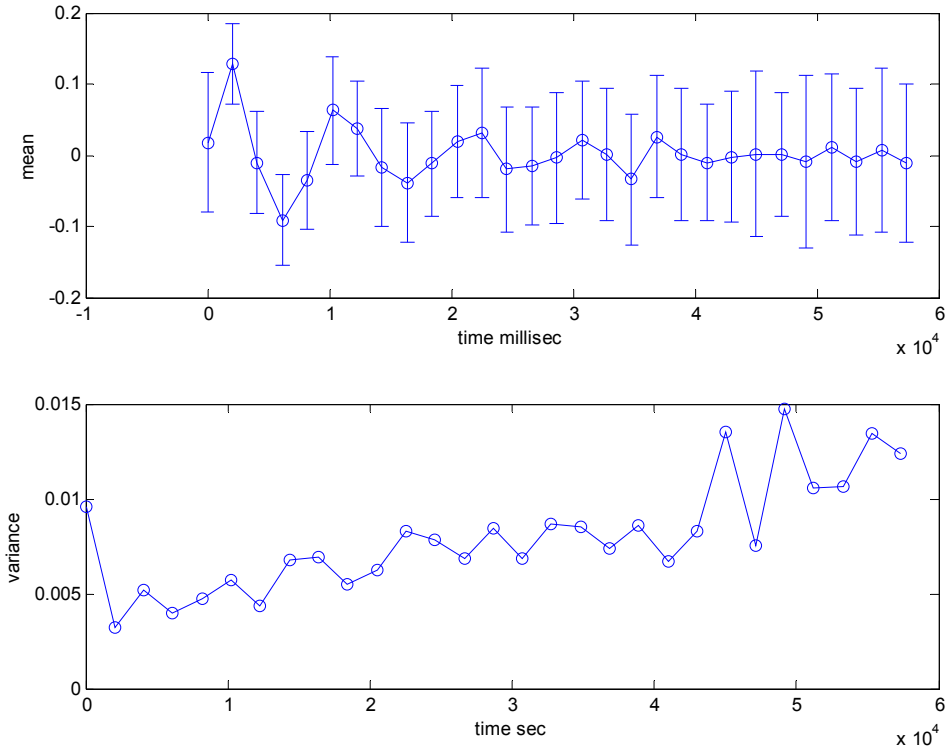


Figure C.23 Running mean and variance for tray 4 time series at reboiler pressure = 31.02 psig

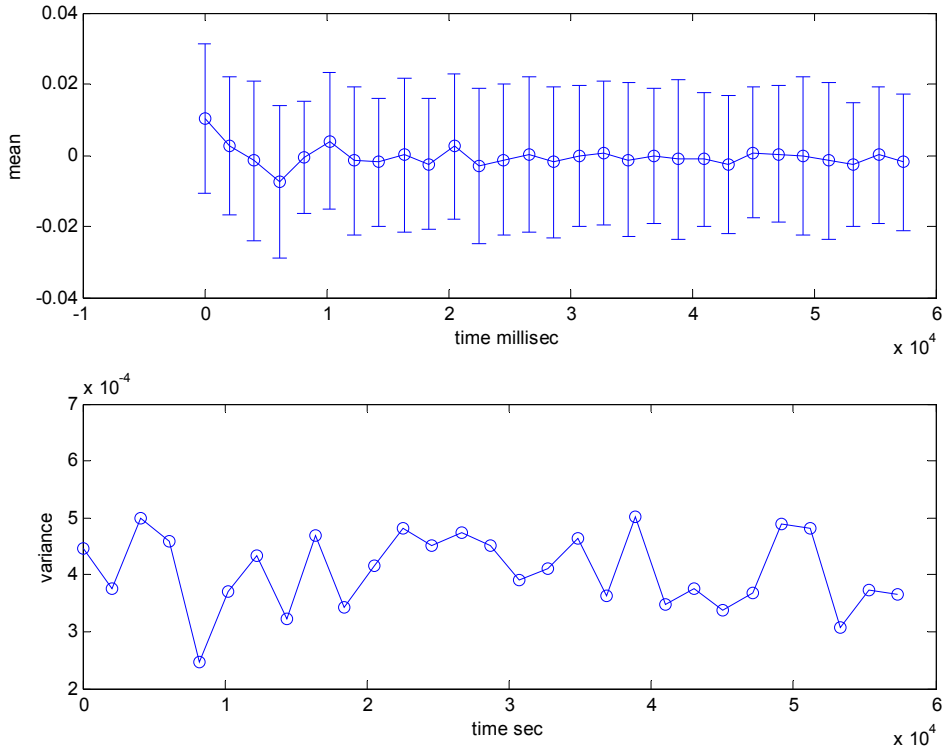


Figure C.24 Running mean and variance for tray 4 time series at reboiler pressure = 15.02 psig

VITA

Alok Maheshbhai Patel was born in Patan, India on July 18th 1979. He graduated from M. G. Amin and V. N. Savani School (Vallabh Ashram) in May 1997. In August 1997, he joined K. K. Wagh College of Engineering in their Civil Engineering program. He transferred to University of Tennessee, Chattanooga in August 1999. He completed his Bachelor's Degree in Chemical Engineering in May 2003. In August 2004, he entered University of Tennessee, Knoxville to earn his Master's Degree in Chemical Engineering.